Naval Research Laboratory

Washington, DC 20375-5320

NRL/MR/5310--20-10,148

Developments in the Finite-Difference Time-Domain Method for Electromagnetic Modeling

Michael S. Kluskens

Radar Analysis Branch
Radar Division

October 19, 2020

REPORT DOCUMENTATION PAGE

Form Approved
OMB No. 0704-0188

1. REPORT DATE *(DD-MM-YYYY)*	**2. REPORT TYPE**	**3. DATES COVERED** *(From - To)*
19-10-2020	NRL Memorandum Report	Oct 2019 – Aug 2020

4. TITLE AND SUBTITLE

Developments in the Finite-Difference Time-Domain Method for Electromagnetic Modeling

5a. CONTRACT NUMBER

5b. GRANT NUMBER

5c. PROGRAM ELEMENT NUMBER
PE-62271N

6. AUTHOR(S)

Michael S. Kluskens

5d. PROJECT NUMBER

5e. TASK NUMBER
EW-271-001

5f. WORK UNIT NUMBER
6B47

7. PERFORMING ORGANIZATION NAME(S) AND ADDRESS(ES)

Naval Research Laboratory
4555 Overlook Avenue, SW
Washington, DC 20375-5320

8. PERFORMING ORGANIZATION REPORT NUMBER

NRL/MR/5310--20-10,148

9. SPONSORING / MONITORING AGENCY NAME(S) AND ADDRESS(ES)

Office of Naval Research
One Liberty Center
875 N. Randolph Street, Suite 1425
Arlington, VA 22203-1995

10. SPONSOR / MONITOR'S ACRONYM(S)

ONR

11. SPONSOR / MONITOR'S REPORT NUMBER(S)

12. DISTRIBUTION / AVAILABILITY STATEMENT

DISTRIBUTION STATEMENT A: Approved for public release; distribution is unlimited.

13. SUPPLEMENTARY NOTES

14. ABSTRACT

This report presents the derivation and evaluation of concepts in the finite-difference time-domain (FDTD) method for electromagnetic modeling. I show that the incident field time derivative required for the scattered-field method can be obtained from the spatial derivative of the incident-field and that a sixth-order central difference equation is a cost effective means to generate the derivative of the incidentfield as opposed to the analytic derivative. I present background on boundary condition concepts starting with one-dimensional FDTD before turning to two-dimensional FDTD where I show that the split-field formulation of the Bérenger Perfectly Matched Layer (PML) method can be generalized with other one-dimensional FDTD boundary conditions rather than just lossy material layers. In the development of one-dimensional boundary conditions, I show that the formula for splitting an electromagnetic field into components traveling in opposite directions can be used to develop a series of one-way boundary conditions, which perform better than those developed from the factorization of the wave equation. In the last section of the report, I develop a split-field, one-way boundary condition for two-dimensional FDTD that is far less expensive than the widely used PML methods, which even for two-dimensional FDTD require over 27 different PML/FDTD update equations along with interface equations between the nine different PML/FDTD regions.

15. SUBJECT TERMS

Finite-difference Time-domain

16. SECURITY CLASSIFICATION OF:			**17. LIMITATION OF ABSTRACT**	**18. NUMBER OF PAGES**	**19a. NAME OF RESPONSIBLE PERSON**
a. REPORT	**b. ABSTRACT**	**c. THIS PAGE**			Michael S. Kluskens
Unclassified Unlimited	Unclassified Unlimited	Unclassified Unlimited	Unclassified Unlimited	68	**19b. TELEPHONE NUMBER** *(include area code)* (202) 404-1818

Standard Form 298 (Rev. 8-98)
Prescribed by ANSI Std. Z39.18

This page intentionally left blank.

CONTENTS

EXECUTIVE SUMMARY E-1

1. INTRODUCTION 1
   - 1.1 Electromagnetic Properties of Materials 1
   - 1.2 Foundations of Finite-Difference Time-Domain 4
   - 1.3 Two-Dimensional Finite-Difference Time-Domain 6
   - 1.4 Three-Dimensional Finite-Difference Time-Domain 7

2. TOTAL-FIELD/SCATTERED-FIELD METHOD 7
   - 2.1 Numerical Dispersion in the Total-Field/Scattered-Field Method 9
   - 2.2 Secondary FDTD Grid for the Total-Field/Scattered-Field Method 13

3. SCATTERED-FIELD METHOD 15
   - 3.1 Numerical Derivatives for the Scattered-Field Method 18
   - 3.2 Alternative Derivative for the Scattered-Field Method 22

4. BOUNDARY CONDITIONS 22
   - 4.1 Boundary Conditions From the Factorization of the Wave Equation 23
   - 4.2 First-Order Wave Equation Boundary Condition 24
   - 4.3 Second Order Wave Equation Boundary Condition 27
   - 4.4 Alternative Second Order Wave Equation Boundary Condition 30

5. ONE-WAY PROPAGATION BOUNDARY CONDITION 33
   - 5.1 First-Order One-Way Propagation Boundary Condition 33
   - 5.2 Second Order One-Way Propagation Boundary Condition 35
   - 5.3 Third Order One-Way Propagation Boundary Condition 38
   - 5.4 Temporal Second Order One-Way Propagation Boundary Condition 40
   - 5.5 Spatial and Temporal Second Order One-Way Propagation Boundary Condition 42
   - 5.6 Summary on One-Dimensional FDTD Boundary Conditions 43

6. BOUNDARY CONDITIONS IN TWO DIMENSIONS 43
   - 6.1 Wave Equation Boundary Condition in Two Dimensions 43
   - 6.2 First-Order One-Way Propagation Boundary Condition in Two Dimensions 45
   - 6.3 Perfectly Matched Layer Boundary Condition in Two Dimensions 49
   - 6.4 Split-Field One-Way Propagation Boundary Condition in Two Dimensions 52

7. CONCLUSION 58

REFERENCES 59

APPENDIX A—FDTD Formulas as Fortran90 Code 61

FIGURES

1 Electrical properties of seawater at 20°C with a salinity of 35 parts per thousand. 3

2 Propagation of an analytic modulated Gaussian pulse (f_c = 300 MHz, f_{BW} = 300 MHz) in a free space region using the total-field/scattered-field method with $\Delta x = 0.05$ meters and $\Delta t = \Delta x/c$. 10

3 Propagation of an analytic modulated Gaussian pulse (f_c = 300 MHz, f_{BW} = 300 MHz) in a free space region using the total-field/scattered-field method with $\Delta x = 0.05$ meters and $\Delta t = \Delta x/(c\sqrt{2})$. 10

4 Propagation of a reduced velocity analytic modulated Gaussian pulse (f_c = 300 MHz, f_{BW} = 300 MHz) in a free space region using the total-field/scattered-field method with $\Delta x = 0.05$ meters and $\Delta t = \Delta x/(c\sqrt{2})$. 11

5 Propagation of a narrow band pulse with the reduced velocity analytic modulated Gaussian pulse (f_c = 300 MHz, f_{BW} = 100 MHz) in a free space region using the total-field/scattered-field method with $\Delta x = 0.05$ meters and $\Delta t = \Delta x/(c\sqrt{2})$. 12

6 Propagation of a numerically-filtered, modulated Gaussian pulse (f_c = 300 MHz, f_{BW} = 100 MHz) in a free space region using the total-field/scattered-field method with $\Delta x = 0.05$ meters and $\Delta t = \Delta x/(c\sqrt{2})$. 13

7 Total-field/scattered-field method for a numerically-filtered, modulated Gaussian pulse (f_c = 300 MHz, f_{BW} = 100 MHz) incident on seven cells centered at 5 meters with a relative dielectric constant of 2, $\Delta x = 0.05$ m, and $\Delta t = \Delta x/(c\sqrt{2})$. 14

8 Scattered-field method for an analytic modulated Gaussian pulse (f_c = 300 MHz, f_{BW} = 100 MHz) incident on seven cells centered at 5 meters with a relative dielectric constant of 2, $\Delta x = 0.05$ m, and $\Delta t = \Delta x/(c\sqrt{2})$. 17

9 Sum of the incident-field and scattered-field calculated via the scattered-field method for an analytic modulated Gaussian pulse (f_c = 300 MHz, f_{BW} = 100 MHz) incident on seven cells centered at 5 meters with a relative dielectric constant of 2, $\Delta x = 0.05$ m, and $\Delta t = \Delta x/(c\sqrt{2})$. 17

10 Analytic time derivative of the modulated Gaussian pulse versus the second order central difference equation calculated from the spatial grid at one time instance. 19

11 Sum of the analytic incident-field and scattered-field calculated via the scattered-field method using the second order central difference equation with an analytic modulated Gaussian pulse (f_c = 300 MHz, f_{BW} = 100 MHz) incident on seven cells centered at 5 meters with a relative dielectric constant of 2, $\Delta x = 0.05$ m, and $\Delta t = \Delta x/(c\sqrt{2})$. 19

12 Sum of the analytic incident-field and scattered-field calculated via the scattered-field method using the fourth order central difference equation with an analytic modulated Gaussian pulse ($f_c = 300$ MHz, $f_{BW} = 100$ MHz) incident on seven cells centered at 5 meters with a relative dielectric constant of 2, $\Delta x = 0.05$ m, and $\Delta t = \Delta x/(c\sqrt{2})$. 20

13 Sum of the analytic incident-field and scattered-field calculated via the scattered-field method using the sixth order central difference equation with an analytic modulated Gaussian pulse ($f_c = 300$ MHz, $f_{BW} = 100$ MHz) incident on seven cells centered at 5 meters with a relative dielectric constant of 2, $\Delta x = 0.05$ m, and $\Delta t = \Delta x/(c\sqrt{2})$. 20

14 Sum of the analytic incident-field and scattered-field calculated via the scattered-field method using the sixth order central difference equation with a modulated Gaussian pulse ($f_c = 300$ MHz, $f_{BW} = 100$ MHz) generated in an FDTD grid and incident on seven cells centered at 5 meters with a relative dielectric constant of 2, $\Delta x = 0.05$ m, and $\Delta t = \Delta x/(c\sqrt{2})$. 21

15 Reflection of a modulated Gaussian pulse ($f_c = 300$ MHz, $f_{BW} = 300$ MHz) from a terminated FDTD grid at $x = 10$ m with $\Delta x = 0.05$ m and $\Delta t = \Delta x/(c\sqrt{2})$. 23

16 Reflection of a modulated Gaussian pulse ($f_c = 300$ MHz, $f_{BW} = 300$ MHz) from a boundary condition derived from the wave equation and forward difference equations with $\Delta x = 0.05$ meters and $\Delta t = \Delta x/(c\sqrt{2})$. 26

17 Reflection of a modulated Gaussian pulse ($f_c = 300$ MHz, $f_{BW} = 300$ MHz) from a second order wave equation boundary condition with $\Delta x = 0.05$ meters and $\Delta t = \Delta x/(c\sqrt{2})$. 29

18 Reflection of a modulated Gaussian pulse ($f_c = 300$ MHz, $f_{BW} = 300$ MHz) from a central difference equation derived boundary condition with $\Delta x = 0.05$ meters and $\Delta t = \Delta x/(c\sqrt{2})$. . 32

19 Reflection of a modulated Gaussian pulse ($f_c = 300$ MHz, $f_{BW} = 300$ MHz) from a central difference equation derived boundary condition with $\Delta x = 0.05$ meters and $\Delta t = \Delta x/(c\sqrt{2})$ at time = 50 ns. 32

20 Reflection of a modulated Gaussian pulse ($f_c = 300$ MHz, $f_{BW} = 300$ MHz) from the first-order $\boldsymbol{\mathcal{E}} = -\eta\hat{x} \times \boldsymbol{\mathcal{H}}$ boundary condition with $\Delta x = 0.05$ meters and $\Delta t = \Delta x/(c\sqrt{2})$. 34

21 Reflection of a modulated Gaussian pulse ($f_c = 300$ MHz, $f_{BW} = 300$ MHz) from the first-order $\boldsymbol{\mathcal{E}} = -\eta\hat{x} \times \boldsymbol{\mathcal{H}}$ boundary condition with $\Delta x = 0.05$ meters and $\Delta t = \Delta x/(c\sqrt{2})$ at time = 50 ns. 35

22 Reflection of a modulated Gaussian pulse ($f_c = 300$ MHz, $f_{BW} = 300$ MHz) from the second order $\boldsymbol{\mathcal{E}} = -\eta\hat{x} \times \boldsymbol{\mathcal{H}}$ boundary condition with $\Delta x = 0.05$ meters and $\Delta t = \Delta x/(c\sqrt{2})$ at time = 50 ns. 36

23 Reflection of a modulated Gaussian pulse ($f_c = 300$ MHz, $f_{BW} = 300$ MHz) from the $\boldsymbol{\mathcal{E}} = -\eta\hat{x} \times \boldsymbol{\mathcal{H}}$ boundary condition created by averaging the first and second-order boundary conditions with $\Delta x = 0.05$ meters and $\Delta t = \Delta x/(c\sqrt{2})$ at time = 50 ns. 37

24 Reflection of a modulated Gaussian pulse (f_c = 300 MHz, f_{BW} = 300 MHz) from the third-order $\boldsymbol{\mathcal{E}} = -\eta\hat{x} \times \boldsymbol{\mathcal{H}}$ boundary condition with $\Delta x = 0.05$ meters and $\Delta t = \Delta x/(c\sqrt{2})$ at time = 50 ns. 39

25 Reflection of a modulated Gaussian pulse (f_c = 300 MHz, f_{BW} = 300 MHz) from the temporal second-order $\boldsymbol{\mathcal{E}} = -\eta\hat{x} \times \boldsymbol{\mathcal{H}}$ boundary condition with $\Delta x = 0.05$ meters and $\Delta t = \Delta x/(c\sqrt{2})$ at time = 50 ns. 41

26 Reflection of a modulated Gaussian pulse (f_c = 300 MHz, f_{BW} = 300 MHz) from the spatial and temporal second order $\boldsymbol{\mathcal{E}} = -\eta\hat{x} \times \boldsymbol{\mathcal{H}}$ boundary condition with $\Delta x = 0.05$ meters and $\Delta t = \Delta x/(c\sqrt{2})$ at time = 50 ns. 43

27 Propagation of a modulated Gaussian pulse (f_c = 300 MHz, f_{BW} = 300 MHz) in a two-dimensional FDTD grid after 20 ns with $\Delta x = 0.05$ meters and $\Delta t = \Delta x/(c\sqrt{2})$. 46

28 Propagation of a modulated Gaussian pulse (f_c = 300 MHz, f_{BW} = 300 MHz) in a two-dimensional FDTD grid after 30 ns with $\pm x$ first-order $\boldsymbol{\mathcal{E}} = -\eta\hat{x} \times \boldsymbol{\mathcal{H}}$ boundary conditions for $\Delta x = 0.05$ meters and $\Delta t = \Delta x/(c\sqrt{2})$. 46

29 Propagation of a modulated Gaussian pulse (f_c = 300 MHz, f_{BW} = 300 MHz) in a two-dimensional FDTD grid after 25 ns (a) and 30 ns (b) with the first-order $\boldsymbol{\mathcal{E}} = -\eta\hat{x} \times \boldsymbol{\mathcal{H}}$ boundary conditions for $\Delta x = 0.05$ meters and $\Delta t = \Delta x/(c\sqrt{2})$. 47

30 Propagation of a modulated Gaussian pulse (f_c = 300 MHz, f_{BW} = 300 MHz) in a two-dimensional FDTD grid after 35 ns (a) and 40 ns (b) with the first-order $\boldsymbol{\mathcal{E}} = -\eta\hat{x} \times \boldsymbol{\mathcal{H}}$ boundary conditions for $\Delta x = 0.05$ meters and $\Delta t = \Delta x/(c\sqrt{2})$. 48

31 Symbolic representation of PML and FDTD equations in a subsection of a two-dimensional FDTD grid..... 50

32 Propagation of a modulated Gaussian pulse (f_c = 300 MHz, f_{BW} = 300 MHz) in a two-dimensional FDTD grid after 25 ns (a) and 30 ns (b) with a ten cell cosine tapered PML boundary condition for $\Delta x = 0.05$ meters and $\Delta t = \Delta x/(c\sqrt{2})$. 53

33 Propagation of a modulated Gaussian pulse (f_c = 300 MHz, f_{BW} = 300 MHz) in a two-dimensional FDTD grid after 35 ns (a) and 40 ns (b) with a ten cell cosine tapered PML boundary condition for $\Delta x = 0.05$ meters and $\Delta t = \Delta x/(c\sqrt{2})$. 54

34 Propagation of a modulated Gaussian pulse (f_c = 300 MHz, f_{BW} = 300 MHz) in a two-dimensional FDTD grid after 25 ns (a) and 30 ns (b) with a first-order, split-field, one-way boundary condition for $\Delta x = 0.05$ meters and $\Delta t = \Delta x/(c\sqrt{2})$. 56

35 Propagation of a modulated Gaussian pulse (f_c = 300 MHz, f_{BW} = 300 MHz) in a two-dimensional FDTD grid after 35 ns (a) and 40 ns (b) with a first-order, split-field, one-way boundary condition for $\Delta x = 0.05$ meters and $\Delta t = \Delta x/(c\sqrt{2})$. 57

EXECUTIVE SUMMARY

This report presents the derivation and evaluation of concepts in the finite-difference time-domain (FDTD) method for electromagnetic modeling. I start with a background on how the electromagnetic properties of materials are treated in FDTD and follow with the foundation of the Yee formulation of FDTD. From this basis, I develop the total-field/scattered-field and scattered-field methods for simulating waves incident on the region modeled in an FDTD grid. For the first method, I show that a secondary FDTD grid is effective in reducing anomalous scattering at the boundary between the total-field and scattered-field regions. I show that the incident-field time derivative required for the scattered-field method can be obtained from the spatial derivative of the incident-field and that a sixth-order central difference equation is a cost effective means to generate the derivative of the incident-field as opposed to the analytic derivative.

I present background on boundary condition concepts starting with one-dimensional FDTD before turning to two-dimensional FDTD where I show that the split-field formulation of the Bérenger Perfectly Matched Layer (PML) method can be generalized with other one-dimensional FDTD boundary conditions rather than just lossy material layers. In the development of one-dimensional boundary conditions, I show that the formula for splitting an electromagnetic field into components traveling in opposite directions can be used to develop a series of one-way boundary conditions, which perform better than those developed from the factorization of the wave equation. In the last section of the report, I develop a split-field, one-way boundary condition for two-dimensional FDTD that is far less expensive than the widely used PML methods, which even for two-dimensional FDTD require over 27 different PML/FDTD update equations along with interface equations between the nine different PML/FDTD regions.

This page intentionally left blank

DEVELOPMENTS IN THE FINITE-DIFFERENCE TIME-DOMAIN METHOD FOR ELECTROMAGNETIC MODELING

1. INTRODUCTION

The field of computational electromagnetics encompasses numerous techniques. The simplest to derive is the finite-difference time-domain (FDTD) method [1]. The derivation can start from the differential form of Maxwell's equations,

$$\nabla \times \boldsymbol{\mathcal{E}}(t) = -\frac{\partial \boldsymbol{\mathcal{B}}(t)}{\partial t}, \tag{1a}$$

$$\nabla \times \boldsymbol{\mathcal{H}}(t) = \frac{\partial \boldsymbol{\mathcal{D}}(t)}{\partial t} + \boldsymbol{\mathcal{J}}(t), \tag{1b}$$

$$\nabla \cdot \boldsymbol{\mathcal{D}}(t) = \rho, \tag{1c}$$

$$\nabla \cdot \boldsymbol{\mathcal{B}}(t) = 0, \tag{1d}$$

or the integral form of Maxwell's equations,

$$\oint \boldsymbol{\mathcal{E}} \cdot d\mathbf{l} = -\frac{\partial}{\partial t} \iint \boldsymbol{\mathcal{B}} \cdot d\mathbf{s}, \tag{2a}$$

$$\oint \boldsymbol{\mathcal{H}} \cdot d\mathbf{l} = \frac{\partial}{\partial t} \iint \boldsymbol{\mathcal{D}} \cdot d\mathbf{s} + \iint \boldsymbol{\mathcal{J}} \cdot d\mathbf{s}, \tag{2b}$$

$$\oiint \boldsymbol{\mathcal{D}} \cdot d\mathbf{s} = \iiint \rho \, dv, \tag{2c}$$

$$\oiint \boldsymbol{\mathcal{B}} \cdot d\mathbf{s} = 0, \tag{2d}$$

where $\boldsymbol{\mathcal{E}}/\boldsymbol{\mathcal{H}}$ are the electric/magnetic field intensities, $\boldsymbol{\mathcal{D}}/\boldsymbol{\mathcal{B}}$ are the electric/magnetic flux densities, and $\boldsymbol{\mathcal{J}}/\rho$ are the electric current/charge densities [2, Section 1-2], [3, Section 1.2].

1.1 Electromagnetic Properties of Materials

For simplistic isotropic materials, field intensities, flux densities, and current density are linked by scalar constitutive relations

$$\boldsymbol{\mathcal{D}}(t) = \epsilon \boldsymbol{\mathcal{E}}(t), \tag{3a}$$

$$\boldsymbol{\mathcal{B}}(t) = \mu \boldsymbol{\mathcal{H}}(t), \tag{3b}$$

$$\boldsymbol{\mathcal{J}}(t) = \sigma_s \boldsymbol{\mathcal{E}}(t) + \boldsymbol{\mathcal{J}}^i(t), \tag{3c}$$

Manuscript approved October 16, 2020.

where ϵ, μ, and σ_s are the permittivity, permeability, and static electric conductivity of the materials, respectively, and $\mathcal{J}^i(t)$ is the impressed (source) electric current. For anisotropic materials, permittivity, permeability, and conductivity are tensors. For example, Equation (3a) expands to [3, Section 2.7]

$$\begin{bmatrix} \mathcal{D}_x(t) \\ \mathcal{D}_y(t) \\ \mathcal{D}_z(t) \end{bmatrix} = \begin{bmatrix} \epsilon_{xx} & \epsilon_{xy} & \epsilon_{xz} \\ \epsilon_{yx} & \epsilon_{yy} & \epsilon_{yz} \\ \epsilon_{zx} & \epsilon_{zy} & \epsilon_{zz} \end{bmatrix} \begin{bmatrix} \mathcal{E}_x(t) \\ \mathcal{E}_y(t) \\ \mathcal{E}_z(t) \end{bmatrix}. \tag{4}$$

As adding anisotropic materials to FDTD is a mathematical exercise, this report concentrates on isotropic materials in the development of advanced FDTD methods.

The electromagnetic properties of real materials are not as simple as implied in Equation (3). An electric field polarizes dielectric materials creating electric dipoles through the movement of bound charges. This interaction occurs at the electron, atomic, and molecular levels with multiple natural frequencies for every material [3, Section 2.8.1] [4]. These natural frequencies are widely spaced in frequency, from radio frequency to ultraviolet and beyond. There are a number of complicated expressions; including the Kramers-Kronig relationship; that describe permittivity as a function of frequency [3, Section 2.8.1]. However, the time varying permittivity of materials is represented in frequency-limited, time-domain[1] calculations via a Debye model [3, Section 2.8.1], or, in the case of plasmas, a Drude model [5]. Given a time varying permittivity, $\epsilon(t)$, the general isotropic form of Equation (3a) is

$$\boldsymbol{\mathcal{D}}(t) = \epsilon(t) * \boldsymbol{\mathcal{E}}(t), \tag{5}$$

where $*$ represents convolution [3, Section 1.3]. As convolution is computationally expensive, a simpler formulation derived via the frequency domain is employed when possible.[2] To determine if a Debye model is required for an FDTD calculation it is necessary to look at both the relative permittivity and the effective electric conductivity versus frequency, rather than the effective electric loss tangent, which is tabulated in most dielectric material tables [4]. For example, a Debye model is usually required for calculations involving seawater owing to its significant relative permittivity variation as a function of frequency. However, the relative permittivity and effective electric conductivity of seawater, based on the Meissner-Somaraju model [6, 7], are constant within three digits below 400 MHz as shown in Figure 1. Therefore, FDTD calculations with seawater below 400 MHz do not require the Debye model.

To determine the basis for the simpler model of time-varying permittivity, I start with the Fourier transform of Equation (5)

$$D(\omega) = \hat{\epsilon}(\omega) E(\omega) \tag{6a}$$

$$= \left[\epsilon'(\omega) - j\epsilon''(\omega)\right] E(\omega) \tag{6b}$$

where ω is angular frequency (2π frequency), $\hat{\epsilon}$ is the complex permittivity, and ϵ' and ϵ'' are the real and imaginary parts of complex permittivity [2, Section 1-11] [3, Section 2.8.1] [4]. In the frequency domain,

[1] All FDTD calculations are frequency limited as the approximations break down with increasing frequency.

[2] This report uses the $e^{j\omega t}$ convention, following the notation of [2–4].

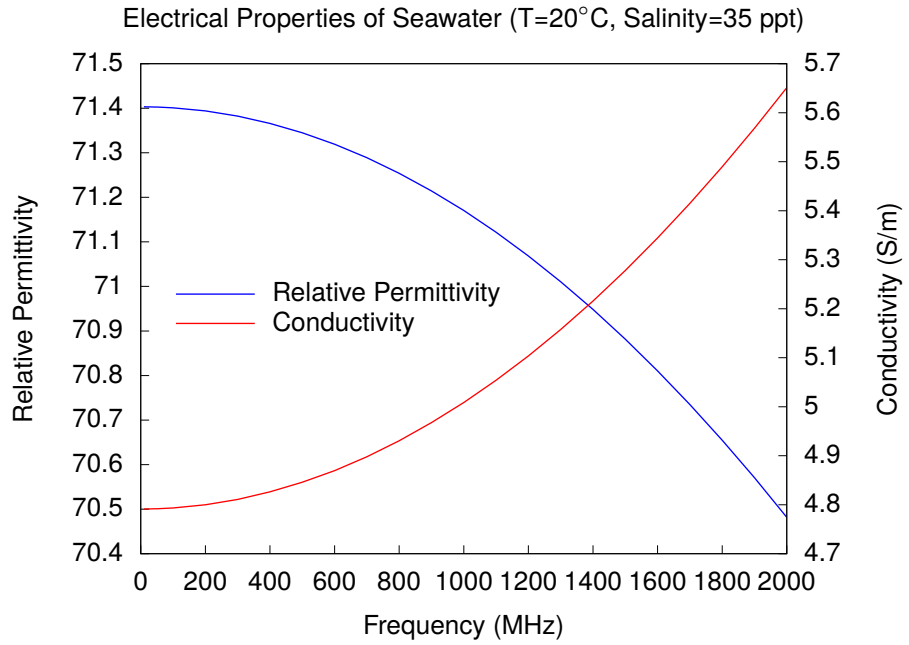

Figure 1—Electrical properties of seawater at 20°C with a salinity of 35 parts per thousand.

Equation (1b) is

$$\begin{aligned}
\nabla \times H(\omega) &= j\omega D(\omega) + \sigma_s E(\omega) + J^i(\omega), && \text{(7a)}\\
&= j\omega \left[\epsilon'(\omega) - j\epsilon''(\omega)\right] E(\omega) + \sigma_s E(\omega) + J^i(\omega), && \text{(7b)}\\
&= \left[j\omega\epsilon'(\omega) + \omega\epsilon''(\omega) + \sigma_s\right] E(\omega) + J^i(\omega), && \text{(7c)}\\
&= \left[j\omega\epsilon'(\omega) + \sigma_e(\omega)\right] E(\omega) + J^i(\omega), && \text{(7d)}\\
&= j\omega \left[\epsilon'(\omega) - j\frac{\sigma_e(\omega)}{\omega}\right] E(\omega) + J^i(\omega), && \text{(7e)}\\
&= j\omega\epsilon'(\omega) \left[1 - j\tan\delta_e(\omega)\right] E(\omega) + J^i(\omega), && \text{(7f)}
\end{aligned}$$

where the effective electric conductivity [3, Section 2.8.1] is given by

$$\sigma_e(\omega) = \omega\epsilon''(\omega) + \sigma_s, \tag{8}$$

and effective electric loss tangent by

$$\tan\delta_e(\omega) = \sigma_e(\omega) / \left[\omega\epsilon'(\omega)\right]. \tag{9}$$

In frequency domain measurements and tables, permittivity is usually presented as relative permittivity,

$$\epsilon_r(\omega) = \epsilon'(\omega)/\epsilon_0, \tag{10}$$

and effective electric loss tangent [4], where ϵ_0 is the permittivity of free space (8.854×10^{-12} farads/meter). If $\epsilon'(\omega)$ and $\sigma_e(\omega)$ are relatively constant with respect to the frequency range of a time-domain calculation, the first-order approximation of the inverse Fourier transform of Equation (7d) is

$$\nabla \times \boldsymbol{\mathcal{H}}(t) = \epsilon' \frac{\partial \boldsymbol{\mathcal{E}}(t)}{\partial t} + \sigma_e \boldsymbol{\mathcal{E}}(t) + \boldsymbol{\mathcal{J}}^i(t), \tag{11}$$

where ϵ' and σ_e are constants with respect to time. Even though this is apparently identical to Equation (1b) with the definition from Equation (3c), this contains a first-order approximation of the time-varying permittivity through the inclusion of ϵ'' in the definition of the effective electric conductivity. To simplify the following developments, the real part of permittivity and the effective electric conductivity are represented by ϵ and σ in the rest of this report. Effective electric conductivity is quickly calculated from tabulated values of loss tangent using the formula

$$\sigma = \epsilon_r f_{GHz} \tan\delta / 18.0, \tag{12}$$

where f_{GHz} is frequency in GHz.

A similar development follows for permeability, such that Maxwell's equations in differential form are often listed as

$$-\nabla \times \boldsymbol{\mathcal{E}}(t) = \mu \frac{\partial \boldsymbol{\mathcal{H}}(t)}{\partial t} + \sigma^* \boldsymbol{\mathcal{H}}(t) + \boldsymbol{\mathcal{M}}^i(t), \tag{13a}$$

$$\nabla \times \boldsymbol{\mathcal{H}}(t) = \epsilon \frac{\partial \boldsymbol{\mathcal{E}}(t)}{\partial t} + \sigma \boldsymbol{\mathcal{E}}(t) + \boldsymbol{\mathcal{J}}^i(t), \tag{13b}$$

$$\nabla \cdot \boldsymbol{\mathcal{E}}(t) = 0, \tag{13c}$$

$$\nabla \cdot \boldsymbol{\mathcal{H}}(t) = 0, \tag{13d}$$

where σ^* is the effective magnetic conductivity and $\boldsymbol{\mathcal{M}}^i(t)$ is the impressed (source) magnetic current. Permeability is usually tabulated in terms of relative permeability, $\mu_r = \mu/\mu_0$, and magnetic loss tangent, $\tan\delta^* = \sigma^*/(\omega\mu)$, where μ_0 is the permeability of free space ($4\pi \times 10^{-7}$ henries/meter) and σ^* is the effective magnetic conductivity due to the imaginary component of permeability. A quick formula for magnetic conductivity is

$$\sigma^* = 7896 \mu_r f_{GHz} \tan\delta^*. \tag{14}$$

1.2 Foundations of Finite-Difference Time-Domain

The key concept in the 1966 paper by K. S. Yee proposing FDTD for electromagnetic modeling is the approximation of the partial derivatives in the differential form of Maxwell's equations by second order central differences, thereby yielding a method that is second-order accurate in space and time [1]. As this report is primarily concerned with developments in FDTD for scattering, the impressed electric and magnetic

currents are not included in the following derivations. As a first step in creating the Yee FDTD equations, I rearrange Equations (13a) – (13b) as follows

$$\mu \frac{\partial \boldsymbol{\mathcal{H}}(t)}{\partial t} + \sigma^* \boldsymbol{\mathcal{H}}(t) = -\nabla \times \boldsymbol{\mathcal{E}}(t), \tag{15a}$$

$$\epsilon \frac{\partial \boldsymbol{\mathcal{E}}(t)}{\partial t} + \sigma \boldsymbol{\mathcal{E}}(t) = \nabla \times \boldsymbol{\mathcal{H}}(t). \tag{15b}$$

Applying second order central differences to Equation (15b) for a one-dimensional problem with the fields $\mathcal{E}_z(x,t)$ and $\mathcal{H}_y(x,t)$ in isotropic material and solving for the future $\mathcal{E}_z$ field results in the following FDTD E-field update equation at the point $(x, t+\frac{\Delta t}{2})$

$$\mathcal{E}_z(x, t+\Delta t) = c_a \mathcal{E}_z(x,t) + \frac{c_b}{\Delta x}\left[\mathcal{H}_y(x+\tfrac{\Delta x}{2}, t+\tfrac{\Delta t}{2}) - \mathcal{H}_y(x-\tfrac{\Delta x}{2}, t+\tfrac{\Delta t}{2})\right], \tag{16}$$

where Δt is the time step, Δx is the spatial step in the x direction, and

$$c_a = \frac{2\epsilon - \sigma \Delta t}{2\epsilon + \sigma \Delta t}, \tag{17a}$$

$$c_b = \frac{2\Delta t}{2\epsilon + \sigma \Delta t}, \tag{17b}$$

with ϵ and σ the material parameters at x. Equation (16) shows that the choice of second order central differences requires that $\boldsymbol{\mathcal{E}}$ and $\boldsymbol{\mathcal{H}}$ are offset in time and space. Following this convention, solving for the future $\mathcal{H}_y$ field using Equation (15a) results in the following FDTD H-field update equation at the point $(x+\frac{\Delta x}{2}, t)$

$$\mathcal{H}_y(x+\tfrac{\Delta x}{2}, t+\tfrac{\Delta t}{2}) = d_a \mathcal{H}_y(x+\tfrac{\Delta x}{2}, t-\tfrac{\Delta t}{2}) + \frac{d_b}{\Delta x}\left[\mathcal{E}_z(x+\Delta x, t) - \mathcal{E}_z(x,t)\right], \tag{18}$$

where

$$d_a = \frac{2\mu - \sigma^* \Delta t}{2\mu + \sigma^* \Delta t}, \tag{19a}$$

$$d_b = \frac{2\Delta t}{2\mu + \sigma^* \Delta t}, \tag{19b}$$

with μ and σ^* the material parameters at $x+\frac{\Delta x}{2}$. I only used half of Maxwell's equations, Equations (1a) and (1b), in these derivations. The remaining equations, Equations (1d) and (1c), are Gauss' Law for electric and magnetic charge and require free charge to be zero in a source-free region. By taking the divergence of Equations (1a) and (1b), it is seen that Equations (1d) and (1c) are redundant [8, Section 2.1]. In addition, it has been shown that the Yee FDTD equations directly satisfy Equations (1d) and (1c) [9, Section 3.6.9].

1.3 Two-Dimensional Finite-Difference Time-Domain

The two-dimensional FDTD update equations for the fields $\mathcal{E}_z(x,y,t)$, $\mathcal{H}_x(x,y,t)$, and $\mathcal{H}_y(x,y,t)$ in isotropic material are

$$\begin{aligned}\mathcal{E}_z(x,y,t+\Delta t) &= c_a\mathcal{E}_z(x,y,t)\\ &\quad+\frac{c_b}{\Delta x}\left[\mathcal{H}_y(x+\tfrac{\Delta x}{2},y,t+\tfrac{\Delta t}{2})-\mathcal{H}_y(x-\tfrac{\Delta x}{2},y,t+\tfrac{\Delta t}{2})\right]\\ &\quad-\frac{c_b}{\Delta y}\left[\mathcal{H}_x(x,y+\tfrac{\Delta y}{2},t+\tfrac{\Delta t}{2})-\mathcal{H}_x(x,y-\tfrac{\Delta y}{2},t+\tfrac{\Delta t}{2})\right],\end{aligned}\tag{20a}$$

$$\mathcal{H}_x(x,y+\tfrac{\Delta y}{2},t+\tfrac{\Delta t}{2}) = d_{ax}\mathcal{H}_x(x,y+\tfrac{\Delta y}{2},t-\tfrac{\Delta t}{2})-\frac{d_{bx}}{\Delta y}\left[\mathcal{E}_z(x,y+\Delta y,t)-\mathcal{E}_z(x,y,t)\right],\tag{20b}$$

$$\mathcal{H}_y(x+\tfrac{\Delta x}{2},y,t+\tfrac{\Delta t}{2}) = d_{ay}\mathcal{H}_y(x+\tfrac{\Delta x}{2},y,t-\tfrac{\Delta t}{2})+\frac{d_{by}}{\Delta x}\left[\mathcal{E}_z(x+\Delta x,y,t)-\mathcal{E}_z(x,y,t)\right],\tag{20c}$$

where Δy is the spatial step in the y direction, (c_a, c_b) use the material at (x,y), (d_{ax}, d_{bx}) use the material at $(x, y+\frac{\Delta y}{2})$, and (d_{ay}, d_{by}) use the material at $(x+\frac{\Delta x}{2}, y)$. Similarly, the two-dimensional FDTD update equations for the fields $\mathcal{H}_z(x,y,t)$, $\mathcal{E}_x(x,y,t)$, and $\mathcal{E}_y(x,y,t)$ in isotropic material are

$$\begin{aligned}\mathcal{H}_z(x+\tfrac{\Delta x}{2},y+\tfrac{\Delta y}{2},t+\tfrac{\Delta t}{2}) &= d_a\mathcal{H}_z(x+\tfrac{\Delta x}{2},y+\tfrac{\Delta y}{2},t-\tfrac{\Delta t}{2})\\ &\quad-\frac{d_b}{\Delta x}\left[\mathcal{E}_y(x+\Delta x,y+\tfrac{\Delta y}{2},t)-\mathcal{E}_y(x,y+\tfrac{\Delta y}{2},t)\right]\\ &\quad+\frac{d_b}{\Delta y}\left[\mathcal{E}_x(x+\tfrac{\Delta x}{2},y+\Delta y,t)-\mathcal{E}_x(x+\tfrac{\Delta x}{2},y,t)\right],\end{aligned}\tag{21a}$$

$$\begin{aligned}\mathcal{E}_x(x+\tfrac{\Delta x}{2},y,t+\Delta t) &= c_{ax}\mathcal{E}_x(x+\tfrac{\Delta x}{2},y,t)\\ &\quad+\frac{c_{bx}}{\Delta y}\left[\mathcal{H}_z(x+\tfrac{\Delta x}{2},y+\tfrac{\Delta y}{2},t+\tfrac{\Delta t}{2})-\mathcal{H}_z(x+\tfrac{\Delta x}{2},y-\tfrac{\Delta y}{2},t+\tfrac{\Delta t}{2})\right],\end{aligned}\tag{21b}$$

$$\begin{aligned}\mathcal{E}_y(x,y+\tfrac{\Delta y}{2},t+\Delta t) &= c_{ay}\mathcal{E}_y(x,y+\tfrac{\Delta y}{2},t)\\ &\quad-\frac{c_{by}}{\Delta x}\left[\mathcal{H}_z(x+\tfrac{\Delta x}{2},y+\tfrac{\Delta y}{2},t+\tfrac{\Delta t}{2})-\mathcal{H}_z(x-\tfrac{\Delta x}{2},y+\tfrac{\Delta y}{2},t+\tfrac{\Delta t}{2})\right].\end{aligned}\tag{21c}$$

These derivations are based on the differential form of Maxwell's equations, which are only valid where the fields are continuous and have continuous derivatives; however, neither are true at material interfaces [2, Section 1-2], [3, Section 1.2.1]. The reason Yee FDTD is not affected by these limitations is that an identical set of equations is derived from the integral form of Maxwell's equations [9, Section 3.6.8]. If I linearly approximate the fields and evaluate Equation (2b) over a Δx by Δy square centered at (x,y), then taking $\mathcal{E}_z$ to be the value of the linear approximation at (x,y), and taking $\mathcal{H}_x$ and $\mathcal{H}_y$ to be the value of the linear approximations at the center of their respective edges, I can derive Equation (20a) and conclude that it is second order accurate. Conversely, if I approximated the fields as constants over the square, I would incorrectly conclude that Equation (20a) was only first-order accurate.

1.4 Three-Dimensional Finite-Difference Time-Domain

The three-dimensional FDTD E-field update equations are

$$\begin{aligned}
\mathcal{E}_x(x+\tfrac{\Delta x}{2}, y, z, t+\Delta t) &= c_{ax}\mathcal{E}_x(x+\tfrac{\Delta x}{2}, y, z, t) \\
&\quad + \frac{c_{bx}}{\Delta y}\left[\mathcal{H}_z(x+\tfrac{\Delta x}{2}, y+\tfrac{\Delta y}{2}, z, t+\tfrac{\Delta t}{2}) - \mathcal{H}_z(x+\tfrac{\Delta x}{2}, y-\tfrac{\Delta y}{2}, z, t+\tfrac{\Delta t}{2})\right] \\
&\quad - \frac{c_{bx}}{\Delta z}\left[\mathcal{H}_y(x+\tfrac{\Delta x}{2}, y, z+\tfrac{\Delta z}{2}, t+\tfrac{\Delta t}{2}) - \mathcal{H}_y(x+\tfrac{\Delta x}{2}, y, z-\tfrac{\Delta z}{2}, t+\tfrac{\Delta t}{2})\right],
\end{aligned} \tag{22a}$$

$$\begin{aligned}
\mathcal{E}_y(x, y+\tfrac{\Delta y}{2}, z, t+\Delta t) &= c_{ay}\mathcal{E}_y(x, y+\tfrac{\Delta y}{2}, z, t) \\
&\quad + \frac{c_{by}}{\Delta z}\left[\mathcal{H}_x(x, y+\tfrac{\Delta y}{2}, z+\tfrac{\Delta z}{2}, t+\tfrac{\Delta t}{2}) - \mathcal{H}_x(x, y+\tfrac{\Delta y}{2}, z-\tfrac{\Delta z}{2}, t+\tfrac{\Delta t}{2})\right] \\
&\quad - \frac{c_{by}}{\Delta x}\left[\mathcal{H}_z(x+\tfrac{\Delta x}{2}, y+\tfrac{\Delta y}{2}, z, t+\tfrac{\Delta t}{2}) - \mathcal{H}_z(x-\tfrac{\Delta x}{2}, y+\tfrac{\Delta y}{2}, z, t+\tfrac{\Delta t}{2})\right],
\end{aligned} \tag{22b}$$

$$\begin{aligned}
\mathcal{E}_z(x, y, z+\tfrac{\Delta z}{2}, t+\Delta t) &= c_{az}\mathcal{E}_z(x, y, z+\tfrac{\Delta z}{2}, t) \\
&\quad + \frac{c_{bz}}{\Delta x}\left[\mathcal{H}_y(x+\tfrac{\Delta x}{2}, y, z+\tfrac{\Delta z}{2}, t+\tfrac{\Delta t}{2}) - \mathcal{H}_y(x-\tfrac{\Delta x}{2}, y, z+\tfrac{\Delta z}{2}, t+\tfrac{\Delta t}{2})\right] \\
&\quad - \frac{c_{bz}}{\Delta y}\left[\mathcal{H}_x(x, y+\tfrac{\Delta y}{2}, z+\tfrac{\Delta z}{2}, t+\tfrac{\Delta t}{2}) - \mathcal{H}_x(x, y-\tfrac{\Delta y}{2}, z+\tfrac{\Delta z}{2}, t+\tfrac{\Delta t}{2})\right],
\end{aligned} \tag{22c}$$

and the H-field update equations are

$$\begin{aligned}
\mathcal{H}_x(x, y+\tfrac{\Delta y}{2}, z+\tfrac{\Delta z}{2}, t+\tfrac{\Delta t}{2}) &= d_{ax}\mathcal{H}_z(x, y+\tfrac{\Delta y}{2}, z+\tfrac{\Delta z}{2}, t-\tfrac{\Delta t}{2}) \\
&\quad + \frac{d_{bx}}{\Delta y}\left[\mathcal{E}_z(x, y+\Delta y, z+\tfrac{\Delta z}{2}, t) - \mathcal{E}_z(x, y, z+\tfrac{\Delta z}{2}, t)\right] \\
&\quad - \frac{d_{bx}}{\Delta z}\left[\mathcal{E}_y(x, y+\tfrac{\Delta y}{2}, z+\Delta z, t) - \mathcal{E}_y(x, y+\tfrac{\Delta y}{2}, z, t)\right],
\end{aligned} \tag{23a}$$

$$\begin{aligned}
\mathcal{H}_y(x+\tfrac{\Delta x}{2}, y, z+\tfrac{\Delta z}{2}, t+\tfrac{\Delta t}{2}) &= d_{ay}\mathcal{H}_z(x+\tfrac{\Delta x}{2}, y, z+\tfrac{\Delta z}{2}, t-\tfrac{\Delta t}{2}) \\
&\quad + \frac{d_{by}}{\Delta z}\left[\mathcal{E}_x(x+\tfrac{\Delta x}{2}, y, z+\Delta z, t) - \mathcal{E}_x(x+\tfrac{\Delta x}{2}, y, z, t)\right] \\
&\quad - \frac{d_{by}}{\Delta x}\left[\mathcal{E}_z(x+\Delta x, y, z+\tfrac{\Delta z}{2}, t) - \mathcal{E}_z(x, y, z+\tfrac{\Delta z}{2}, t)\right],
\end{aligned} \tag{23b}$$

$$\begin{aligned}
\mathcal{H}_z(x+\tfrac{\Delta x}{2}, y+\tfrac{\Delta y}{2}, z, t+\tfrac{\Delta t}{2}) &= d_{az}\mathcal{H}_z(x+\tfrac{\Delta x}{2}, y+\tfrac{\Delta y}{2}, z, t-\tfrac{\Delta t}{2}) \\
&\quad + \frac{d_{bz}}{\Delta x}\left[\mathcal{E}_y(x+\Delta x, y+\tfrac{\Delta y}{2}, z, t) - \mathcal{E}_y(x, y+\tfrac{\Delta y}{2}, z, t)\right] \\
&\quad - \frac{d_{bz}}{\Delta y}\left[\mathcal{E}_x(x+\tfrac{\Delta x}{2}, y+\Delta y, z, t) - \mathcal{E}_x(x+\tfrac{\Delta x}{2}, y, z, t)\right].
\end{aligned} \tag{23c}$$

2. TOTAL-FIELD/SCATTERED-FIELD METHOD

The total-field/scattered-field method is a technique to simulate scattering calculations in FDTD by dividing the FDTD space into total-field and scattered-field regions [9, Section 5.6], [10–17]. The scattered-field region surrounds the total-field region and the incident-field enters into the equations at the boundary

between the two regions. I start the derivation with $\mathcal{E}_z^t = \mathcal{E}_z^s + \mathcal{E}_z^i$ and $\mathcal{H}_y^t = \mathcal{H}_y^s + \mathcal{H}_y^i$, where t = total-field, s = scattered-field, and i = incident-field. In one-dimensional Yee FDTD, if x_L is the leftmost total-field point and aligned with the $\mathcal{E}_z$ field points I write Equation (16) at x_L as

$$\mathcal{E}_z^t(x_L, t+\Delta t) = c_a \mathcal{E}_z^t(x_L, t) + \frac{c_b}{\Delta x}\left[\mathcal{H}_y^t(x_L + \tfrac{\Delta x}{2}, t+\tfrac{\Delta t}{2}) - \mathcal{H}_y^s(x_L - \tfrac{\Delta x}{2}, t+\tfrac{\Delta t}{2}) - \mathcal{H}_y^i(x_L - \tfrac{\Delta x}{2}, t+\tfrac{\Delta t}{2})\right], \tag{24}$$

and Equation (18) at $x_L - \frac{\Delta x}{2}$ as

$$\mathcal{H}_y^s(x_L - \tfrac{\Delta x}{2}, t+\tfrac{\Delta t}{2}) = d_a \mathcal{H}_y^s(x_L - \tfrac{\Delta x}{2}, t-\tfrac{\Delta t}{2}) + \frac{d_b}{\Delta x}\left[\mathcal{E}_z^t(x_L, t) - \mathcal{E}_z^i(x_L, t) - \mathcal{E}_z^s(x_L - \Delta x, t)\right]. \tag{25}$$

Similarly, if x_R is the rightmost total-field point and aligned with the $\mathcal{E}_z$ field points I write Equation (16) at x_R as

$$\mathcal{E}_z^t(x_R, t+\Delta t) = c_a \mathcal{E}_z^t(x_R, t) + \frac{c_b}{\Delta x}\left[\mathcal{H}_y^s(x_R + \tfrac{\Delta x}{2}, t+\tfrac{\Delta t}{2}) + \mathcal{H}_y^i(x_R + \tfrac{\Delta x}{2}, t+\tfrac{\Delta t}{2}) - \mathcal{H}_y^t(x_R - \tfrac{\Delta x}{2}, t+\tfrac{\Delta t}{2})\right], \tag{26}$$

and Equation (18) at $x_R + \frac{\Delta x}{2}$ as

$$\mathcal{H}_y^s(x_R + \tfrac{\Delta x}{2}, t+\tfrac{\Delta t}{2}) = d_a \mathcal{H}_y^s(x_R + \tfrac{\Delta x}{2}, t-\tfrac{\Delta t}{2}) + \frac{d_b}{\Delta x}\left[\mathcal{E}_z^s(x_R + \Delta x, t) - \mathcal{E}_z^t(x_R, t) + \mathcal{E}_z^i(x_R, t)\right]. \tag{27}$$

The total-field/scattered-field boundary is aligned with either the $\mathcal{E}_z$ or $\mathcal{H}_y$ field points on either side. Rather than having special update equations at the boundary, it is more efficient to have update equations equivalent to the global update equations

$$\mathcal{E}_z^{t'}(x_L, t+\Delta t) = c_a \mathcal{E}_z^t(x_L, t) + \frac{c_b}{\Delta x}\left[\mathcal{H}_y^t(x_L + \tfrac{\Delta x}{2}, t+\tfrac{\Delta t}{2}) - \mathcal{H}_y^s(x_L - \tfrac{\Delta x}{2}, t+\tfrac{\Delta t}{2})\right], \tag{28a}$$

$$\mathcal{E}_z^{t'}(x_R, t+\Delta t) = c_a \mathcal{E}_z^t(x_R, t) + \frac{c_b}{\Delta x}\left[\mathcal{H}_y^s(x_R + \tfrac{\Delta x}{2}, t+\tfrac{\Delta t}{2}) - \mathcal{H}_y^t(x_R - \tfrac{\Delta x}{2}, t+\tfrac{\Delta t}{2})\right], \tag{28b}$$

$$\mathcal{H}_y^{s'}(x_L - \tfrac{\Delta x}{2}, t+\tfrac{\Delta t}{2}) = d_a \mathcal{H}_y^s(x_L - \tfrac{\Delta x}{2}, t-\tfrac{\Delta t}{2}) + \frac{d_b}{\Delta x}\left[\mathcal{E}_z^t(x_L, t) - \mathcal{E}_z^s(x_L - \Delta x, t)\right], \tag{28c}$$

$$\mathcal{H}_y^{s'}(x_R + \tfrac{\Delta x}{2}, t+\tfrac{\Delta t}{2}) = d_a \mathcal{H}_y^s(x_R + \tfrac{\Delta x}{2}, t-\tfrac{\Delta t}{2}) + \frac{d_b}{\Delta x}\left[\mathcal{E}_z^s(x_R + \Delta x, t) - \mathcal{E}_z^t(x_R, t)\right], \tag{28d}$$

with corrections handled separately,

$$\mathcal{E}_z^t(x_L, t+\Delta t) = \mathcal{E}_z^{t'}(x_L, t+\Delta t) - \frac{c_b}{\Delta x}\mathcal{H}_y^i(x_L - \tfrac{\Delta x}{2}, t+\tfrac{\Delta t}{2}), \tag{29a}$$

$$\mathcal{E}_z^t(x_R, t+\Delta t) = \mathcal{E}_z^{t'}(x_R, t+\Delta t) + \frac{c_b}{\Delta x}\mathcal{H}_y^i(x_R + \tfrac{\Delta x}{2}, t+\tfrac{\Delta t}{2}), \tag{29b}$$

$$\mathcal{H}_y^s(x_L - \tfrac{\Delta x}{2}, t+\tfrac{\Delta t}{2}) = \mathcal{H}_y^{s'}(x_L - \tfrac{\Delta x}{2}, t+\tfrac{\Delta t}{2}) - \frac{d_b}{\Delta x}\mathcal{E}_z^i(x_L, t), \tag{29c}$$

$$\mathcal{H}_y^s(x_R + \tfrac{\Delta x}{2}, t+\tfrac{\Delta t}{2}) = \mathcal{H}_y^{s'}(x_R + \tfrac{\Delta x}{2}, t+\tfrac{\Delta t}{2}) + \frac{d_b}{\Delta x}\mathcal{E}_z^i(x_R, t), \tag{29d}$$

where $\mathcal{E}_z^{t'}$ and $\mathcal{H}_y^{s'}$ represent the uncorrected fields. To include both propagation directions, I define the propagation direction as ϕ relative to the $+x$ axis, so that $\phi = 180°$ is equivalent to propagation in the $-x$ direction, then the incident-field corrections are

$$\mathcal{E}_z^t(x_L, t+\Delta t) = \mathcal{E}_z^{t'}(x_L, t+\Delta t) + \cos(\phi)\frac{c_b}{\Delta x}\frac{\mathcal{E}_z^i(x_L - \frac{\Delta x}{2}, t+\frac{\Delta t}{2})}{\eta}, \tag{30a}$$

$$\mathcal{E}_z^t(x_R, t+\Delta t) = \mathcal{E}_z^{t'}(x_R, t+\Delta t) - \cos(\phi)\frac{c_b}{\Delta x}\frac{\mathcal{E}_z^i(x_R + \frac{\Delta x}{2}, t+\frac{\Delta t}{2})}{\eta}, \tag{30b}$$

$$\mathcal{H}_y^s(x_L - \tfrac{\Delta x}{2}, t+\tfrac{\Delta t}{2}) = \mathcal{H}_y^{s'}(x_L - \tfrac{\Delta x}{2}, t+\tfrac{\Delta t}{2}) - \frac{d_b}{\Delta x}\mathcal{E}_z^i(x_L, t), \tag{30c}$$

$$\mathcal{H}_y^s(x_R + \tfrac{\Delta x}{2}, t+\tfrac{\Delta t}{2}) = \mathcal{H}_y^{s'}(x_R + \tfrac{\Delta x}{2}, t+\tfrac{\Delta t}{2}) + \frac{d_b}{\Delta x}\mathcal{E}_z^i(x_R, t), \tag{30d}$$

where $\eta = \sqrt{\mu/\epsilon}$ is wave-impedance and $\mathcal{H}_y^i(x,t) = -\mathcal{E}_z^i(x,t)/\eta$ for a plane-wave propagating in the $+x$ direction. The incident-field is a modulated Gaussian pulse given by

$$\mathcal{E}_z^i(x,t) = \sin(\omega_c t')e^{-(t'/\tau)^2}, \tag{31}$$

where $\omega_c = 2\pi f_c$ (f_c = center frequency), $\tau = 2/(\pi f_{BW})$ (f_{BW} = pulse bandwidth), and

$$t' = t - 3\tau - \cos(\phi)(x - x_{L,R})/c, \tag{32}$$

where c is the speed of light. The pulse is offset in time 3τ to lower the relative starting amplitude to ~ 0.0001, thereby reducing the high frequency noise. Similarly, the leading edge of the pulse is offset in x to align the start of the pulse with the appropriate boundary, i.e. x_L or x_R, depending on the propagation direction.

2.1 Numerical Dispersion in the Total-Field/Scattered-Field Method

A key parameter in Yee FDTD is the time step. For one-dimensional Yee FDTD, the maximum time step for numerical stability is $\Delta x\sqrt{\mu\epsilon}$, or in free space $\Delta x/c$ [9, Section 2.7.1]. One-dimensional Yee FDTD with this time-step has no numerical dispersion, meaning that all frequencies in the pulse travel at the same velocity [9, Section 2.5]. Under these conditions the total-field/scattered-field method with direct application of an analytic incident-field works very well, as shown in the waterfall[3] plot in Figure 2. However, this is only true for one-dimensional Yee FDTD and only with this time-step. For a more realistic test, consider two-dimensional Yee FDTD where the maximum Δt for numerical stability in free space is [9, Section 4.7]

$$\Delta t = \frac{\Delta x \Delta y}{c\sqrt{\Delta x^2 + \Delta y^2}}. \tag{33}$$

The equivalent condition in one-dimensional Yee FDTD is $\Delta t = \Delta x/(c\sqrt{2})$. The numerical dispersion is clearly visible at the total-field/scattered-field boundary after only 180 cells, as shown in Figure 3. The

[3] A waterfall plot is a standard means to display data that changes with time, each subplot here has a magnitude of ±1.

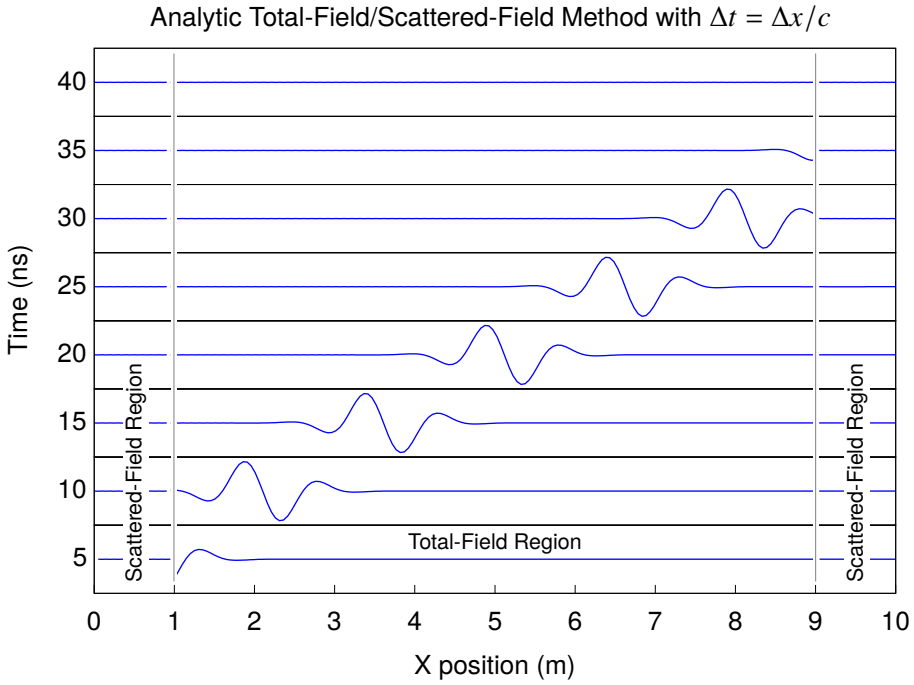

Figure 2—Propagation of an analytic modulated Gaussian pulse ($f_c = 300$ MHz, $f_{BW} = 300$ MHz) in a free space region using the total-field/scattered-field method with $\Delta x = 0.05$ meters and $\Delta t = \Delta x/c$.

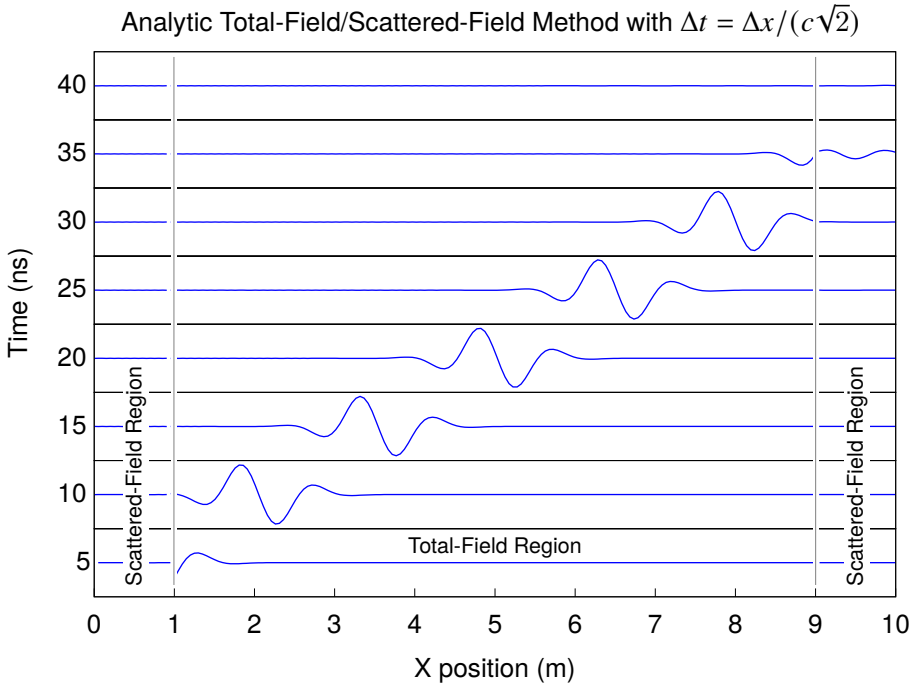

Figure 3—Propagation of an analytic modulated Gaussian pulse ($f_c = 300$ MHz, $f_{BW} = 300$ MHz) in a free space region using the total-field/scattered-field method with $\Delta x = 0.05$ meters and $\Delta t = \Delta x/(c\sqrt{2})$.

dispersion equation for one-dimensional Yee FDTD is given by [9, Section 2.6]

$$\tilde{k} = \frac{1}{\Delta x} \cos^{-1} \left\{ 1 + \left(\frac{\Delta x}{c \Delta t} \right)^2 \left[\cos(\omega \Delta t) - 1 \right] \right\}. \tag{34}$$

Using the half-angle trigonometric formula Equation (34) is simplified to

$$\tilde{k} = \frac{2}{\Delta x} \sin^{-} 1 \left[\frac{\Delta x}{c \Delta t} \left| \sin \frac{\omega \Delta t}{2} \right| \right]. \tag{35}$$

If $\Delta t = \Delta x / c$ as in Figure 2, then $\tilde{k} = \omega / c$, which is the continuous space value for k. One possible correction for the analytic Gaussian pulse in Figure 3 is to adjust propagation velocity, c, in Equation (32) by 0.9979, which is $k / \tilde{k}$ at the center frequency. This approach is only slightly effective, as shown in Figure 4, because over the bandwidth of the pulse the correction factor should range from 0.9995 to 0.9953. The effects of the bandwidth on this correction approach is seen by comparing Figure 4 with Figure 5, where the latter has one-third the bandwidth of the first.

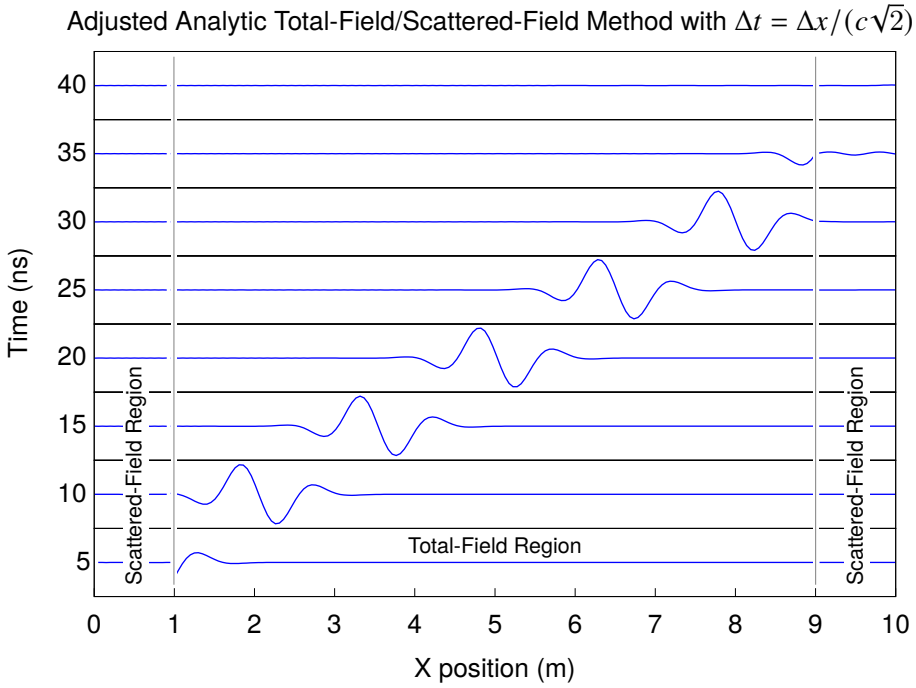

Figure 4—Propagation of a reduced velocity analytic modulated Gaussian pulse (f_c = 300 MHz, f_{BW} = 300 MHz) in a free space region using the total-field/scattered-field method with Δx = 0.05 meters and $\Delta t = \Delta x/(c\sqrt{2})$.

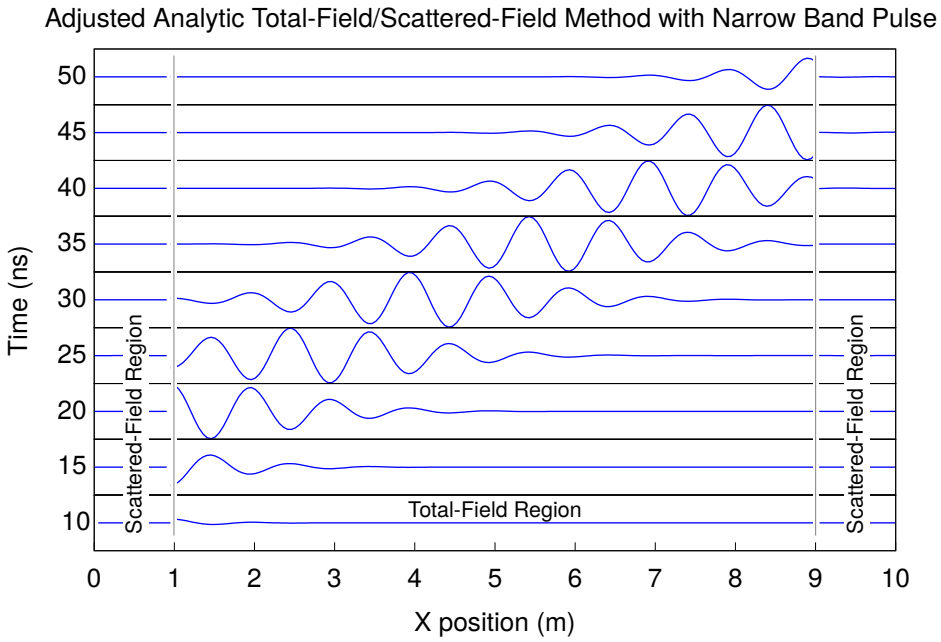

Figure 5—Propagation of a narrow band pulse with the reduced velocity analytic modulated Gaussian pulse (f_c = 300 MHz, f_{BW} = 100 MHz) in a free space region using the total-field/scattered-field method with $\Delta x = 0.05$ meters and $\Delta t = \Delta x/(c\sqrt{2})$.

2.2 Secondary FDTD Grid for the Total-Field/Scattered-Field Method

The simplest method to generate a Gaussian pulse with matching propagation velocity over all frequencies is to filter the analytic Gaussian pulse numerically via a secondary Yee FDTD grid. In this case, the secondary Yee FDTD grid is excited by an analytic Gaussian pulse and the total-field region of this grid is used to excite the primary Yee FDTD grid. As shown in Figure 6, this results in a clean transition from the total-field region

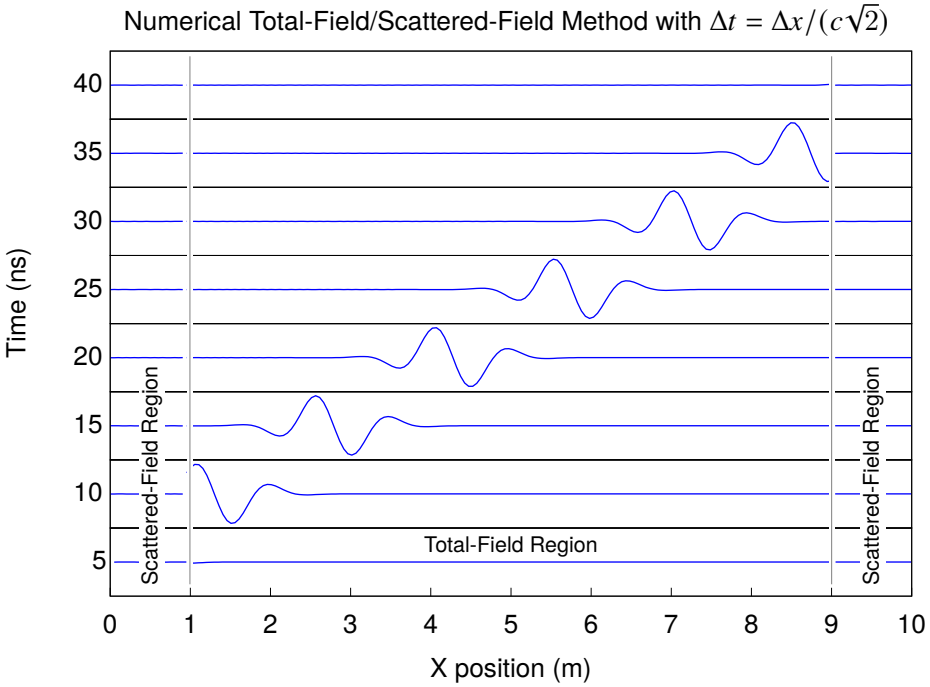

Figure 6—Propagation of a numerically-filtered, modulated Gaussian pulse (f_c = 300 MHz, f_{BW} = 100 MHz) in a free space region using the total-field/scattered-field method with Δx = 0.05 meters and $\Delta t = \Delta x/(c\sqrt{2})$.

to the scattered-field region. While not perfect, this technique works well for inducing plane-waves into two and three-dimensional FDTD grids with minimal additional cost. When using a secondary, one-dimensional FDTD grid for the incident-field in two and three-dimensional FDTD I use the ratio of the dispersion factors from both grids to reduce the dispersion mismatch.

Next, I consider the numerically generated modulated Gaussian pulse incident on a seven-cell region centered at x = 5 meters with a relative dielectric constant of two. In Figure 7 I see that the field reflected from the dielectric propagates to the left across the total-field/scattered-field boundary without distortion. The transmitted field in the total-field region visually looks to be the same as the incident pulse because the dielectric region is roughly one-half the wavelength at the center frequency. I compare the scattered-field regions of Figure 7 with the results in the next section.

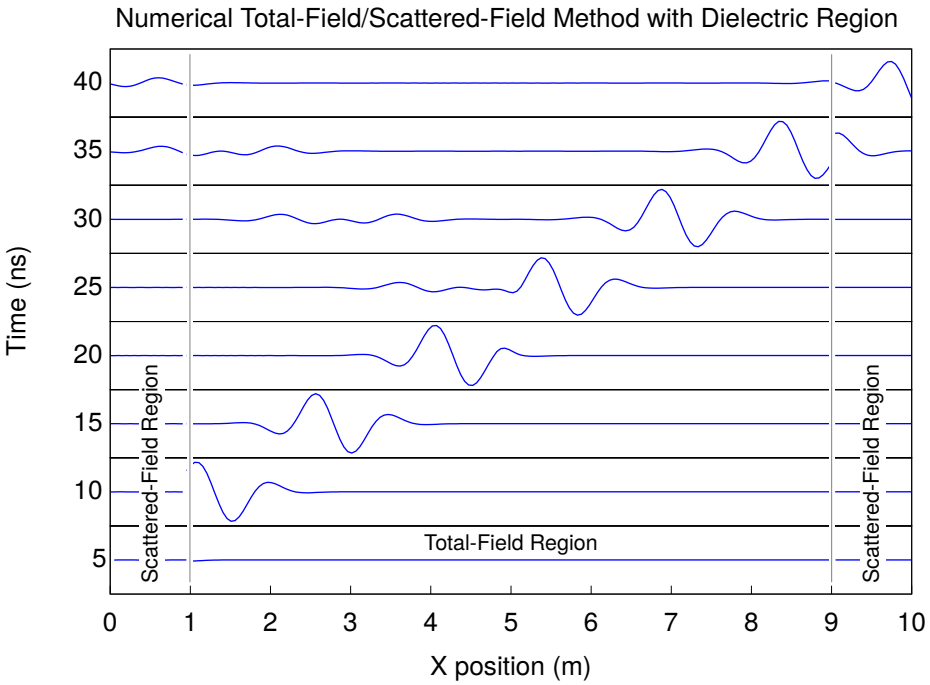

Figure 7—Total-field/scattered-field method for a numerically-filtered, modulated Gaussian pulse (f_c = 300 MHz, f_{BW} = 100 MHz) incident on seven cells centered at 5 meters with a relative dielectric constant of 2, $\Delta x = 0.05$ m, and $\Delta t = \Delta x/(c\sqrt{2})$.

3. SCATTERED-FIELD METHOD

The scattered-field method is an alternative technique to simulate scattering calculations in FDTD with only the scattered-field calculations in the FDTD grid [9, Section 5.9]. The incident-fields are handled analytically, or via a secondary FDTD grid, and are governed by the following equations

$$\mu_0 \frac{\partial \boldsymbol{\mathcal{H}}^i(t)}{\partial t} = -\nabla \times \boldsymbol{\mathcal{E}}^i(t), \tag{36a}$$

$$\epsilon_0 \frac{\partial \boldsymbol{\mathcal{E}}^i(t)}{\partial t} = \nabla \times \boldsymbol{\mathcal{H}}^i(t). \tag{36b}$$

Expanding the total fields in Equation (15) as the sum of the scattered fields and the incident fields, and subtracting Equation (36) for the incident-field I get [8, Section 2.2]

$$\mu \frac{\partial \boldsymbol{\mathcal{H}}^s(t)}{\partial t} + (\mu - \mu_0) \frac{\partial \boldsymbol{\mathcal{H}}^i(t)}{\partial t} + \sigma^* \boldsymbol{\mathcal{H}}^s(t) + \sigma^* \boldsymbol{\mathcal{H}}^i(t) = -\nabla \times \boldsymbol{\mathcal{E}}^s(t), \tag{37a}$$

$$\epsilon \frac{\partial \boldsymbol{\mathcal{E}}^s(t)}{\partial t} + (\epsilon - \epsilon_0) \frac{\partial \boldsymbol{\mathcal{E}}^i(t)}{\partial t} + \sigma \boldsymbol{\mathcal{E}}^s(t) + \sigma \boldsymbol{\mathcal{E}}^i(t) = \nabla \times \boldsymbol{\mathcal{H}}^s(t). \tag{37b}$$

As a first step in creating the scattered-field Yee FDTD equations and for comparison with Equation (15), I rearrange the equations as follows [9, Section 5.9.2]

$$\mu \frac{\partial \boldsymbol{\mathcal{H}}^s(t)}{\partial t} + \sigma^* \boldsymbol{\mathcal{H}}^s(t) = -\nabla \times \boldsymbol{\mathcal{E}}^s(t) - \sigma^* \boldsymbol{\mathcal{H}}^i(t) - (\mu - \mu_0) \frac{\partial \boldsymbol{\mathcal{H}}^i(t)}{\partial t}, \tag{38a}$$

$$\epsilon \frac{\partial \boldsymbol{\mathcal{E}}^s(t)}{\partial t} + \sigma \boldsymbol{\mathcal{E}}^s(t) = \nabla \times \boldsymbol{\mathcal{H}}^s(t) - \sigma \boldsymbol{\mathcal{E}}^i(t) - (\epsilon - \epsilon_0) \frac{\partial \boldsymbol{\mathcal{E}}^i(t)}{\partial t}. \tag{38b}$$

Applying second order central differences to Equation (38) for a one-dimensional problem with the fields $\mathcal{E}_z(x,t)$ and $\mathcal{H}_y(x,t)$ in isotropic material and solving for the future $\mathcal{E}_z$ and $\mathcal{H}_y$ fields results in the scattered-field Yee FDTD update equations

$$\begin{aligned} \mathcal{H}_y^s(x+\tfrac{\Delta x}{2}, t+\tfrac{\Delta t}{2}) = d_a \mathcal{H}_y^s(x+\tfrac{\Delta x}{2}, t-\tfrac{\Delta t}{2}) + \frac{d_b}{\Delta x}\left[\mathcal{E}_z^s(x+\Delta x, t) - \mathcal{E}_z^s(x,t)\right] \\ -d_b\left[\sigma^* \mathcal{H}_y^i(x+\tfrac{\Delta x}{2}, t) + (\mu - \mu_0)\frac{\partial \mathcal{H}_y^i(x+\frac{\Delta x}{2}, t)}{\partial t}\right], \end{aligned} \tag{39a}$$

$$\begin{aligned} \mathcal{E}_z^s(x, t+\Delta t) = c_a \mathcal{E}_z^s(x,t) + \frac{c_b}{\Delta x}\left[\mathcal{H}_y^s(x+\tfrac{\Delta x}{2}, t+\tfrac{\Delta t}{2}) - \mathcal{H}_y^s(x-\tfrac{\Delta x}{2}, t+\tfrac{\Delta t}{2})\right] \\ -c_b\left[\sigma \mathcal{E}_z^i(x, t+\tfrac{\Delta t}{2}) + (\epsilon - \epsilon_0)\frac{\partial \mathcal{E}_z^i(x, t+\frac{\Delta t}{2})}{\partial t}\right]. \end{aligned} \tag{39b}$$

As in the previous section, I write these equations in a form equivalent to the standard global update equations

$$\mathcal{H}_y'^s(x+\tfrac{\Delta x}{2}, t+\tfrac{\Delta t}{2}) = d_a \mathcal{H}_y^s(x+\tfrac{\Delta x}{2}, t-\tfrac{\Delta t}{2}) + \frac{d_b}{\Delta x}\left[\mathcal{E}_z^s(x+\Delta x, t) - \mathcal{E}_z^s(x,t)\right], \tag{40a}$$

$$\mathcal{E}_z'^s(x, t+\Delta t) = c_a \mathcal{E}_z^s(x,t) + \frac{c_b}{\Delta x}\left[\mathcal{H}_y^s(x+\tfrac{\Delta x}{2}, t+\tfrac{\Delta t}{2}) - \mathcal{H}_y^s(x-\tfrac{\Delta x}{2}, t+\tfrac{\Delta t}{2})\right], \tag{40b}$$

with corrections

$$\mathcal{H}_y^s(x+\tfrac{\Delta x}{2}, t+\tfrac{\Delta t}{2}) = \mathcal{H}_y'^s(x+\tfrac{\Delta x}{2}, t-\tfrac{\Delta t}{2}) - d_b \left[\sigma^* \mathcal{H}_y^i(x+\tfrac{\Delta x}{2}, t) + (\mu - \mu_0) \frac{\partial \mathcal{H}_y^i(x+\frac{\Delta x}{2}, t)}{\partial t} \right], \tag{41a}$$

$$\mathcal{E}_z^s(x, t+\Delta t) = \mathcal{E}_z'^s(x, t) - c_b \left[\sigma \mathcal{E}_z^i(x, t+\tfrac{\Delta t}{2}) + (\epsilon - \epsilon_0) \frac{\partial \mathcal{E}_z^i(x, t+\frac{\Delta t}{2})}{\partial t} \right]. \tag{41b}$$

As in the previous section, the incident-field is a modulated Gaussian pulse given by

$$\mathcal{E}_z^i(x, t) = \sin(\omega_c t') e^{-(t'/\tau)^2}, \tag{42}$$

with a time derivative of

$$\frac{\partial \mathcal{E}_z^i(x, t)}{\partial t} = \left[\omega_c \cos(\omega_c t') - \frac{2t'}{\tau^2} \sin(\omega_c t') \right] e^{-(t'/\tau)^2}, \tag{43}$$

and $\mathcal{H}_y^i(x, t) = -\mathcal{E}_z^i(x, t)/\eta$ for a plane-wave propagating in the $+x$ direction. The scattered-field generated by this analytic, modulated Gaussian pulse incident on seven material cells with a dielectric constant of 2 is shown in Figure 8. The reflected field for $x < 5$ meters matches that in Figure 7 for time greater than 25 ns when the incident pulse has passed $x = 5$ meters. Similarly, the scattered-field in Figure 8 matches that in the scattered-field region of Figure 7 for $x > 9$ meters. Figure 9 shows the sum of the incident-field plus the scattered-field and is a reasonable match to the total-field region in Figure 7.

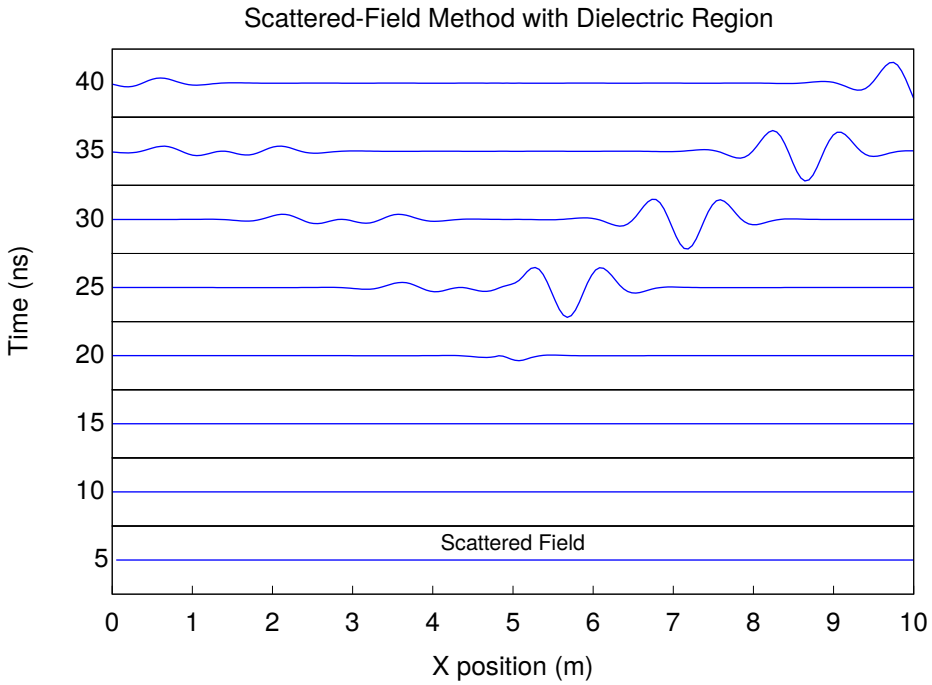

Figure 8—Scattered-field method for an analytic modulated Gaussian pulse (f_c = 300 MHz, f_{BW} = 100 MHz) incident on seven cells centered at 5 meters with a relative dielectric constant of 2, Δx = 0.05 m, and $\Delta t = \Delta x/(c\sqrt{2})$.

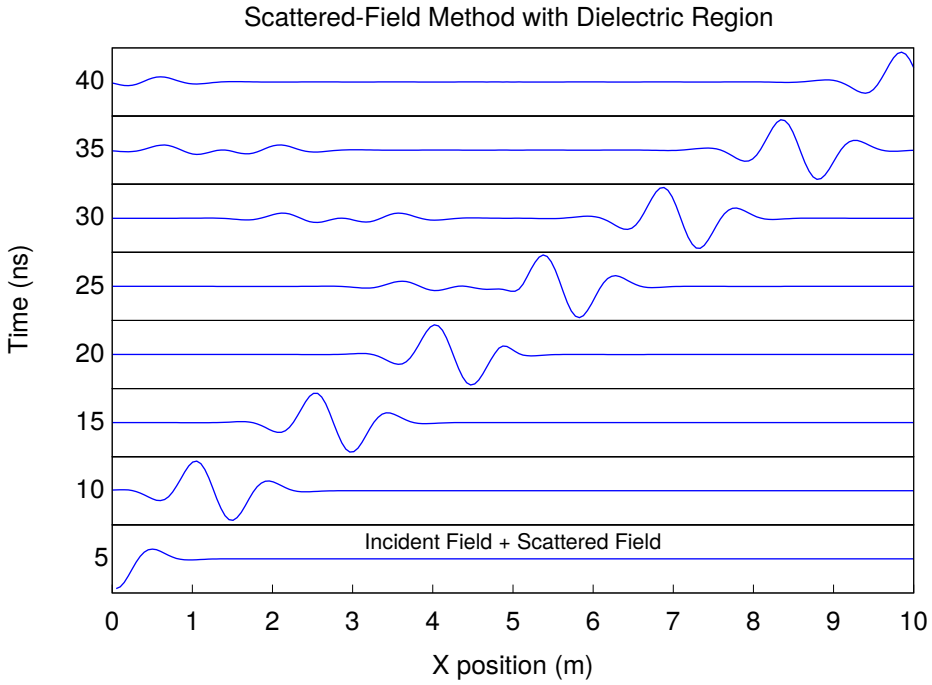

Figure 9—Sum of the incident-field and scattered-field calculated via the scattered-field method for an analytic modulated Gaussian pulse (f_c = 300 MHz, f_{BW} = 100 MHz) incident on seven cells centered at 5 meters with a relative dielectric constant of 2, Δx = 0.05 m, and $\Delta t = \Delta x/(c\sqrt{2})$.

3.1 Numerical Derivatives for the Scattered-Field Method

While the computational cost of Equation (43) is minor for these one-dimensional examples, it becomes significant when it must be computed at every time-step for every cell with a material for a large three-dimensional FDTD problem [9, Section 5.9.2]. I use central difference equations to approximate the time derivative to reduce the computational cost of computing the derivative of the incident-field. The second, fourth, and sixth order central difference equations are [18, Section 43],

$$f'(x_0) \approx \frac{1}{2h}\left[f(x_1) - f(x_{-1})\right] \tag{44a}$$

$$f'(x_0) \approx \frac{1}{12h}\left[-f(x_2) + 8f(x_1) - 8f(x_{-1}) + f(x_{-2})\right] \tag{44b}$$

$$f'(x_0) \approx \frac{1}{60h}\left[2f(x_3) - 13f(x_2) + 50f(x_1) - 50f(x_{-1}) + 13f(x_{-2}) - 2f(x_{-3})\right]. \tag{44c}$$

The obvious approach would be to calculate and store Equation (42) for multiple time steps everywhere it is required in order to use one of the central difference equations. However, it is simpler to calculate the incident-field across the entire grid for the current time only and calculate the time derivative from the appropriately scaled spatial derivative. From Equation (32) I see that using $h = -\Delta x/c$ in Equation (44) corresponds to the time-derivative of the incident-field giving us the following approximations to the time derivative of the incident-field

$$\frac{\partial \mathcal{E}_z(x,t)}{\partial t} \approx -\frac{c}{2\Delta x}\left[\mathcal{E}_z(x{+}\Delta x,t) - \mathcal{E}_z(x{-}\Delta x,t)\right] \tag{45a}$$

$$\frac{\partial \mathcal{E}_z(x,t)}{\partial t} \approx -\frac{c}{12\Delta x}\left[-\mathcal{E}_z(x{+}2\Delta x,t) + 8\mathcal{E}_z(x{+}\Delta x,t) - 8\mathcal{E}_z(x{-}\Delta x,t) + \mathcal{E}_z(x{-}2\Delta x,t)\right] \tag{45b}$$

$$\begin{aligned}\frac{\partial \mathcal{E}_z(x,t)}{\partial t} \approx -\frac{c}{60\Delta x}\big[&2\mathcal{E}_z(x{+}3\Delta x,t) - 13\mathcal{E}_z(x{+}2\Delta x,t) + 50\mathcal{E}_z(x{+}\Delta x,t)\\ &-50\mathcal{E}_z(x{-}\Delta x,t) + 13\mathcal{E}_z(x{-}2\Delta x,t) - 2\mathcal{E}_z(x{-}3\Delta x,t)\big].\end{aligned} \tag{45c}$$

I show in Figure 10 that the second order central difference equation calculated this way gives nearly the same result as the analytic time derivative for the example problem, where $\omega = 2\pi 3x10^8$, $\tau = 2.12x10^{-9}$, $\Delta x = 0.05$, and $h = -1.67x10^{-10}$. The results from the higher order central difference equations are visually identical to the analytic time derivative. The sum of the incident-field plus the scattered-field using each of the central difference equations with the analytic modulated Gaussian pulse is shown in Figures 11 – 13. As the computational cost of Equation (42) also becomes significant for large three-dimensional FDTD problems, the alternative is to generate the incident-field in a secondary one-dimensional FDTD grid [9, Section 5.9.2] and calculate the derivative of the incident-field numerically using Equation (44). The result of using a secondary FDTD grid with the sixth order central spatial difference for the time derivative is shown in Figure 14.

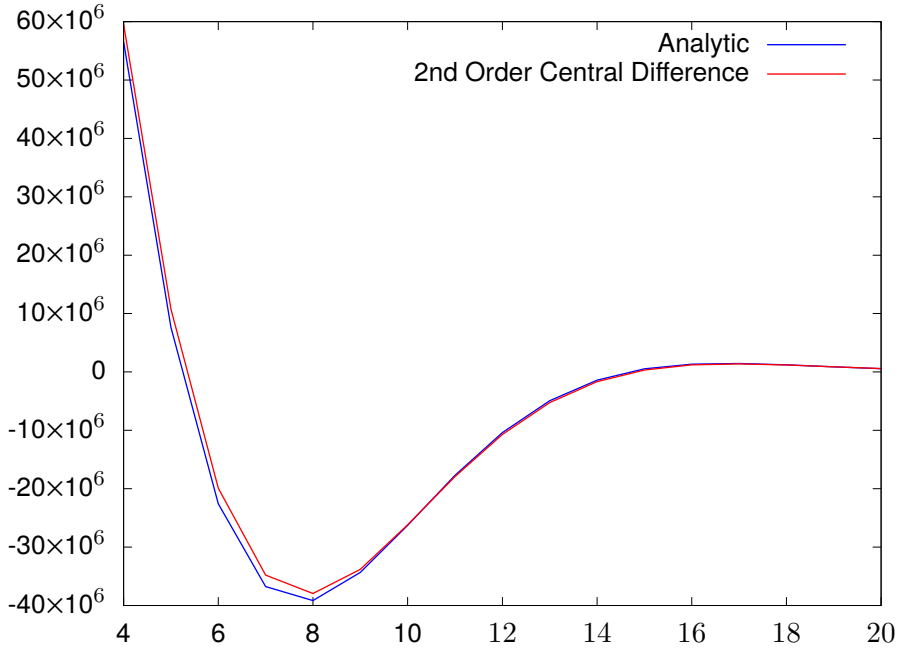

Figure 10—Analytic time derivative of the modulated Gaussian pulse versus the second order central difference equation calculated from the spatial grid at one time instance.

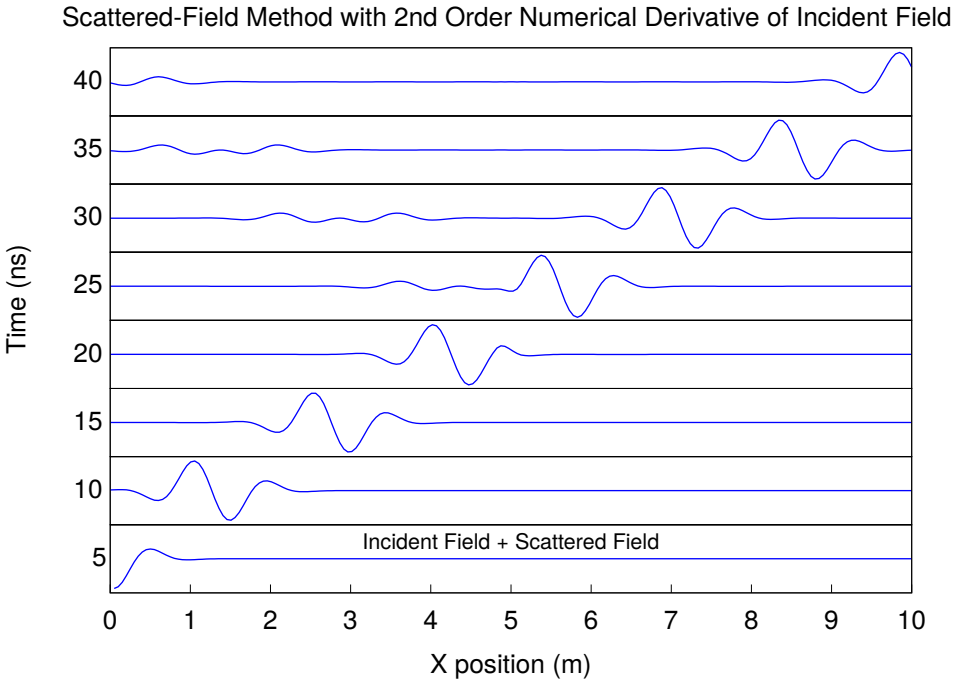

Figure 11—Sum of the analytic incident-field and scattered-field calculated via the scattered-field method using the second order central difference equation with an analytic modulated Gaussian pulse (f_c = 300 MHz, f_{BW} = 100 MHz) incident on seven cells centered at 5 meters with a relative dielectric constant of 2, Δx = 0.05 m, and $\Delta t = \Delta x/(c\sqrt{2})$.

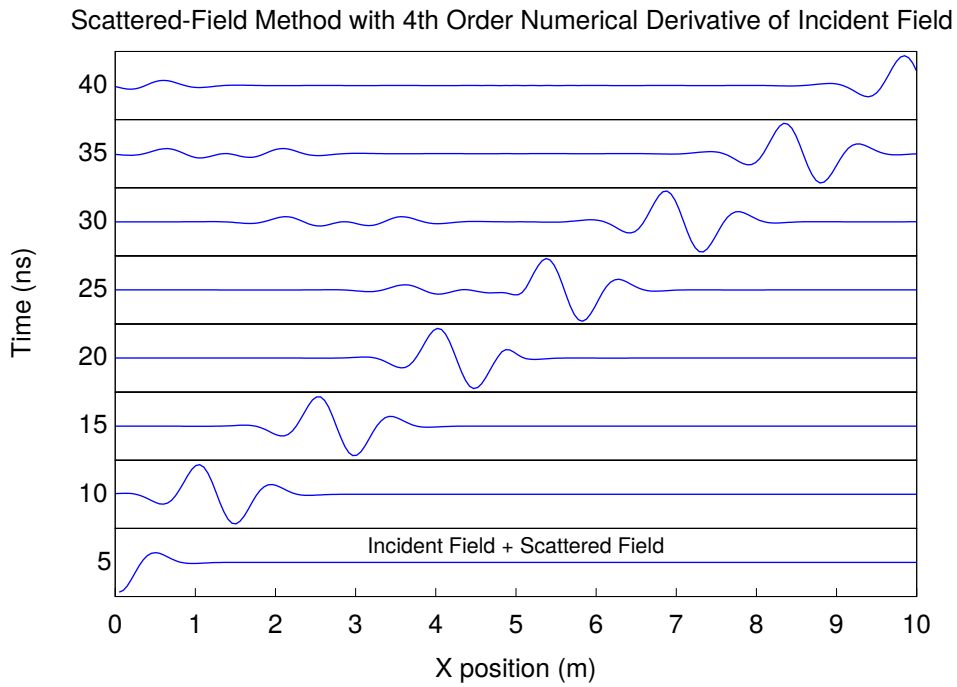

Figure 12—Sum of the analytic incident-field and scattered-field calculated via the scattered-field method using the fourth order central difference equation with an analytic modulated Gaussian pulse (f_c = 300 MHz, f_{BW} = 100 MHz) incident on seven cells centered at 5 meters with a relative dielectric constant of 2, $\Delta x = 0.05$ m, and $\Delta t = \Delta x/(c\sqrt{2})$.

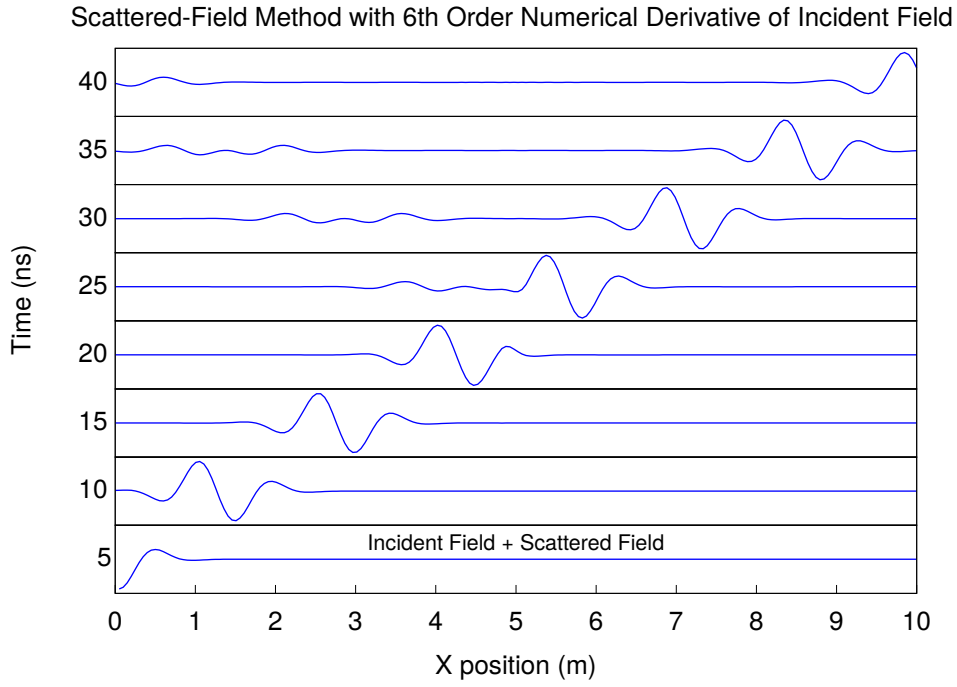

Figure 13—Sum of the analytic incident-field and scattered-field calculated via the scattered-field method using the sixth order central difference equation with an analytic modulated Gaussian pulse (f_c = 300 MHz, f_{BW} = 100 MHz) incident on seven cells centered at 5 meters with a relative dielectric constant of 2, $\Delta x = 0.05$ m, and $\Delta t = \Delta x/(c\sqrt{2})$.

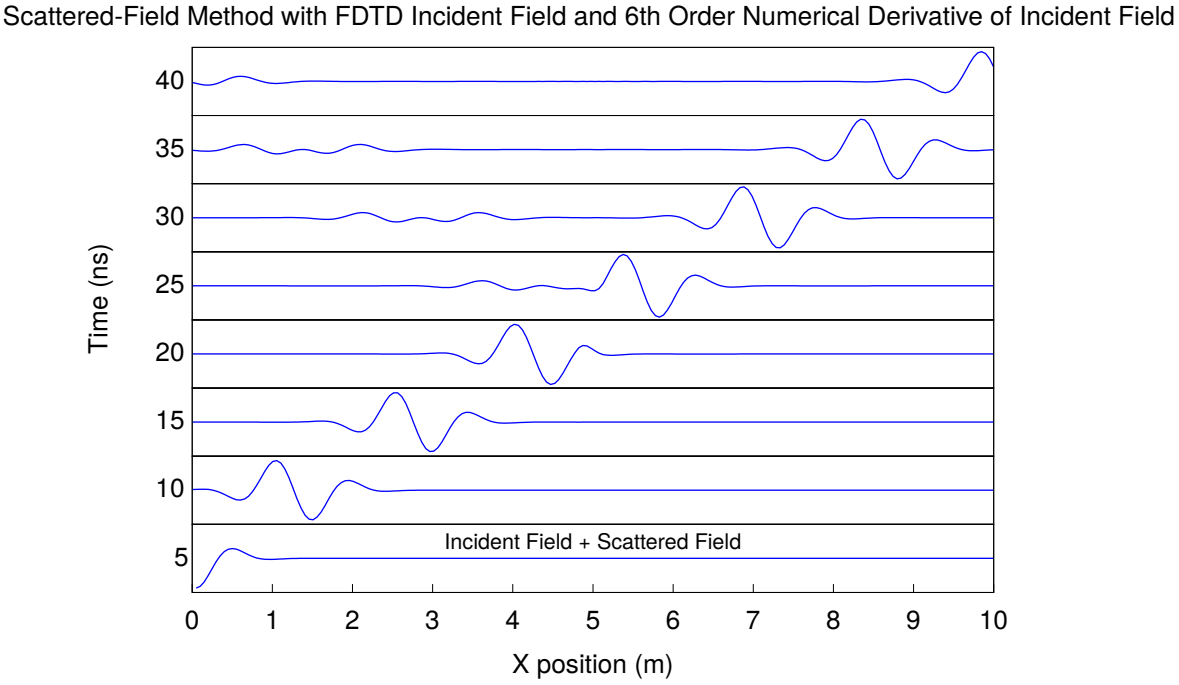

Figure 14—Sum of the analytic incident-field and scattered-field calculated via the scattered-field method using the sixth order central difference equation with a modulated Gaussian pulse (f_c = 300 MHz, f_{BW} = 100 MHz) generated in an FDTD grid and incident on seven cells centered at 5 meters with a relative dielectric constant of 2, $\Delta x = 0.05$ m, and $\Delta t = \Delta x/(c\sqrt{2})$.

3.2 Alternative Derivative for the Scattered-Field Method

Alternatively, from Equation (36b), the derivative of the incident-field with respect to time is obtained directly from the $\mathcal{H}_y$ field in the secondary FDTD grid used to generate the incident-field. In this case, I only expand the spatial derivatives using the second order central difference equation to get

$$\frac{\partial \mathcal{E}_z^i(x, t+\frac{\Delta t}{2})}{\partial t} \approx \frac{1}{\epsilon_0 \Delta x}\left[\mathcal{H}_y^i(x+\tfrac{\Delta x}{2}, t+\tfrac{\Delta t}{2}) - \mathcal{H}_y^i(x-\tfrac{\Delta x}{2}, t+\tfrac{\Delta t}{2})\right]. \tag{46}$$

Since the incident-field in the secondary FDTD grid is a plane wave propagating in the $+x$ direction in free space, I use $\mathcal{H}_y^i(x,t) = -\mathcal{E}_z^i(x,t)/\eta$ with Equation (46) to get

$$\frac{\partial \mathcal{E}_z^i(x, t+\frac{\Delta t}{2})}{\partial t} \approx -\frac{1}{\epsilon_0 \eta \Delta x}\left[\mathcal{E}_z^i(x+\tfrac{\Delta x}{2}, t+\tfrac{\Delta t}{2}) - \mathcal{E}_z^i(x-\tfrac{\Delta x}{2}, t+\tfrac{\Delta t}{2})\right]. \tag{47}$$

Knowing that $\epsilon_0 \eta = \sqrt{\mu_0 \epsilon_0} = 1/c$ I transform Equation (47) to

$$\frac{\partial \mathcal{E}_z^i(x, t+\frac{\Delta t}{2})}{\partial t} \approx -\frac{c}{\Delta x}\left[\mathcal{E}_z^i(x+\tfrac{\Delta x}{2}, t+\tfrac{\Delta t}{2}) - \mathcal{E}_z^i(x-\tfrac{\Delta x}{2}, t+\tfrac{\Delta t}{2})\right]. \tag{48}$$

Comparing Equation (48) with Equation (45a) I see that they are essentially identical. The disadvantage of using Equation (46) or Equation (48) is that they do not match the spatial or time steps that would be available when calculating the secondary grid. More specifically to calculate $\mathcal{E}_z(x, t+\frac{\Delta t}{2})$ for Equation (41b), the secondary grid would be also calculating $\mathcal{H}_y(x+\frac{\Delta x}{2}, t)$ since Yee FDTD with second order central differences offsets the $\mathcal{E}$ and $\mathcal{H}$ fields in time and space.

4. BOUNDARY CONDITIONS

The FDTD method solves for fields in a finite region. The surface where the FDTD update equations terminate acts like a perfect reflector as there are no fields beyond that surface. Using the same parameters as in Figure 3 I use the total-field/scattered-field method only at $x = 1$ m with no boundary condition at $x = 10$ m to demonstrate this effect in Figure 15. Here I see total reflection from the end of the FDTD grid at $x = 10$ m. This is the reason that FDTD simulations of open regions have to be terminated by a boundary condition that minimizes the reflection of the incident-fields and does not distort the fields inside the FDTD region [8, Chapter 18], [9, Chapter 6].

The analytical and the perfectly matched layer (PML) boundary conditions are the primary classes of boundary conditions for FDTD. Analytical boundary conditions are based on analytical derivations at the boundary of the FDTD region. PML boundary conditions are based on a nonphysical anisotropic multilayer material covering between ten and twenty cells at the edge of the FDTD region, which adds greatly to the computational cost of an FDTD simulation [19]. With a PML boundary condition, only fields propagating perpendicular to the external surface are absorbed by the multilayer material while fields propagating parallel

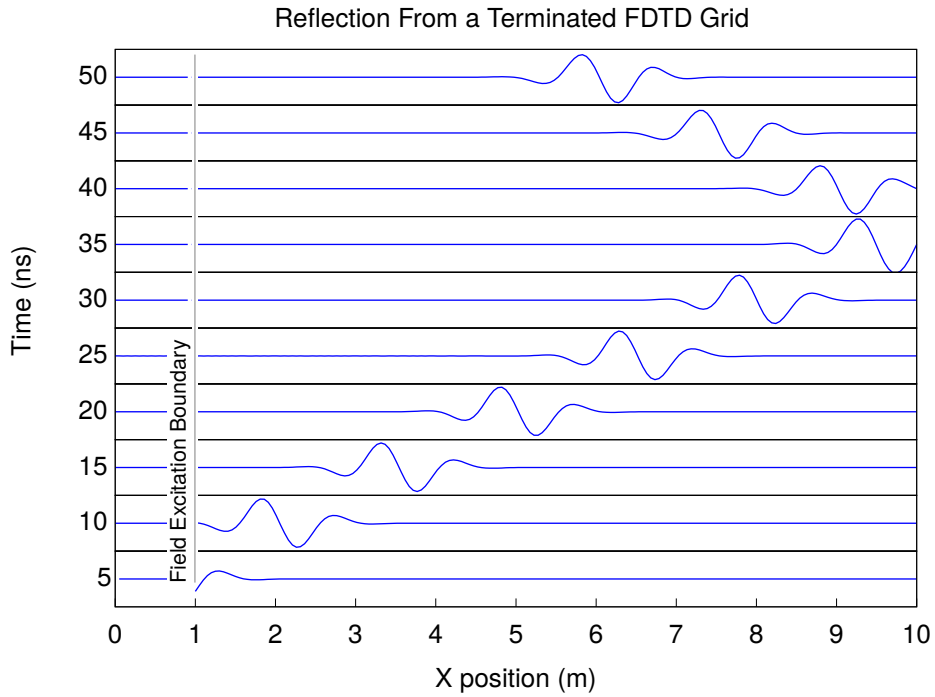

Figure 15—Reflection of a modulated Gaussian pulse (f_c = 300 MHz, f_{BW} = 300 MHz) from a terminated FDTD grid at x = 10 m with Δx = 0.05 m and $\Delta t = \Delta x/(c\sqrt{2})$.

to the surface are unaffected. This concept is a direct result of these two equations describing the separation of an electromagnetic field into fields propagating in opposite directions [20]

$$\vec{\mathcal{E}} = \frac{1}{2}\left(\mathcal{E} - \eta\hat{n}\times\mathcal{H}\right), \tag{49a}$$

$$\overleftarrow{\mathcal{E}} = \frac{1}{2}\left(\mathcal{E} + \eta\hat{n}\times\mathcal{H}\right). \tag{49b}$$

If I take $\hat{n}$ to be the normal to a surface than setting the appropriate equation to zero does not restrict the electric fields propagating parallel to the surface. In the following, I evaluate boundary conditions based on the wave equation, the PML method, and the one-way propagation equation, Equation (49). Finally, I combine the split-field concepts of the PML method inherent in Equation (49) with a boundary condition directly based on Equation (49) as opposed to the lossy material layer concept of PML.

4.1 Boundary Conditions From the Factorization of the Wave Equation

Several analytical, absorbing boundary conditions are based on the factorization of the wave equation into components representing waves traveling in each direction [9, Section 6.3]. The electric field wave equation in free space is obtained from Equation (36) as follows

$$\nabla\times\left[\mu_0\frac{\partial\mathcal{H}(t)}{\partial t}\right] = -\nabla\times\nabla\times\mathcal{E}(t), \tag{50a}$$

$$\mu_0\frac{\partial}{\partial t}\left[\nabla\times\mathcal{H}(t)\right] = -\nabla\times\nabla\times\mathcal{E}(t), \tag{50b}$$

$$\mu_0 \frac{\partial}{\partial t}\left[\epsilon_0 \frac{\partial \boldsymbol{\mathcal{E}}(t)}{\partial t}\right] = -\nabla \times \nabla \times \boldsymbol{\mathcal{E}}(t), \tag{50c}$$

$$\mu_0 \epsilon_0 \frac{\partial^2 \boldsymbol{\mathcal{E}}(t)}{\partial t^2} = -\nabla \times \nabla \times \boldsymbol{\mathcal{E}}(t), \tag{50d}$$

$$\frac{1}{c^2}\frac{\partial^2 \boldsymbol{\mathcal{E}}(t)}{\partial t^2} = \nabla^2 \boldsymbol{\mathcal{E}}(t) - \nabla\left(\nabla \cdot \boldsymbol{\mathcal{E}}(t)\right) \tag{50e}$$

$$\frac{1}{c^2}\frac{\partial^2 \boldsymbol{\mathcal{E}}(t)}{\partial t^2} = \nabla^2 \boldsymbol{\mathcal{E}}(t) \tag{50f}$$

since $\nabla \cdot \boldsymbol{\mathcal{E}}(t) = 0$ in a source free region.

4.2 First-Order Wave Equation Boundary Condition

In one dimension, with only $\mathcal{E}_z$ field components and propagation in the x direction, the electric field wave equation is written as

$$\frac{\partial^2 \mathcal{E}_z(x,t)}{\partial x^2} - \frac{1}{c^2}\frac{\partial \mathcal{E}_z(x,t)}{\partial t} = 0, \tag{51a}$$

$$\left(\frac{\partial}{\partial x} + \frac{1}{c}\frac{\partial}{\partial t}\right)\left(\frac{\partial}{\partial x} - \frac{1}{c}\frac{\partial}{\partial t}\right)\mathcal{E}_z(x,t) = 0. \tag{51b}$$

The first component of Equation (51b) corresponds to waves propagating in the $-x$ direction, and the second component corresponds to waves propagating in the $+x$ direction. To eliminate reflections from the $+x$ boundary, I set the $-x$ propagating wave to zero at the $+x$ boundary using the first component of Equation (51b),

$$\frac{\partial \mathcal{E}_z(x,t)}{\partial x} + \frac{1}{c}\frac{\partial \mathcal{E}_z(x,t)}{\partial t} = 0. \tag{52}$$

To get $\mathcal{E}_z$ field values at points on the FDTD grid related to the $-x$ propagating wave, our first approach is to apply first-order forward difference equations for both derivatives to Equation (52) at the point $(x-\Delta x, t)$,

$$\frac{1}{\Delta x}\left[\mathcal{E}_z(x,t) - \mathcal{E}_z(x-\Delta x,t)\right] = -\frac{1}{c\Delta t}\left[\mathcal{E}_z(x-\Delta x,t+\Delta t) - \mathcal{E}_z(x-\Delta x,t)\right], \tag{53a}$$

$$\mathcal{E}_z(x,t) = \mathcal{E}_z(x-\Delta x,t)\left[1 + \frac{\Delta x}{c\Delta t}\right] - \frac{\Delta x}{c\Delta t}\mathcal{E}_z(x-\Delta x,t+\Delta t). \tag{53b}$$

To evaluate the boundary problem in one dimension, I define the finite region with $\mathcal{E}_z$ FDTD grid points at $x = \Delta x$ through $x = n_x \Delta x$. Similarly, I define the $\mathcal{H}_y$ FDTD grid points at $x = \Delta x + \frac{\Delta x}{2}$ through $x = (n_x - 1)\Delta x + \frac{\Delta x}{2}$. With this definition, the grid points $\mathcal{E}_z(\Delta x, t)$ and $\mathcal{E}_z(n_x \Delta x, t)$ can not be updated using the update equation, Equation (16), as this would require $\mathcal{H}_y$ field values outside the grid, that is $\mathcal{H}_y(\frac{\Delta x}{2}, t)$ and $\mathcal{H}_y(n_x \Delta x + \frac{\Delta x}{2}, t)$.

As a first step to find the value of $\mathcal{E}_z(n_x \Delta x, t)$ I use Equation (53b) with array notation[4] to get

$$\mathcal{E}_z(n_x,t) = \mathcal{E}_z(n_x-1,t)\left[1 + \frac{\Delta x}{c\Delta t}\right] - \frac{\Delta x}{c\Delta t}\mathcal{E}_z(n_x-1,t+\Delta t). \tag{54}$$

[4] Using the array notation where I drop the Δx multiplier on the $\mathcal{E}_z$ / $\mathcal{H}_y$ fields and the $\frac{\Delta x}{2}$ offset on the $\mathcal{H}_y$ fields.

Equation (54) requires $\mathcal{E}_z$ at $t+\Delta t$ so I use the update equation to relate the future $\mathcal{E}_z$ field to earlier $\mathcal{H}_y$ fields. From Equation (16) I have

$$\mathcal{E}_z(n_x-1,t+\Delta t) = c_a\mathcal{E}_z(n_x-1,t) + \frac{c_b}{\Delta x}\left[\mathcal{H}_y(n_x-1,t+\tfrac{\Delta t}{2}) - \mathcal{H}_y(n_x-2,t+\tfrac{\Delta t}{2})\right], \tag{55}$$

then

$$\begin{aligned}\mathcal{E}_z(n_x,t) =& \mathcal{E}_z(n_x-1,t)\left[1+\frac{\Delta x}{c\Delta t}\right] - \frac{c_a\Delta x}{c\Delta t}\mathcal{E}_z(n_x-1,t) \\ &- \frac{c_b}{c\Delta t}\left[\mathcal{H}_y(n_x-1,t+\tfrac{\Delta t}{2}) - \mathcal{H}_y(n_x-2,t+\tfrac{\Delta t}{2})\right], \end{aligned} \tag{56a}$$

$$\begin{aligned}=& \mathcal{E}_z(n_x-1,t)\left[1+\frac{(1-c_a)\Delta x}{c\Delta t}\right] \\ &- \frac{c_b}{c\Delta t}\left[\mathcal{H}_y(n_x-1,t+\tfrac{\Delta t}{2}) - \mathcal{H}_y(n_x-2,t+\tfrac{\Delta t}{2})\right]. \end{aligned} \tag{56b}$$

However, I need $\mathcal{E}_z(n_x,t)$ to calculate $\mathcal{H}_y(n_x-1,t+\frac{\Delta t}{2})$, so again I use an update equation, in this case Equation (18),

$$\mathcal{H}_y(n_x-1,t+\tfrac{\Delta t}{2}) = d_a\mathcal{H}_y(n_x-1,t-\tfrac{\Delta t}{2}) + \frac{d_b}{\Delta x}\left[\mathcal{E}_z(n_x,t) - \mathcal{E}_z(n_x-1,t)\right], \tag{57}$$

and to simplify the final equation I also expand $\mathcal{H}_y(n_x-2,t+\frac{\Delta t}{2})$ using

$$\mathcal{H}_y(n_x-2,t+\tfrac{\Delta t}{2}) = d_a\mathcal{H}_y(n_x-2,t-\tfrac{\Delta t}{2}) + \frac{d_b}{\Delta x}\left[\mathcal{E}_z(n_x-1,t) - \mathcal{E}_z(n_x-2,t)\right]. \tag{58}$$

Then I have

$$\begin{aligned}\mathcal{E}_z(n_x,t) =& \mathcal{E}_z(n_x-1,t)\left[1+\frac{(1-c_a)\Delta x}{c\Delta t}\right] \\ &- \frac{c_b}{c\Delta t}\left[d_a\mathcal{H}_y(n_x-1,t-\tfrac{\Delta t}{2}) + \frac{d_b}{\Delta x}\left[\mathcal{E}_z(n_x,t) - \mathcal{E}_z(n_x-1,t)\right]\right. \\ &\left. - d_a\mathcal{H}_y(n_x-2,t-\tfrac{\Delta t}{2}) - \frac{d_b}{\Delta x}\left[\mathcal{E}_z(n_x-1,t) - \mathcal{E}_z(n_x-2,t)\right]\right]. \end{aligned} \tag{59}$$

Rearranging I get

$$\begin{aligned}\mathcal{E}_z(n_x,t)\left(1+\frac{c_bd_b}{c\Delta t\Delta x}\right) =& \mathcal{E}_z(n_x-1,t)\left[1+\frac{(1-c_a)\Delta x}{c\Delta t}+\frac{2c_bd_b}{c\Delta t\Delta x}\right] - \frac{c_bd_b}{c\Delta t\Delta x}\mathcal{E}_z(n_x-2,t) \\ &- \frac{c_bd_a}{c\Delta t}\left[\mathcal{H}_y(n_x-1,t-\tfrac{\Delta t}{2}) - \mathcal{H}_y(n_x-2,t-\tfrac{\Delta t}{2})\right]. \end{aligned} \tag{60}$$

In a free space region, I reduce the constants as follows,

$$c_a = 1, \tag{61a}$$

$$d_a = 1, \tag{61b}$$

$$c_b = \frac{\Delta t}{\epsilon_0}, \tag{61c}$$

$$d_b = \frac{\Delta t}{\mu_0}, \tag{61d}$$

$$\frac{c_b d_a}{c\Delta t} = \eta_0, \tag{61e}$$

$$\frac{c_b d_b}{c\Delta t} = c\Delta t. \tag{61f}$$

Then a first-order wave equation $+x$ boundary condition in free space is

$$\begin{aligned}\mathcal{E}_z(n_x,t) =& \frac{2c\Delta t + \Delta x}{c\Delta t + \Delta x}\mathcal{E}_z(n_x-1,t) - \frac{c\Delta t}{c\Delta t + \Delta x}\mathcal{E}_z(n_x-2,t) \\ & - \frac{\eta_0 \Delta x}{c\Delta t + \Delta x}\left[\mathcal{H}_y(n_x-1,t-\tfrac{\Delta t}{2}) - \mathcal{H}_y(n_x-2,t-\tfrac{\Delta t}{2})\right].\end{aligned} \tag{62}$$

As this is derived starting with first-order difference equations the error is substantial and the reflection from the boundary is easily visible in Figure 16.

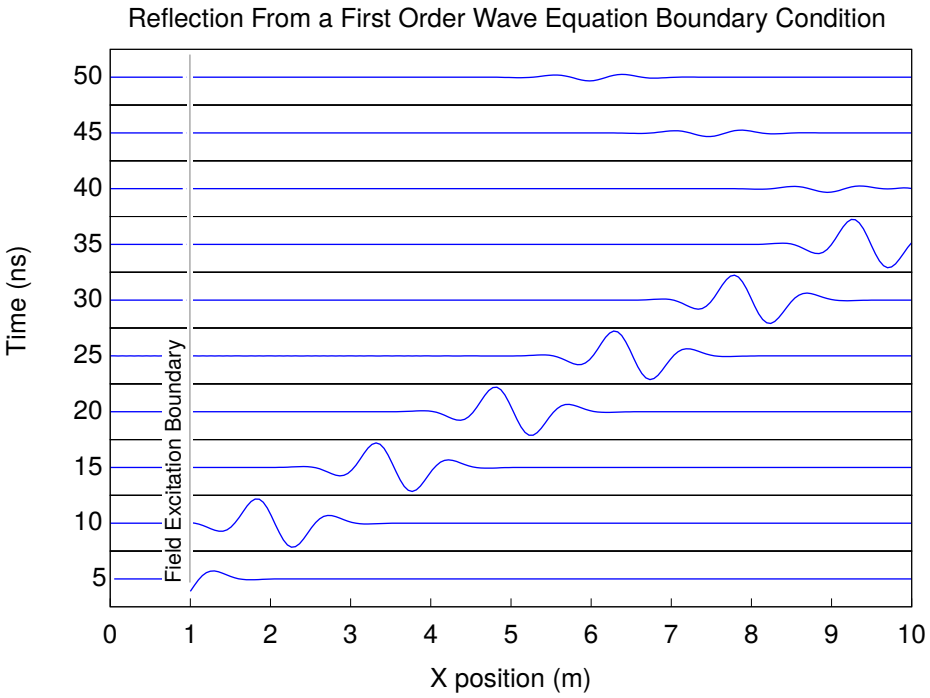

Figure 16—Reflection of a modulated Gaussian pulse (f_c = 300 MHz, f_{BW} = 300 MHz) from a boundary condition derived from the wave equation and forward difference equations with Δx = 0.05 meters and $\Delta t = \Delta x/(c\sqrt{2})$.

4.3 Second Order Wave Equation Boundary Condition

A second order boundary condition is obtained by applying the central difference equations to Equation (52) at the point $(x-\frac{\Delta x}{2}, t)$,

$$\frac{1}{\Delta x}\left[\mathcal{E}_z(x,t) - \mathcal{E}_z(x-\Delta x,t)\right] = -\frac{1}{c\Delta t}\left[\mathcal{E}_z(x-\tfrac{\Delta x}{2}, t+\tfrac{\Delta t}{2}) - \mathcal{E}_z(x-\tfrac{\Delta x}{2}, t-\tfrac{\Delta t}{2})\right]. \tag{63}$$

$\mathcal{E}_z(x-\frac{\Delta x}{2}, t-\frac{\Delta t}{2})$ is obtained from a linear interpolation of the four nearest electric field points in space and time,

$$\mathcal{E}_z(x-\tfrac{\Delta x}{2}, t-\tfrac{\Delta t}{2}) = \frac{1}{4}\left[\mathcal{E}_z(x,t) + \mathcal{E}_z(x-\Delta x,t) + \mathcal{E}_z(x,t-\Delta t) + \mathcal{E}_z(x-\Delta x,t-\Delta t)\right]. \tag{64}$$

$\mathcal{E}_z(x-\frac{\Delta x}{2}, t+\frac{\Delta t}{2})$ is obtained via a spatial/temporal linear interpolation of the electric field,

$$\mathcal{E}_z(x-\tfrac{\Delta x}{2}, t+\tfrac{\Delta t}{2}) = \frac{1}{2}\left[\mathcal{E}_z(x,t) + \mathcal{E}_z(x-\Delta x,t+\Delta t)\right]. \tag{65}$$

Combining Equations (63) – (65) with Equation (55) and converting to array notation for the boundary at $x = n_x\Delta x$, I get

$$\begin{aligned}\mathcal{E}_z(n_x,t) - \mathcal{E}_z(n_x-1,t) = -\frac{\Delta x}{4c\Delta t}\Big\{&\mathcal{E}_z(x,t) - \mathcal{E}_z(n_x-1,t) - \mathcal{E}_z(n_x,t-\Delta t)\\ &- \mathcal{E}_z(n_x-1,t-\Delta t) + 2\mathcal{E}_z(n_x-1,t+\Delta t)\Big\},\end{aligned} \tag{66a}$$

$$\begin{aligned}= -\frac{\Delta x}{4c\Delta t}\Big\{&\mathcal{E}_z(x,t) + (2c_a-1)\mathcal{E}_z(n_x-1,t) - \mathcal{E}_z(n_x,t-\Delta t) - \mathcal{E}_z(n_x-1,t-\Delta t)\\ &+ \frac{2c_b}{\Delta x}\left[\mathcal{H}_y(n_x-1,t+\tfrac{\Delta t}{2}) - \mathcal{H}_y(n_x-2,t+\tfrac{\Delta t}{2})\right]\Big\}.\end{aligned} \tag{66b}$$

Combining with Equations (57) – (58), I get

$$\begin{aligned}\mathcal{E}_z(n_x,t) - \mathcal{E}_z(n_x-1,t) = -\frac{\Delta x}{4c\Delta t}\Big\{&\mathcal{E}_z(x,t) + (2c_a-1)\mathcal{E}_z(n_x-1,t) - \mathcal{E}_z(n_x,t-\Delta t) - \mathcal{E}_z(n_x-1,t-\Delta t)\\ &+ \frac{2c_b}{\Delta x}\Big[d_a\mathcal{H}_y(n_x-1,t-\tfrac{\Delta t}{2}) + \frac{d_b}{\Delta x}\left[\mathcal{E}_z(n_x,t) - \mathcal{E}_z(n_x-1,t)\right]\\ &- d_a\mathcal{H}_y(n_x-2,t-\tfrac{\Delta t}{2}) - \frac{d_b}{\Delta x}\left[\mathcal{E}_z(n_x-1,t) - \mathcal{E}_z(n_x-2,t)\right]\Big]\Big\},\end{aligned} \tag{67a}$$

$$\begin{aligned}= \frac{\Delta x}{4c\Delta t}\Big\{&-\mathcal{E}_z(x,t) + (1-2c_a)\mathcal{E}_z(n_x-1,t) + \mathcal{E}_z(n_x,t-\Delta t) + \mathcal{E}_z(n_x-1,t-\Delta t)\\ &- \frac{2c_bd_a}{\Delta x}\left[\mathcal{H}_y(n_x-1,t-\tfrac{\Delta t}{2}) - \mathcal{H}_y(n_x-2,t-\tfrac{\Delta t}{2})\right]\\ &+ \frac{2c_bd_b}{\Delta x^2}\left[-\mathcal{E}_z(n_x,t) + 2\mathcal{E}_z(n_x-1,t) - \mathcal{E}_z(n_x-2,t)\right]\Big\}.\end{aligned} \tag{67b}$$

Then

$$\mathcal{E}_z(n_x,t)\left(1+\frac{\Delta x}{4c\Delta t}+\frac{c_b d_b}{\Delta x^2}\right)=\left[1+\frac{\Delta x}{4c\Delta t}\left(\frac{4c_b d_b}{\Delta x^2}+1-2c_a\right)\right]\mathcal{E}_z(n_x-1,t)$$
$$+\frac{\Delta x}{4c\Delta t}\left\{\mathcal{E}_z(n_x,t-\Delta t)+\mathcal{E}_z(n_x-1,t-\Delta t)-\frac{2c_b d_b}{\Delta x^2}\mathcal{E}_z(n_x-2,t)\right.$$
$$\left.-\frac{2c_b d_a}{\Delta x}\left[\mathcal{H}_y(n_x-1,t-\tfrac{\Delta t}{2})-\mathcal{H}_y(n_x-2,t-\tfrac{\Delta t}{2})\right]\right\}. \quad (68)$$

For the $+x$ boundary in a free space region I get

$$\mathcal{E}_z(n_x,t)\left[1+\frac{\Delta x}{4c\Delta t}+\left(\frac{c\Delta t}{\Delta x}\right)^2\right]=\left[1+\frac{c\Delta t}{\Delta x}-\frac{\Delta x}{4c\Delta t}\right]\mathcal{E}_z(n_x-1,t)$$
$$+\frac{\Delta x}{4c\Delta t}\left\{\mathcal{E}_z(n_x,t-\Delta t)+\mathcal{E}_z(n_x-1,t-\Delta t)-2\left(\frac{c\Delta t}{\Delta x}\right)^2\mathcal{E}_z(n_x-2,t)\right.$$
$$\left.-2\eta_0\frac{c\Delta t}{\Delta x}\left[\mathcal{H}_y(n_x-1,t-\tfrac{\Delta t}{2})-\mathcal{H}_y(n_x-2,t-\tfrac{\Delta t}{2})\right]\right\}. \quad (69)$$

Even though this is derived using the second order central difference equations the error is substantial and the reflection from the boundary is easily visible for times greater than 40 ns in Figure 17. The cause of the error is the first-order linear interpolation to get the electric fields for the spatial and temporal central differences.

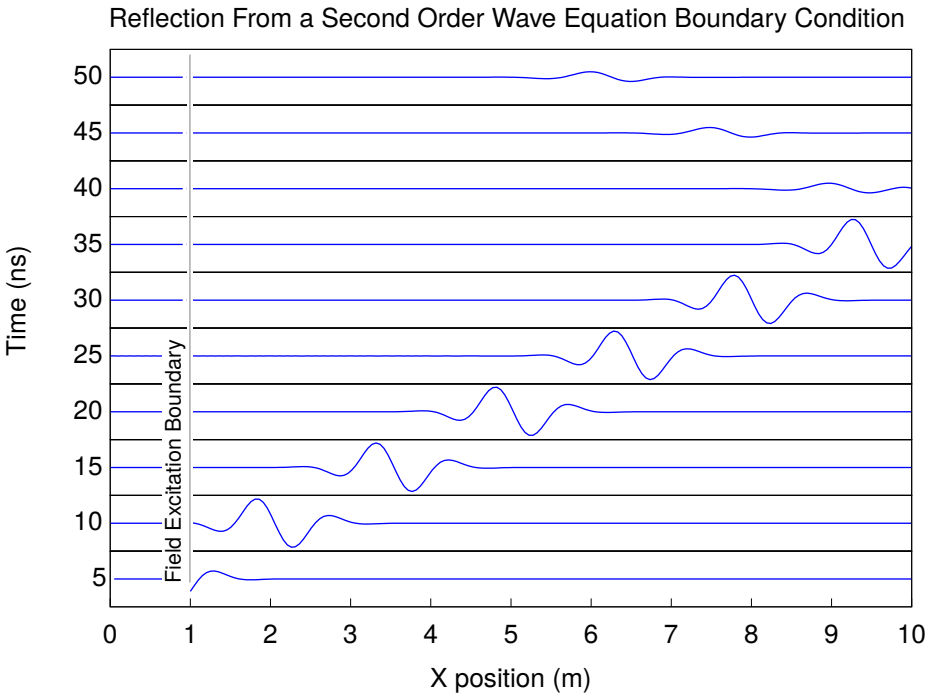

Figure 17—Reflection of a modulated Gaussian pulse (f_c = 300 MHz, f_{BW} = 300 MHz) from a second order wave equation boundary condition with $\Delta x = 0.05$ meters and $\Delta t = \Delta x/(c\sqrt{2})$.

4.4 Alternative Second Order Wave Equation Boundary Condition

Alternatively, I apply the central difference equations at the point $(x-\Delta x, t)$ with twice the spatial and temporal step size,

$$\frac{1}{2\Delta x}\left[\mathcal{E}_z(x,t) - \mathcal{E}_z(x-2\Delta x,t)\right] = -\frac{1}{2c\Delta t}\left[\mathcal{E}_z(x-\Delta x,t+\Delta t) - \mathcal{E}_z(x-\Delta x,t-\Delta t)\right], \tag{70a}$$

$$\mathcal{E}_z(x,t) = \frac{\Delta x}{c\Delta t}\mathcal{E}_z(x-\Delta x,t-\Delta t) + \mathcal{E}_z(x-2\Delta x,t) - \frac{\Delta x}{c\Delta t}\mathcal{E}_z(x-\Delta x,t+\Delta t). \tag{70b}$$

No linear interpolation is needed to get either the spatial or temporal electric fields for the central difference equations. Converting Equation (70b) to array notation for the boundary at $x = n_x\Delta x$, I get

$$\mathcal{E}_z(n_x,t) = \frac{\Delta x}{c\Delta t}\mathcal{E}_z(n_x-1,t-\Delta t) + \mathcal{E}_z(n_x-2,t) - \frac{\Delta x}{c\Delta t}\mathcal{E}_z(n_x-1,t+\Delta t). \tag{71}$$

Using Equation (55)

$$\mathcal{E}_z(n_x-1,t+\Delta t) = c_a\mathcal{E}_z(n_x-1,t) + \frac{c_b}{\Delta x}\left[\mathcal{H}_y(n_x-1,t+\tfrac{\Delta t}{2}) - \mathcal{H}_y(n_x-2,t+\tfrac{\Delta t}{2})\right], \tag{72}$$

then

$$\begin{aligned}\mathcal{E}_z(n_x,t) = \frac{\Delta x}{c\Delta t}\mathcal{E}_z(n_x-1,t-\Delta t) + \mathcal{E}_z(n_x-2,t) - \frac{c_a\Delta x}{c\Delta t}\mathcal{E}_z(n_x-1,t)\\ -\frac{c_b}{c\Delta t}\left[\mathcal{H}_y(n_x-1,t+\tfrac{\Delta t}{2}) - \mathcal{H}_y(n_x-2,t+\tfrac{\Delta t}{2})\right].\end{aligned} \tag{73}$$

For the future $\mathcal{H}_y$ fields I use Equations (57) – (58),

$$\mathcal{H}_y(n_x-1,t+\tfrac{\Delta t}{2}) = d_a\mathcal{H}_y(n_x-1,t-\tfrac{\Delta t}{2}) + \frac{d_b}{\Delta x}\left[\mathcal{E}_z(n_x,t) - \mathcal{E}_z(n_x-1,t)\right], \tag{74a}$$

$$\mathcal{H}_y(n_x-2,t+\tfrac{\Delta t}{2}) = d_a\mathcal{H}_y(n_x-2,t-\tfrac{\Delta t}{2}) + \frac{d_b}{\Delta x}\left[\mathcal{E}_z(n_x-1,t) - \mathcal{E}_z(n_x-2,t)\right], \tag{74b}$$

to get,

$$\begin{aligned}\mathcal{E}_z(n_x,t) = \frac{\Delta x}{c\Delta t}\mathcal{E}_z(n_x-1,t-\Delta t) - \frac{c_a\Delta x}{c\Delta t}\mathcal{E}_z(n_x-1,t) + \mathcal{E}_z(n_x-2,t)\\ -\frac{c_b}{c\Delta t}\left[d_a\mathcal{H}_y(n_x-1,t-\tfrac{\Delta t}{2}) + \frac{d_b}{\Delta x}\left[\mathcal{E}_z(n_x,t) - \mathcal{E}_z(n_x-1,t)\right]\right.\\ \left. - d_a\mathcal{H}_y(n_x-2,t-\tfrac{\Delta t}{2}) - \frac{d_b}{\Delta x}\left[\mathcal{E}_z(n_x-1,t) - \mathcal{E}_z(n_x-2,t)\right]\right].\end{aligned} \tag{75}$$

Rearranging I get

$$\begin{aligned}\mathcal{E}_z(n_x,t)\left(1+\frac{c_b d_b}{c\Delta t\Delta x}\right) &= \frac{\Delta x}{c\Delta t}\mathcal{E}_z(n_x-1,t-\Delta t)\\ &+\left[\frac{2c_b d_b}{c\Delta t\Delta x}-\frac{c_a\Delta x}{c\Delta t}\right]\mathcal{E}_z(n_x-1,t)\\ &+\left[1-\frac{c_b d_b}{c\Delta t\Delta x}\right]\mathcal{E}_z(n_x-2,t)\\ &-\frac{c_b d_a}{c\Delta t}\left[\mathcal{H}_y(n_x-1,t-\tfrac{\Delta t}{2})-\mathcal{H}_y(n_x-2,t-\tfrac{\Delta t}{2})\right].\end{aligned} \tag{76}$$

For the $+x$ boundary in a free space region I get

$$\begin{aligned}\mathcal{E}_z(n_x,t)\left(1+\frac{c\Delta t}{\Delta x}\right) &= \frac{\Delta x}{c\Delta t}\mathcal{E}_z(n_x-1,t-\Delta t)\\ &+\left[\frac{2c\Delta t}{\Delta x}-\frac{\Delta x}{c\Delta t}\right]\mathcal{E}_z(n_x-1,t)\\ &+\left[1-\frac{c\Delta t}{\Delta x}\right]\mathcal{E}_z(n_x-2,t)\\ &-\eta_0\left[\mathcal{H}_y(n_x-1,t-\tfrac{\Delta t}{2})-\mathcal{H}_y(n_x-2,t-\tfrac{\Delta t}{2})\right].\end{aligned} \tag{77}$$

The primary source of error in this one-dimensional boundary condition is the use of the central difference equation with twice the step size used in the Yee FDTD update equations. However, as the formulation closely matches the Yee update equations the error is not visible in Figure 18 (the amplitude in the waterfall charts is ± 1).

Expanding the scale to ± 0.004 and only looking at the 50 ns time slice, I see a 0.0035 magnitude pulse propagating in the $-x$ direction in Figure 19. This corresponds to a 50 dB reduction in the reflection from the boundary.

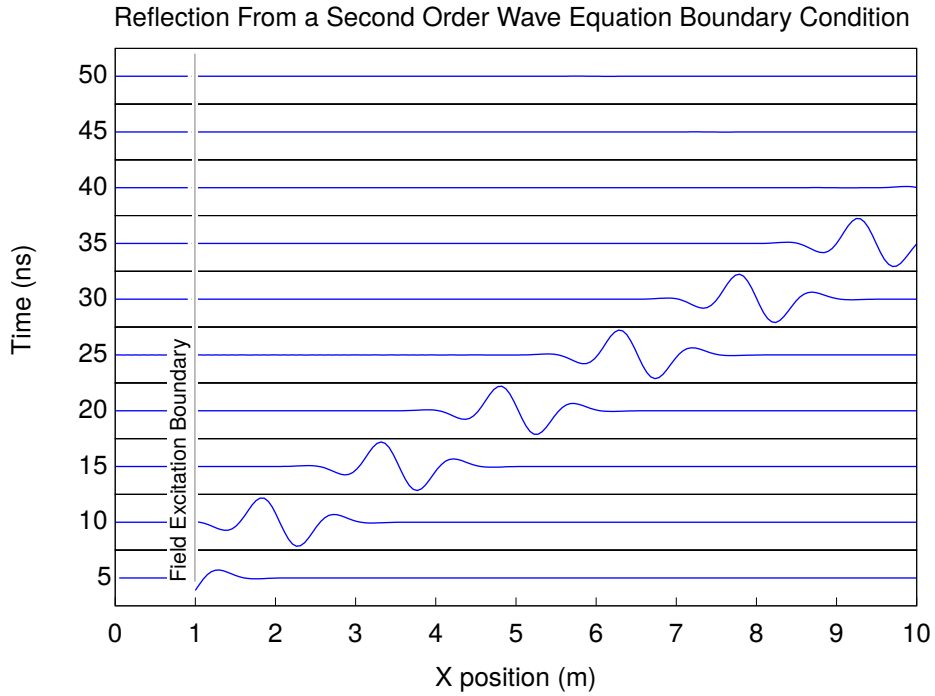

Figure 18—Reflection of a modulated Gaussian pulse (f_c = 300 MHz, f_{BW} = 300 MHz) from a central difference equation derived boundary condition with $\Delta x = 0.05$ meters and $\Delta t = \Delta x/(c\sqrt{2})$.

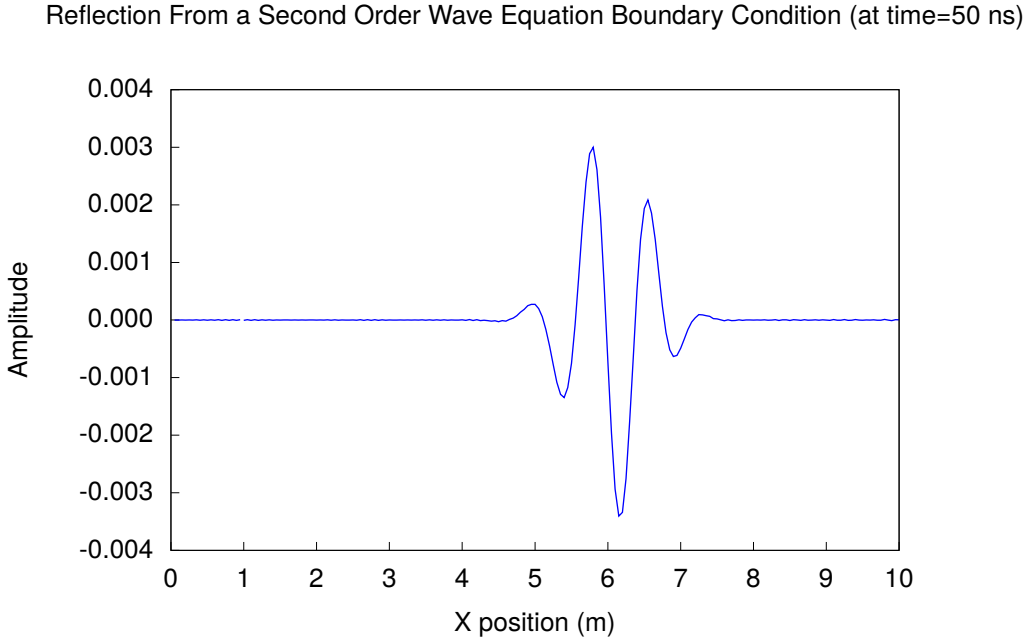

Figure 19—Reflection of a modulated Gaussian pulse (f_c = 300 MHz, f_{BW} = 300 MHz) from a central difference equation derived boundary condition with $\Delta x = 0.05$ meters and $\Delta t = \Delta x/(c\sqrt{2})$ at time = 50 ns.

5. ONE-WAY PROPAGATION BOUNDARY CONDITION

Rather than continue with the factorization of the wave equation, I consider a different approach, the direct application of Equation (49). To eliminate reflections from the $+x$ boundary I set the $-x$ propagating electric field to zero at the $+x$ boundary,

$$\overleftarrow{\boldsymbol{\mathcal{E}}} = 0, \tag{78a}$$

$$\boldsymbol{\mathcal{E}} = -\eta\hat{x} \times \boldsymbol{\mathcal{H}} \tag{78b}$$

In one dimension, with only $\mathcal{E}_z$ field components and propagation in the x direction, I get

$$\mathcal{E}_z(x,t) = -\eta\mathcal{H}_y(x,t) \tag{79}$$

5.1 First-Order One-Way Propagation Boundary Condition

Since the electric and magnetic fields are spatially and temporally offset, I start with spatial linear interpolation of the electric field combined with temporal linear interpolation of the magnetic field at $(x-\frac{\Delta x}{2}, t)$,

$$\frac{1}{2}\left[\mathcal{E}_z(x,t) + \mathcal{E}_z(x-\Delta x,t)\right] = -\frac{\eta}{2}\left[\mathcal{H}_y(x-\tfrac{\Delta x}{2}, t+\tfrac{\Delta t}{2}) + \mathcal{H}_y(x-\tfrac{\Delta x}{2}, t-\tfrac{\Delta t}{2})\right]. \tag{80}$$

Converting to array notation for the boundary at $x = n_x\Delta x$, I get

$$\mathcal{E}_z(n_x,t) + \mathcal{E}_z(n_x-1,t) = -\eta\left[\mathcal{H}_y(n_x-1, t+\tfrac{\Delta t}{2}) + \mathcal{H}_y(n_x-1, t-\tfrac{\Delta t}{2})\right]. \tag{81}$$

For the future $\mathcal{H}_y$ field I use Equation (57),

$$\mathcal{H}_y(n_x-1, t+\tfrac{\Delta t}{2}) = d_a\mathcal{H}_y(n_x-1, t-\tfrac{\Delta t}{2}) + \frac{d_b}{\Delta x}\left[\mathcal{E}_z(n_x,t) - \mathcal{E}_z(n_x-1,t)\right], \tag{82}$$

to get

$$\mathcal{E}_z(n_x,t) = -\mathcal{E}_z(n_x-1,t) - \eta\left[(1+d_a)\mathcal{H}_y(n_x-1, t-\tfrac{\Delta t}{2}) + \frac{d_b}{\Delta x}\left[\mathcal{E}_z(n_x,t) - \mathcal{E}_z(n_x-1,t)\right]\right]. \tag{83}$$

Solving for $\mathcal{E}_z(n_x,t)$ I get

$$\left(\frac{\eta d_b}{\Delta x} + 1\right)\mathcal{E}_z(n_x,t) = \left(\frac{\eta d_b}{\Delta x} - 1\right)\mathcal{E}_z(n_x-1,t) - \eta(1+d_a)\mathcal{H}_y(n_x-1, t-\tfrac{\Delta t}{2}), \tag{84a}$$

$$\mathcal{E}_z(n_x,t) = \frac{\eta d_b - \Delta x}{\eta d_b + \Delta x}\mathcal{E}_z(n_x-1,t) - \frac{\eta(1+d_a)\Delta x}{\eta d_b + \Delta x}\mathcal{H}_y(n_x-1, t-\tfrac{\Delta t}{2}). \tag{84b}$$

For a free space region I have

$$\eta d_b = c\Delta t \tag{85}$$

then the $+x$ boundary condition is

$$\mathcal{E}_z(n_x,t) = \frac{c\Delta t - \Delta x}{c\Delta t + \Delta x}\mathcal{E}_z(n_x-1,t) - \frac{2\eta\Delta x}{c\Delta t + \Delta x}\mathcal{H}_y(n_x-1,t-\tfrac{\Delta t}{2}). \tag{86}$$

The corresponding equation for the $-x$ boundary condition is

$$\mathcal{E}_z(1,t) = \frac{c\Delta t - \Delta x}{c\Delta t + \Delta x}\mathcal{E}_z(2,t) + \frac{2\eta\Delta x}{c\Delta t + \Delta x}\mathcal{H}_y(1,t-\tfrac{\Delta t}{2}). \tag{87}$$

The primary source of error in this boundary condition is the spatial and temporal linear interpolation on the electric and magnetic fields, respectively. However, the resulting error is not visible in Figure 20. Expanding

Figure 20—Reflection of a modulated Gaussian pulse (f_c = 300 MHz, f_{BW} = 300 MHz) from the first-order $\mathcal{E} = -\eta\hat{x} \times \mathcal{H}$ boundary condition with $\Delta x = 0.05$ meters and $\Delta t = \Delta x/(c\sqrt{2})$.

the scale to ± 0.004 and only looking at the 50 ns time slice, I see a 0.0035 magnitude pulse propagating in the $-x$ direction in Figure 21. This corresponds to a 50 dB reduction in the reflection from the boundary for an equation much simpler then Equation (77). Equations (86) – (87) are the boundary conditions used to generate all the calculations in the total-field/scattered-field and the scattered-field sections.

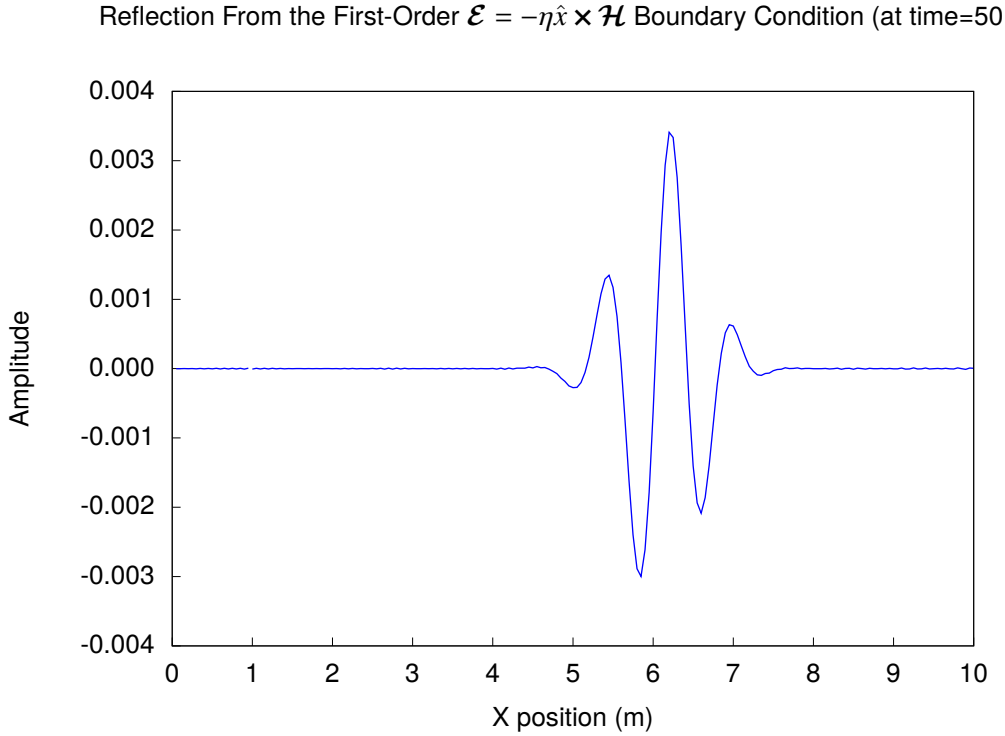

Figure 21—Reflection of a modulated Gaussian pulse (f_c = 300 MHz, f_{BW} = 300 MHz) from the first-order $\mathcal{E} = -\eta\hat{x} \times \mathcal{H}$ boundary condition with $\Delta x = 0.05$ meters and $\Delta t = \Delta x/(c\sqrt{2})$ at time = 50 ns.

5.2 Second Order One-Way Propagation Boundary Condition

To further reduce the error, I use quadratic interpolation,[5]

$$f(i-\tfrac{1}{2})_{\text{quadratic}} = \frac{3}{8}f(i) + \frac{3}{4}f(i-1) - \frac{1}{8}f(i-2), \tag{88}$$

instead of linear interpolation as in Equation (81), to get

$$\frac{3}{4}\mathcal{E}_z(n_x,t) + \frac{3}{2}\mathcal{E}_z(n_x-1,t) - \frac{1}{4}\mathcal{E}_z(n_x-2,t) = -\eta\left[\mathcal{H}_y(n_x-1,t+\tfrac{\Delta t}{2}) + \mathcal{H}_y(n_x-1,t-\tfrac{\Delta t}{2})\right], \tag{89a}$$

$$= -\eta\left[(1+d_a)\mathcal{H}_y(n_x-1,t-\tfrac{\Delta t}{2}) + \frac{d_b}{\Delta x}\left[\mathcal{E}_z(n_x,t) - \mathcal{E}_z(n_x-1,t)\right]\right]. \tag{89b}$$

Combining terms and rearranging I get

$$\left(\frac{\eta d_b}{\Delta x} + \frac{3}{4}\right)\mathcal{E}_z(n_x,t) = \left(\frac{\eta d_b}{\Delta x} - \frac{3}{2}\right)\mathcal{E}_z(n_x-1,t) + \frac{1}{4}\mathcal{E}_z(n_x-2,t) - \eta(1+d_a)\mathcal{H}_y(n_x-1,t-\tfrac{\Delta t}{2}). \tag{90}$$

[5] Same as the Lagrange three point interpolation formula from [21, Eq. 25.2.11]

Then solving for $\mathcal{E}_z(n_x,t)$ I get

$$\mathcal{E}_z(n_x,t) = \frac{\left(\frac{\eta d_b}{\Delta x} - \frac{3}{2}\right)\mathcal{E}_z(n_x-1,t) + \frac{1}{4}\mathcal{E}_z(n_x-2,t) - \eta(1+d_a)\mathcal{H}_y(n_x-1,t-\frac{\Delta t}{2})}{\left(\frac{\eta d_b}{\Delta x} + \frac{3}{4}\right)}. \tag{91}$$

The resulting $+x$ boundary condition in free space is

$$\mathcal{E}_z(n_x,t) = \frac{\left(\frac{c\Delta t}{\Delta x} - \frac{3}{2}\right)\mathcal{E}_z(n_x-1,t) + \frac{1}{4}\mathcal{E}_z(n_x-2,t) - 2\eta\mathcal{H}_y(n_x-1,t-\frac{\Delta t}{2})}{\left(\frac{c\Delta t}{\Delta x} + \frac{3}{4}\right)}, \tag{92}$$

which is very similar to Equation (86). The corresponding equation for the $-x$ boundary condition is

$$\mathcal{E}_z(1,t) = \frac{\left(\frac{c\Delta t}{\Delta x} - \frac{3}{2}\right)\mathcal{E}_z(2,t) + \frac{1}{4}\mathcal{E}_z(3,t) + 2\eta\mathcal{H}_y(1,t-\frac{\Delta t}{2})}{\left(\frac{c\Delta t}{\Delta x} + \frac{3}{4}\right)}. \tag{93}$$

As shown in Figure 22, the reflection is virtually identical to the negative of that from the boundary condition with linear interpolation.

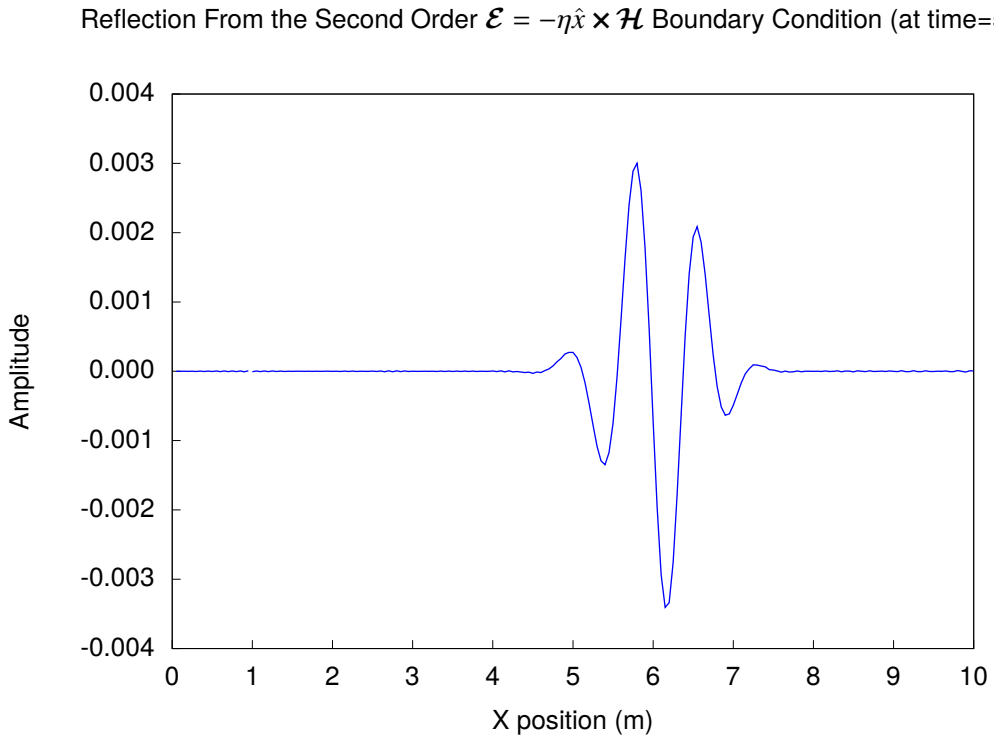

Figure 22—Reflection of a modulated Gaussian pulse (f_c = 300 MHz, f_{BW} = 300 MHz) from the second order $\mathcal{E} = -\eta\hat{x} \times \mathcal{H}$ boundary condition with $\Delta x = 0.05$ meters and $\Delta t = \Delta x/(c\sqrt{2})$ at time = 50 ns.

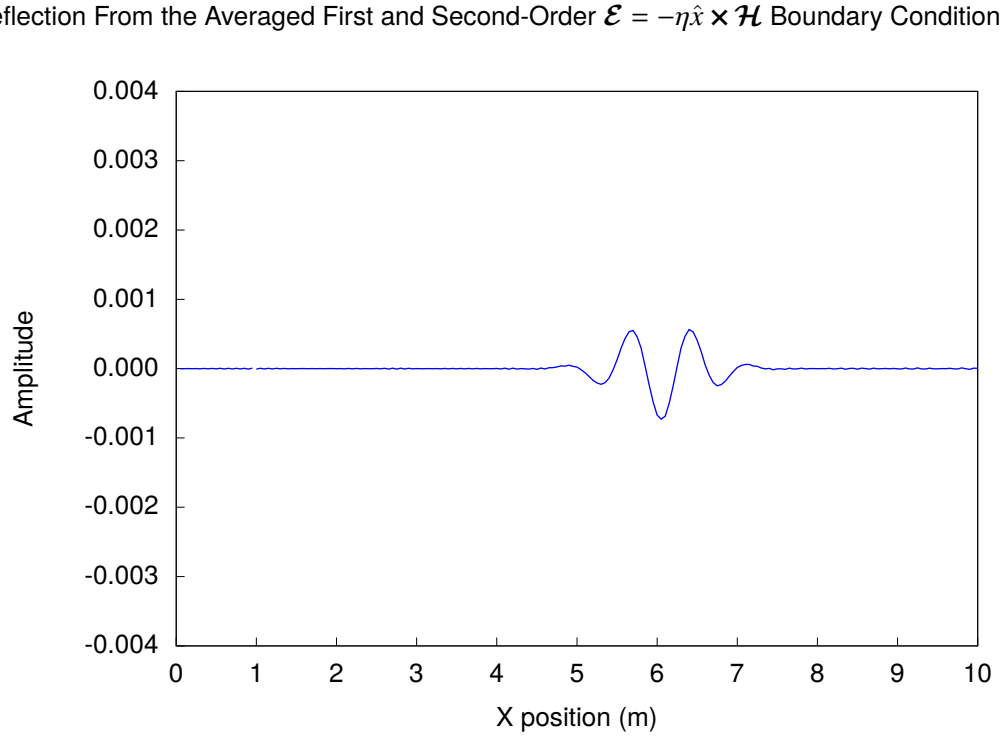

Figure 23—Reflection of a modulated Gaussian pulse (f_c = 300 MHz, f_{BW} = 300 MHz) from the $\mathcal{E} = -\eta\hat{x} \times \mathcal{H}$ boundary condition created by averaging the first and second-order boundary conditions with $\Delta x = 0.05$ meters and $\Delta t = \Delta x/(c\sqrt{2})$ at time = 50 ns.

Based on this observation I calculated both boundary conditions and averaged the value for $\mathcal{E}_z(n_x, t)$. This results in a 0.001 reflection from the boundary as shown in Figure 23. I can determine if this is a general result or specific to this Gaussian pulse by examining the accuracy of the linear interpolation I used in Section 5.1. The accuracy of this linear interpolation is determined by expanding the function values, $f(\pm\frac{1}{2})$, as Taylor series about the interpolated point, $f(0)$, where $f(0)$ represents $\mathcal{E}_z(x - \frac{\Delta x}{2})$,

$$f(\tfrac{1}{2}) = f(0) + \tfrac{1}{2}f'(0) + \tfrac{1}{2}\left(\tfrac{1}{2}\right)^2 f''(0) + \tfrac{1}{6}\left(\tfrac{1}{2}\right)^3 f'''(0) + \tfrac{1}{24}\left(\tfrac{1}{2}\right)^4 f''''(0) + \cdots \tag{94a}$$

$$f(-\tfrac{1}{2}) = f(0) - \tfrac{1}{2}f'(0) + \tfrac{1}{2}\left(\tfrac{1}{2}\right)^2 f''(0) - \tfrac{1}{6}\left(\tfrac{1}{2}\right)^3 f'''(0) + \tfrac{1}{24}\left(\tfrac{1}{2}\right)^4 f''''(0) - \cdots . \tag{94b}$$

Then the error in the linear interpolation formula,

$$f_{\text{linear}}(0) = f(0) + \tfrac{1}{8}f''(0) + \tfrac{1}{384}f''''(0) + \cdots , \tag{95}$$

is dependent on the values of the second, fourth, and higher-order even derivatives of the function. Next, I examine the accuracy of the quadratic interpolation combining Equation (88),

$$f_{\text{quadratic}}(0) = \frac{3}{8}f(\tfrac{1}{2}) + \frac{3}{4}f(-\tfrac{1}{2}) - \frac{1}{8}f(-\tfrac{3}{2}), \tag{96}$$

with the Taylor series for $f(-\frac{3}{2})$,

$$f(-\tfrac{3}{2}) = f(0) - \tfrac{3}{2}f'(0) + \tfrac{1}{2}\left(\tfrac{3}{2}\right)^2 f''(0) - \tfrac{1}{6}\left(\tfrac{3}{2}\right)^3 f'''(0) + \tfrac{1}{24}\left(\tfrac{3}{2}\right)^4 f''''(0) - \cdots , \tag{97}$$

then

$$f_{\text{quadratic}}(0) = f(0) + \tfrac{1}{16} f'''(0) - \tfrac{3}{128} f''''(0) + \cdots . \tag{98}$$

I see that if the second derivative is half the third derivative then the results would be roughly of the same magnitude.

5.3 Third Order One-Way Propagation Boundary Condition

The averaging of the first and second order equations is not a mathematically general solution and depends on the relative magnitudes of the derivatives. So I continue to the Lagrange four point interpolation formula from [21, Eq. 25.2.13] and get

$$f_{\text{cubic}}(0) = \tfrac{5}{16} f(\tfrac{1}{2}) + \tfrac{15}{16} f(-\tfrac{1}{2}) - \tfrac{5}{16} f(-\tfrac{3}{2}) + \tfrac{1}{16} f(-\tfrac{5}{2}). \tag{99}$$

Using the Taylor series from Equation (94), Equation (97), and that for $x = 5/2$, I get

$$f_{\text{cubic}}(0) = f(0) + \tfrac{5}{128} f''''(0) + \cdots . \tag{100}$$

Following the same steps as for the linear and quadratic interpolations I get

$$\mathcal{E}_z(n_x, t) = \frac{\left(\frac{\eta d_b}{\Delta x} - \frac{15}{8}\right) \mathcal{E}_z(n_x - 1, t) + \frac{5}{8}\mathcal{E}_z(n_x - 2, t) - \frac{1}{8}\mathcal{E}_z(n_x - 3, t) - \eta(1 + d_a)\mathcal{H}_y(n_x - 1, t - \frac{\Delta t}{2})}{\left(\frac{\eta d_b}{\Delta x} + \frac{5}{8}\right)}. \tag{101}$$

The resulting boundary condition in free space is

$$\mathcal{E}_z(n_x, t) = \frac{\left(\frac{c\Delta t}{\Delta x} - \frac{15}{8}\right) \mathcal{E}_z(n_x - 1, t) + \frac{5}{8}\mathcal{E}_z(n_x - 2, t) - \frac{1}{8}\mathcal{E}_z(n_x - 3, t) - 2\eta\mathcal{H}_y(n_x - 1, t - \frac{\Delta t}{2})}{\left(\frac{c\Delta t}{\Delta x} + \frac{5}{8}\right)}. \tag{102}$$

As shown in Figure 24, the reflection from this boundary condition is slightly larger than the second order boundary condition implying either the spatial interpolation is not converging, which is highly unlikely for a smooth function like this Gaussian pulse, or another source of error.

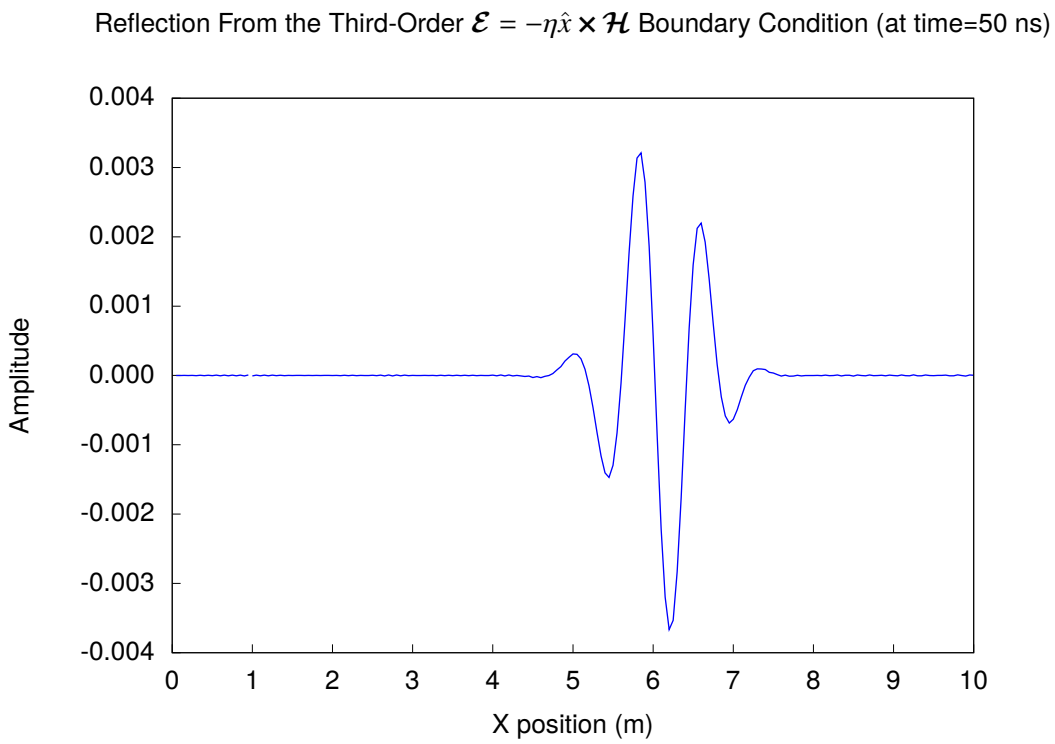

Figure 24—Reflection of a modulated Gaussian pulse (f_c = 300 MHz, f_{BW} = 300 MHz) from the third-order $\mathcal{E} = -\eta\hat{x} \times \mathcal{H}$ boundary condition with $\Delta x = 0.05$ meters and $\Delta t = \Delta x/(c\sqrt{2})$ at time = 50 ns.

5.4 Temporal Second Order One-Way Propagation Boundary Condition

So far I have not considered the error effect of linear interpolation in time. As a first step I start with spatial linear and temporal quadratic interpolation at $(x-\frac{\Delta x}{2}, t)$,

$$\mathcal{E}_z(n_x,t)+\mathcal{E}_z(n_x-1,t)=-\eta\left[\frac{3}{4}\mathcal{H}_y(n_x-1,t+\tfrac{\Delta t}{2})+\frac{3}{2}\mathcal{H}_y(n_x-1,t-\tfrac{\Delta t}{2})-\frac{1}{4}\mathcal{H}_y(n_x-1,t-\tfrac{3\Delta t}{2})\right]. \quad (103)$$

For the future $\mathcal{H}_y$ field I use Equation (57),

$$\mathcal{H}_y(n_x-1,t+\tfrac{\Delta t}{2})=d_a\mathcal{H}_y(n_x-1,t-\tfrac{\Delta t}{2})+\frac{d_b}{\Delta x}\left[\mathcal{E}_z(n_x,t)-\mathcal{E}_z(n_x-1,t)\right], \quad (104)$$

to get

$$\begin{aligned}\mathcal{E}_z(n_x,t)=-\mathcal{E}_z(n_x-1,t)-\eta\left[\frac{3}{2}\left(1+\frac{d_a}{2}\right)\mathcal{H}_y(n_x-1,t-\tfrac{\Delta t}{2})-\frac{1}{4}\mathcal{H}_y(n_x-1,t-\tfrac{3\Delta t}{2})\right.\\ \left.+\frac{3d_b}{4\Delta x}\left[\mathcal{E}_z(n_x,t)-\mathcal{E}_z(n_x-1,t)\right]\right].\end{aligned} \quad (105)$$

Combining the $\mathcal{E}_z(n_x,t)$ terms

$$\left(\frac{3\eta d_b}{4\Delta x}+1\right)\mathcal{E}_z(n_x,t)=\left(\frac{3\eta d_b}{4\Delta x}-1\right)\mathcal{E}_z(n_x-1,t)-\frac{3\eta}{2}\left(1+\frac{d_a}{2}\right)\mathcal{H}_y(n_x-1,t-\tfrac{\Delta t}{2})+\frac{\eta}{4}\mathcal{H}_y(n_x-1,t-\tfrac{3\Delta t}{2}), \quad (106)$$

then solving for $\mathcal{E}_z(n_x,t)$ I get

$$\mathcal{E}_z(n_x,t)=\frac{3\eta d_b-4\Delta x}{3\eta d_b+4\Delta x}\mathcal{E}_z(n_x-1,t)-\frac{3\eta(2+d_a)\Delta x}{3\eta d_b+4\Delta x}\mathcal{H}_y(n_x-1,t-\tfrac{\Delta t}{2})+\frac{\eta\Delta x}{3\eta d_b+4\Delta x}\mathcal{H}_y(n_x-1,t-\tfrac{3\Delta t}{2}). \quad (107)$$

For the $+x$ boundary condition in a free space region I get

$$\mathcal{E}_z(n_x,t)=\frac{3c\Delta t-4\Delta x}{3c\Delta t+4\Delta x}\mathcal{E}_z(n_x-1,t)-\frac{9\eta\Delta x}{3c\Delta t+4\Delta x}\mathcal{H}_y(n_x-1,t-\tfrac{\Delta t}{2})+\frac{\eta\Delta x}{3c\Delta t+4\Delta x}\mathcal{H}_y(n_x-1,t-\tfrac{3\Delta t}{2}). \quad (108)$$

Figure 25 unexpectedly shows an increase in the magnitude of the reflected pulse of approximately 0.0065 versus 0.0035 in Figures 21 and 22, for linear and quadratic interpolation, respectiviely. As I show in the next section, this is because the temporal error was canceling some of the spatial error in the linear interpolation. This is also why increasing the order of the spatial interpolation did not have the expected result of reducing the magnitude of the reflection.

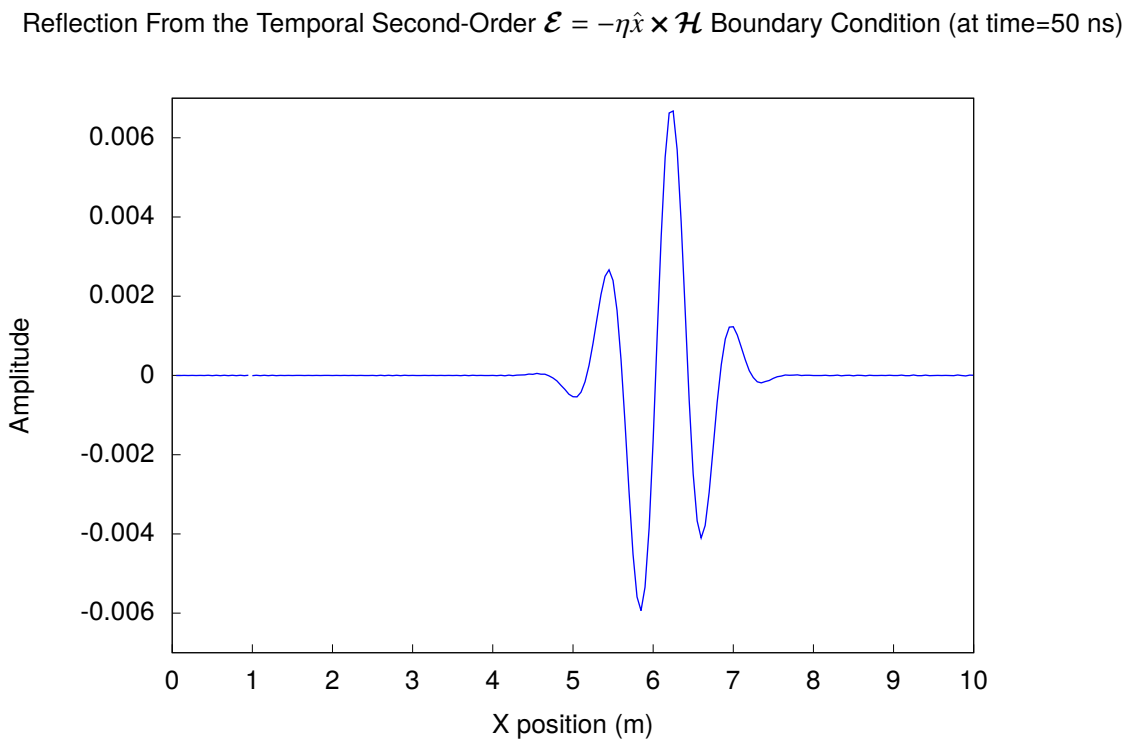

Figure 25—Reflection of a modulated Gaussian pulse (f_c = 300 MHz, f_{BW} = 300 MHz) from the temporal second-order $\mathcal{E} = -\eta\hat{x} \times \mathcal{H}$ boundary condition with $\Delta x = 0.05$ meters and $\Delta t = \Delta x/(c\sqrt{2})$ at time = 50 ns.

5.5 Spatial and Temporal Second Order One-Way Propagation Boundary Condition

To further explore the impacts of spatial and temporal quadratic interpolation, I combine the quadratic components of Equation (89) and Equation (103) to get

$$\frac{3}{4}\mathcal{E}_z(n_x,t)+\frac{3}{2}\mathcal{E}_z(n_x-1,t)-\frac{1}{4}\mathcal{E}_z(n_x-2,t)=-\eta\left[\frac{3}{4}\mathcal{H}_y(n_x-1,t+\tfrac{\Delta t}{2})+\frac{3}{2}\mathcal{H}_y(n_x-1,t-\tfrac{\Delta t}{2})-\frac{1}{4}\mathcal{H}_y(n_x-1,t-\tfrac{3\Delta t}{2})\right]. \tag{109}$$

Combining terms and rearranging I get

$$\frac{3}{4}\left(\frac{\eta d_b}{\Delta x}+1\right)\mathcal{E}_z(n_x,t)=\frac{3}{4}\left(\frac{\eta d_b}{\Delta x}-2\right)\mathcal{E}_z(n_x-1,t)+\frac{1}{4}\mathcal{E}_z(n_x-2,t)-\frac{3\eta}{4}(2+d_a)\mathcal{H}_y(n_x-1,t-\tfrac{\Delta t}{2})+\frac{\eta}{4}\mathcal{H}_y(n_x-1,t-\tfrac{3\Delta t}{2}). \tag{110}$$

Then solving for $\mathcal{E}_z(n_x,t)$ I get

$$\mathcal{E}_z(n_x,t)=\frac{\eta d_b-2\Delta x}{\eta d_b+\Delta x}\mathcal{E}_z(n_x-1,t)+\frac{\Delta x}{3\,(\eta d_b+\Delta x)}\mathcal{E}_z(n_x-2,t)-\frac{\eta\Delta x(2+d_a)}{\eta d_b+\Delta x)}\mathcal{H}_y(n_x-1,t-\tfrac{\Delta t}{2})+\frac{\eta\Delta x}{3\,(\eta d_b+\Delta x)}\mathcal{H}_y(n_x-1,t-\tfrac{3\Delta t}{2}). \tag{111}$$

For the $+x$ boundary condition in a free space region I get

$$\mathcal{E}_z(n_x,t)=\frac{c\Delta t-2\Delta x}{c\Delta t+\Delta x}\mathcal{E}_z(n_x-1,t)+\frac{\Delta x}{3\,(c\Delta t+\Delta x)}\mathcal{E}_z(n_x-2,t)-\frac{3\eta\Delta x}{c\Delta t+\Delta x}\mathcal{H}_y(n_x-1,t-\tfrac{\Delta t}{2})+\frac{\eta\Delta x}{3\,(c\Delta t+\Delta x)}\mathcal{H}_y(n_x-1,t-\tfrac{3\Delta t}{2}). \tag{112}$$

The corresponding $-x$ boundary condition is

$$\mathcal{E}_z(1,t)=\frac{c\Delta t-2\Delta x}{c\Delta t+\Delta x}\mathcal{E}_z(2,t)+\frac{\Delta x}{3\,(c\Delta t+\Delta x)}\mathcal{E}_z(3,t)+\frac{3\eta\Delta x}{c\Delta t+\Delta x}\mathcal{H}_y(1,t-\tfrac{\Delta t}{2})-\frac{\eta\Delta x}{3\,(c\Delta t+\Delta x)}\mathcal{H}_y(1,t-\tfrac{3\Delta t}{2}). \tag{113}$$

The results of using this boundary condition are shown in Figure 26 with a 0.0018 reflection (-55 dB) from the boundary. Given that increasing the order of the temporal interpolation produces a significant reduction in the magnitude of the reflection (from 0.0035 to 0.0018) I see that the error from the temporal linear interpolation was counteracting a portion of the error from the spatial linear interpolation thereby masking the expected improvement when going to spatial quadratic and cubic interpolation without an corresponding increase in the order of the temporal interpolation. For further reduction in the reflection from the one-way boundary condition I would need to continue to increase the order of both the temporal and spatial interpolations.

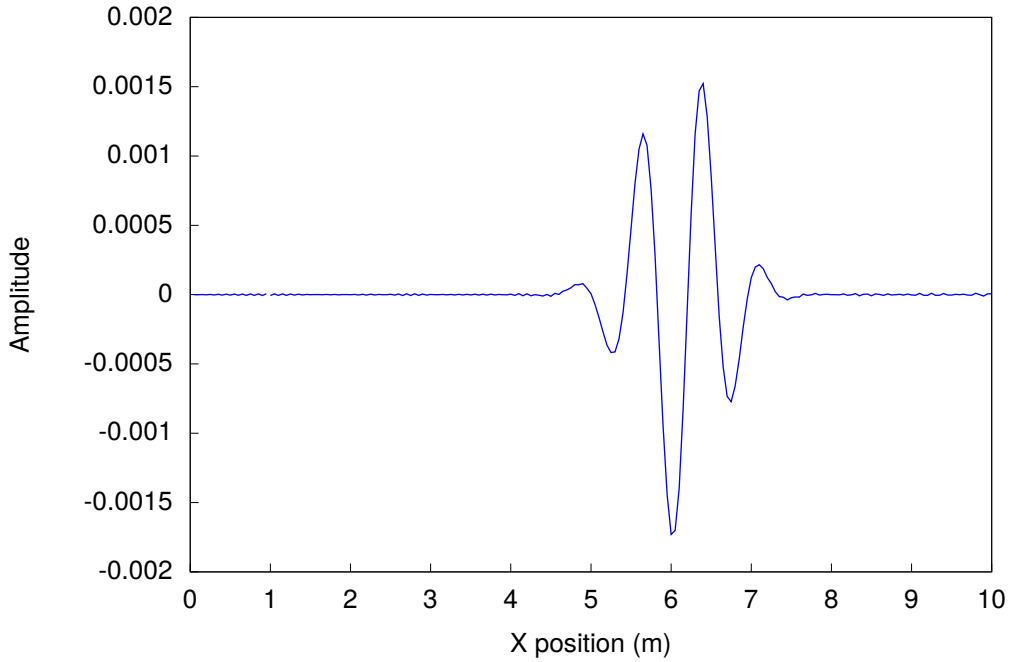

Figure 26—Reflection of a modulated Gaussian pulse (f_c = 300 MHz, f_{BW} = 300 MHz) from the spatial and temporal second order $\mathcal{E} = -\eta\hat{x} \times \mathcal{H}$ boundary condition with $\Delta x = 0.05$ meters and $\Delta t = \Delta x/(c\sqrt{2})$ at time = 50 ns.

5.6 Summary on One-Dimensional FDTD Boundary Conditions

Even though these developments are only for one-dimensional Yee FDTD grids, they are useful when creating secondary grids to generate the incident-fields for both the total-field/scattered-field method and the scattered-field method. Another use of these results is in development of boundary conditions for non-Yee FDTD methods, that is, techniques related to Yee FDTD but not using the standard Yee update equations. In the next section, I examine if the one-dimensional boundary conditions can be used in two-dimensional FDTD with field splitting as developed by Bérenger in 1994 [19].

6. BOUNDARY CONDITIONS IN TWO DIMENSIONS

Boundary conditions in two dimensions are significantly more complicated than in one-dimension. For example, the wave equation is factored only in an approximate sense, as shown in Section 6.1. As an alternative, in Section 6.2, I evaluate using the one-way propagation equations in two-dimensions. Then, in Section 6.3, I present an alternative formulation of the perfectly matched layer boundary condition.

6.1 Wave Equation Boundary Condition in Two Dimensions

First I consider the standard wave equation approach to boundary conditions in two dimensions. With only $\mathcal{E}_z$ field components and propagation in the $x-y$ plane, the electric field wave equation is written as

$$\frac{\partial^2 \mathcal{E}_z(x,y,t)}{\partial x^2} + \frac{\partial^2 \mathcal{E}_z(x,y,t)}{\partial y^2} - \frac{1}{c^2}\frac{\partial \mathcal{E}_z(x,y,t)}{\partial t} = 0, \tag{114}$$

which is written as

$$\left(\frac{\partial}{\partial x}+\frac{1}{c}\frac{\partial}{\partial t}\sqrt{1-S^2}\right)\left(\frac{\partial}{\partial x}-\frac{1}{c}\frac{\partial}{\partial t}\sqrt{1-S^2}\right)\mathcal{E}_z(x,y,t)=0, \tag{115}$$

where

$$S=\frac{c\dfrac{\partial}{\partial y}}{\dfrac{\partial}{\partial t}}. \tag{116}$$

As calculating $\sqrt{1-S^2}$ is not possible, the simplest solution is a single term Taylor series [9, Section 6.3.1],

$$\sqrt{1-S^2}\approx 1, \tag{117}$$

which is the same as the one-dimension wave equation and works best for plane waves incident perpendicular to a boundary. The simplest improvement is the two term Taylor series

$$\sqrt{1-S^2}\approx 1-\tfrac{1}{2}S^2. \tag{118}$$

Then the first term of Equation (115) (for the $+x$ boundary) is approximated as

$$\frac{\partial}{\partial x}+\frac{1}{c}\frac{\partial}{\partial t}\left[1-\frac{S^2}{2}\right] \tag{119a}$$

$$\frac{\partial}{\partial x}+\frac{1}{c}\frac{\partial}{\partial t}\left[1-\frac{1}{2}\left(\frac{c\dfrac{\partial}{\partial y}}{\dfrac{\partial}{\partial t}}\right)^2\right] \tag{119b}$$

$$\frac{\partial}{\partial x}+\frac{1}{c}\frac{\partial}{\partial t}-\frac{c}{2}\frac{\partial^2}{\partial y^2}\Big/\frac{\partial}{\partial t} \tag{119c}$$

which is transformed into the differential equation [9, Section 6.3.1]

$$\frac{\partial^2\mathcal{E}_z}{\partial x\partial t}+\frac{1}{c}\frac{\partial^2\mathcal{E}_z}{\partial t^2}-\frac{c}{2}\frac{\partial^2\mathcal{E}_z}{\partial y^2}=0 \tag{120}$$

for the $+x$ boundary and similarly for the other boundaries. These equations are the basis of the Mur boundary conditions and only achieve a -25 to -40 dB reduction in the reflected signal [9, Section 6.3.2]. Padé and other rational functions have been applied to approximate $\sqrt{1-S^2}$; however, these higher-order approximations do not result in a significant reduction in the reflected signal [9, Section 6.3.4]. Due to the complexity and limitations of the wave-equation approach, I instead consider the application of the one-way propagation equations next.

6.2 First-Order One-Way Propagation Boundary Condition in Two Dimensions

I consider the $\mathcal{E} = \pm\eta\hat{n} \times \mathcal{H}$ approach to boundary conditions in two dimensions. With only $\mathcal{E}_z$ field components and propagation in the $x-y$ plane, Equation (49) gives us

$$\mathcal{E}_z(x,y,t) = \begin{cases} -\eta\mathcal{H}_y(x,y,t) & \text{at } +x \text{ boundary} \\ \eta\mathcal{H}_y(x,y,t) & \text{at } -x \text{ boundary} \\ \eta\mathcal{H}_x(x,y,t) & \text{at } +y \text{ boundary} \\ -\eta\mathcal{H}_x(x,y,t) & \text{at } -y \text{ boundary.} \end{cases} \tag{121}$$

The FDTD grid in two dimensions is defined as a n_x by n_y grid with a uniform spatial separation of Δx in both dimensions.[6] Then, for a free space region with the array notation, the first-order boundary condition is given by

$$\mathcal{E}_z(n_x,y,t) = b_a\mathcal{E}_z(n_x-1,y,t) - b_b\mathcal{H}_y(n_x-1,y,t-\tfrac{\Delta t}{2}) \tag{122a}$$

$$\mathcal{E}_z(1,y,t) = b_a\mathcal{E}_z(2,y,t) + b_b\mathcal{H}_y(1,y,t-\tfrac{\Delta t}{2}) \tag{122b}$$

$$\mathcal{E}_z(x,n_y,t) = b_a\mathcal{E}_z(x,n_y-1,t) + b_b\mathcal{H}_x(x,n_y-1,t-\tfrac{\Delta t}{2}) \tag{122c}$$

$$\mathcal{E}_z(x,1,t) = b_a\mathcal{E}_z(x,2,t) - b_b\mathcal{H}_x(x,1,t-\tfrac{\Delta t}{2}). \tag{122d}$$

where

$$b_a = \frac{c\Delta t - \Delta x}{c\Delta t + \Delta x} \tag{123a}$$

$$b_b = \frac{2\eta\Delta x}{c\Delta t + \Delta x}. \tag{123b}$$

To test boundary conditions in two-dimensional FDTD, I introduce a modulated Gaussian pulse as an electric field at the center of the FDTD grid, as shown in Figure 27 after the pulse has propagated out from the center but before reaching the borders. Figure 28 shows the same test after the pulse has interacted with the boundaries for the case with boundary conditions only implemented on the $\pm x$ boundaries. With the reflections from the $\pm y$ boundaries, the reflections from the $\pm x$ boundaries are barely visible. Two time slices are shown in Figure 29 where all four boundary conditions from Equation (122) have been implemented. Here I see that the fields reflected from the boundaries have been reduced by approximately the same amount as in one dimension with this boundary condition but not immediately. However, the one-way propagation boundary conditions in Sections 5.2 – 5.5 fail when applied using Equation (49) to directly zero the field reflected from each boundary. In the next section, I consider an alternative formulation of the perfectly matched layer boundary condition, and from an examination of the PML method I see that a better application of Equation (49) to the two-dimensional problem is formulated.

[6] The spatial grid is different in x and y; however, here I are making them the same to simplify the development.

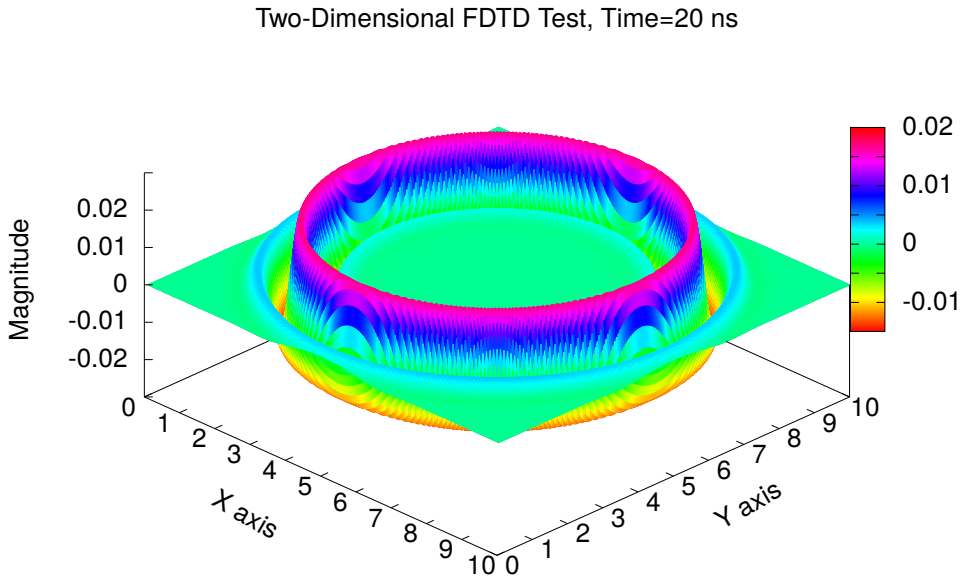

Figure 27—Propagation of a modulated Gaussian pulse (f_c = 300 MHz, f_{BW} = 300 MHz) in a two-dimensional FDTD grid after 20 ns with $\Delta x = 0.05$ meters and $\Delta t = \Delta x/(c\sqrt{2})$.

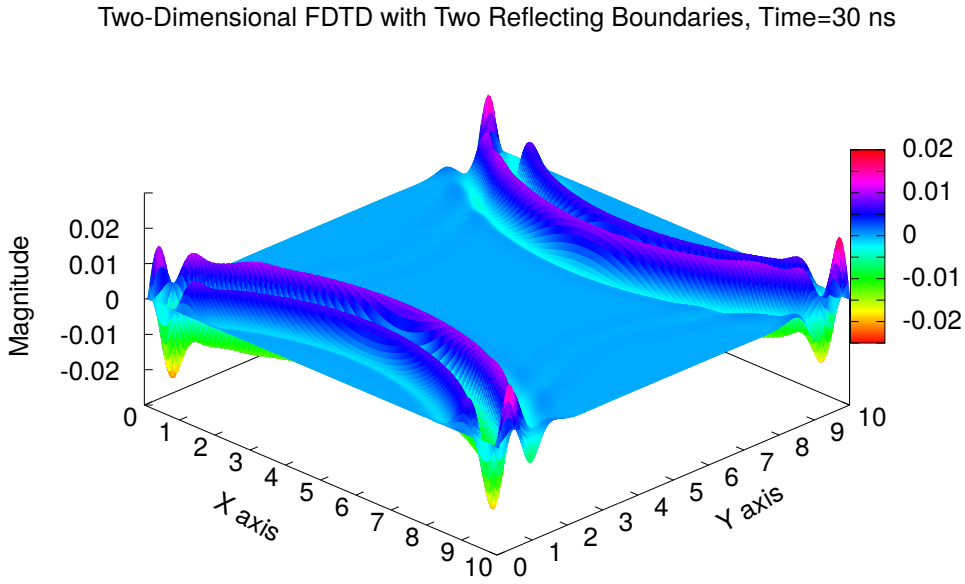

Figure 28—Propagation of a modulated Gaussian pulse (f_c = 300 MHz, f_{BW} = 300 MHz) in a two-dimensional FDTD grid after 30 ns with $\pm x$ first-order $\boldsymbol{\mathcal{E}} = -\eta\hat{x} \times \boldsymbol{\mathcal{H}}$ boundary conditions for $\Delta x = 0.05$ meters and $\Delta t = \Delta x/(c\sqrt{2})$.

a) Two-Dimensional FDTD with $\boldsymbol{\mathcal{E}} = -\eta\hat{x} \times \boldsymbol{\mathcal{H}}$ Boundary Condition, Time=25 ns

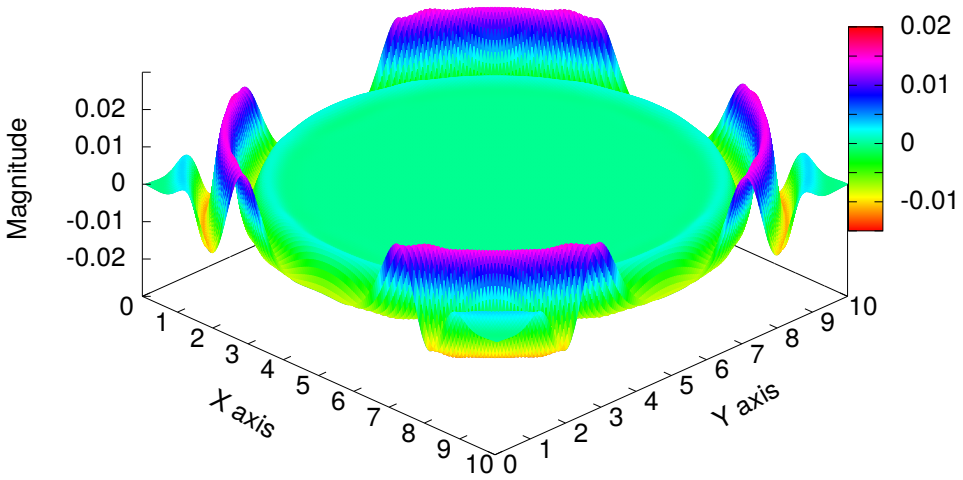

b) Two-Dimensional FDTD with $\boldsymbol{\mathcal{E}} = -\eta\hat{x} \times \boldsymbol{\mathcal{H}}$ Boundary Condition, Time=30 ns

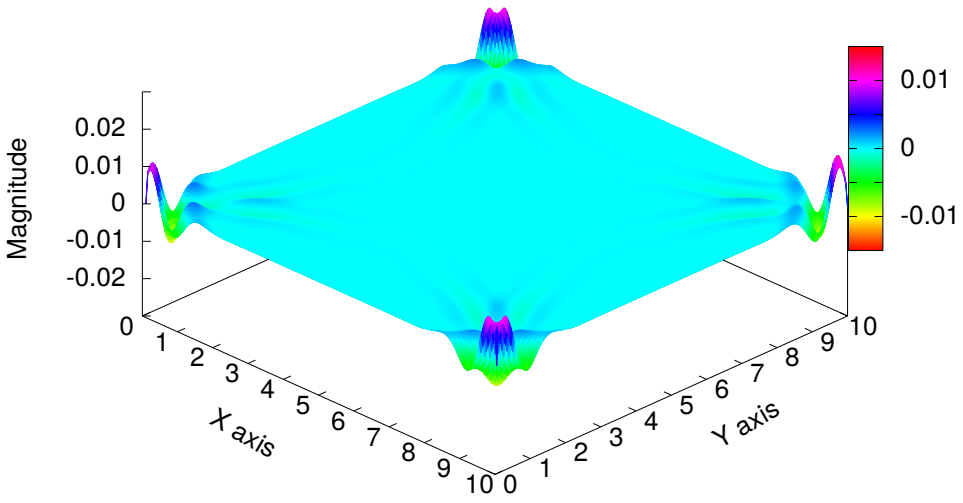

Figure 29—Propagation of a modulated Gaussian pulse (f_c = 300 MHz, f_{BW} = 300 MHz) in a two-dimensional FDTD grid after 25 ns (a) and 30 ns (b) with the first-order $\boldsymbol{\mathcal{E}} = -\eta\hat{x} \times \boldsymbol{\mathcal{H}}$ boundary conditions for $\Delta x = 0.05$ meters and $\Delta t = \Delta x/(c\sqrt{2})$.

a) Two-Dimensional FDTD with $\mathcal{E} = -\eta\hat{x} \times \mathcal{H}$ Boundary Condition, Time=35 ns

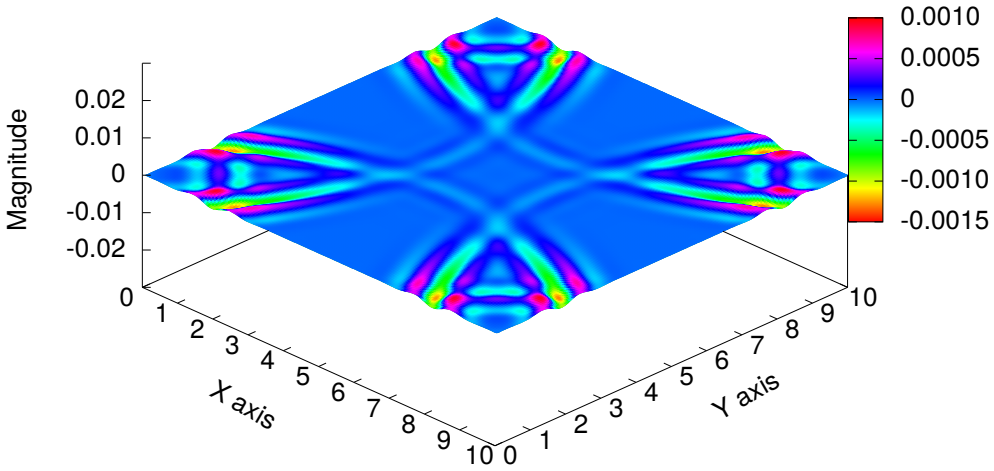

b) Two-Dimensional FDTD with $\mathcal{E} = -\eta\hat{x} \times \mathcal{H}$ Boundary Condition, Time=40 ns

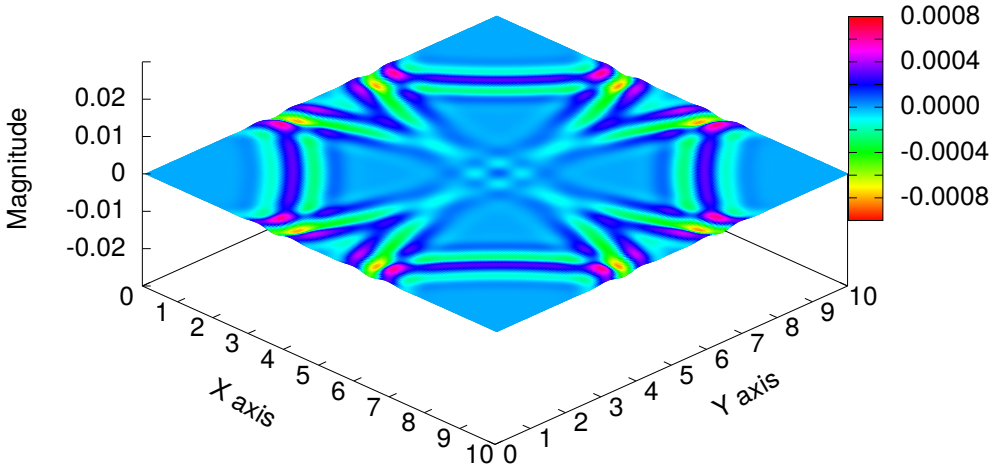

Figure 30—Propagation of a modulated Gaussian pulse (f_c = 300 MHz, f_{BW} = 300 MHz) in a two-dimensional FDTD grid after 35 ns (a) and 40 ns (b) with the first-order $\mathcal{E} = -\eta\hat{x} \times \mathcal{H}$ boundary conditions for $\Delta x = 0.05$ meters and $\Delta t = \Delta x/(c\sqrt{2})$.

6.3 Perfectly Matched Layer Boundary Condition in Two Dimensions

The PML boundary condition is a series of artificial lossy anisotropic material layers surrounding the FDTD space [19]. First developed by Bérenger in 1994, the PML method achieves very high reductions in the reflection from the exterior boundaries of an FDTD grid. For a two-dimensional FDTD grid with only $\mathcal{E}_z$ field components and propagation in the $x-y$ plane, the modified Maxwell's equations forming the basis of the PML method are given by [9, Section 7.3.2]

$$\mu\frac{\partial\mathcal{H}_x(t)}{\partial t}+\sigma_y^*\mathcal{H}_x(t)=-\frac{\partial\mathcal{E}_z(t)}{\partial y}, \tag{124a}$$

$$\mu\frac{\partial\mathcal{H}_y(t)}{\partial t}+\sigma_x^*\mathcal{H}_y(t)=\frac{\partial\mathcal{E}_z(t)}{\partial x}, \tag{124b}$$

$$\epsilon\frac{\partial\mathcal{E}_{zx}(t)}{\partial t}+\sigma_x\mathcal{E}_{zx}(t)=\frac{\partial\mathcal{H}_y(t)}{\partial x}, \tag{124c}$$

$$\epsilon\frac{\partial\mathcal{E}_{zy}(t)}{\partial t}+\sigma_y\mathcal{E}_{zy}(t)=-\frac{\partial\mathcal{H}_x(t)}{\partial y}, \tag{124d}$$

where $\mathcal{E}_z(t)=\mathcal{E}_{zx}(t)+\mathcal{E}_{zy}(t)$. If $\sigma_x=\sigma_y=\sigma$ and $\sigma_x^*=\sigma_y^*=\sigma^*$ I transform Equation (124) into Maxwell's equations for isotropic materials in two dimensions, see Equation (15).

The reflection of a plane wave incident perpendicular to an interface between two materials is zero if $\mu_1/\epsilon_1=\mu_2/\epsilon_2$ and $\sigma^*/\mu=\sigma/\epsilon$ in both materials [9, Section 7.2]. The split-field formulation of the PML method extends the zero reflection to off-axis incidence under the same restrictions [9, Section 7.3.1]. A plane wave propagating in the x direction will only be attenuated if σ_x or σ_x^* are nonzero. Similarly, a plane wave propagating in the y direction will only be attenuated if σ_y or σ_y^* are nonzero. Therefore, one solution for a PML boundary is a series of materials with an increasing conductivity $(\sigma_{(x,y)},\sigma^*_{(x,y)})$ that minimizes the reflection while absorbing waves incident on the boundary before they reach the outer FDTD grid boundary and reflect back. A simple isotropic material ($\sigma_x=\sigma_y$, $\sigma_x^*=\sigma_y^*$) will not work well because it would distort waves propagating parallel to the boundary [9, Section 7.1].

An alternative to optimizing the conductivity profile versus reflection is to gradually zero the FDTD equation parameters (c_a,c_b,d_a,d_b) with a continuous function starting at the edge of the PML boundary and transitioning toward zero at the outer edge of the FDTD grid. As this approach is more closely tied to the FDTD equations the implementation is less complex. One choice is the cosine function, where I define the FDTD equation parameters in the PML region by

$$c_{a,s}=c_a\cos\left(\frac{0.3\pi s}{N_{PML}}\right), \tag{125a}$$

$$c_{b,s}=c_b\cos\left(\frac{0.3\pi s}{N_{PML}}\right), \tag{125b}$$

$$d_{a,s}=d_a\cos\left(\frac{0.3\pi s}{N_{PML}}\right), \tag{125c}$$

$$d_{b,s}=d_b\cos\left(\frac{0.3\pi s}{N_{PML}}\right), \tag{125d}$$

where s is the distance from outer most non-PML grid point to the PML grid point. In Figure 31 I explain the PML method by placing notational FDTD update equations in the appropriate locations in the $-x/+y$ quadrant of a simplified two-dimensional FDTD grid with a nominal two cell PML boundary.

$c_{a,1.5}\mathcal{E}_{zx} + c_{b,1.5}\Delta\mathcal{H}_y$ $c_{a,1.5}\mathcal{E}_{zy} + c_{b,1.5}\Delta\mathcal{H}_x$	$d_{a,1}\mathcal{H}_y + d_{b,1}\Delta\mathcal{E}_z$	$c_{a,0.5}\mathcal{E}_{zx} + c_{b,0.5}\Delta\mathcal{H}_y$ $c_{a,1.5}\mathcal{E}_{zy} + c_{b,1.5}\Delta\mathcal{H}_x$	$d_a\mathcal{H}_y + d_b\Delta\mathcal{E}_z$	$c_a\mathcal{E}_{zx} + c_b\Delta\mathcal{H}_y$ $c_{a,1.5}\mathcal{E}_{zy} + c_{b,1.5}\Delta\mathcal{H}_x$
$d_{a,1}\mathcal{H}_x + d_{b,1}\Delta\mathcal{E}_z$		$d_{a,1}\mathcal{H}_x + d_{b,1}\Delta\mathcal{E}_z$		$d_{a,1}\mathcal{H}_x + d_{b,1}\Delta\mathcal{E}_z$
$c_{a,1.5}\mathcal{E}_{zx} + c_{b,1.5}\Delta\mathcal{H}_y$ $c_{a,0.5}\mathcal{E}_{zy} + c_{b,0.5}\Delta\mathcal{H}_x$	$d_{a,1}\mathcal{H}_y + d_{b,1}\Delta\mathcal{E}_z$	$c_{a,0.5}\mathcal{E}_{zx} + c_{b,0.5}\Delta\mathcal{H}_y$ $c_{a,0.5}\mathcal{E}_{zy} + c_{b,0.5}\Delta\mathcal{H}_x$	$d_a\mathcal{H}_y + d_b\Delta\mathcal{E}_z$	$c_a\mathcal{E}_{zx} + c_b\Delta\mathcal{H}_y$ $c_{a,0.5}\mathcal{E}_{zy} + c_{b,0.5}\Delta\mathcal{H}_x$
$d_a\mathcal{H}_x + d_b\Delta\mathcal{E}_z$		$d_a\mathcal{H}_x + d_b\Delta\mathcal{E}_z$		$d_a\mathcal{H}_x + d_b\Delta\mathcal{E}_z$
$c_{a,1.5}\mathcal{E}_{zx} + c_{b,1.5}\Delta\mathcal{H}_y$ $c_a\mathcal{E}_{zy} + c_b\Delta\mathcal{H}_x$	$d_{a,1}\mathcal{H}_y + d_{b,1}\Delta\mathcal{E}_z$	$c_{a,0.5}\mathcal{E}_{zx} + c_{b,0.5}\Delta\mathcal{H}_y$ $c_a\mathcal{E}_{zy} + c_b\Delta\mathcal{H}_x$	$d_a\mathcal{H}_y + d_b\Delta\mathcal{E}_z$	$c_a\mathcal{E}_z + c_b\Delta\mathcal{H}_y$ $+c_b\Delta\mathcal{H}_x$

Figure 31—Symbolic representation of PML and FDTD equations in a subsection of a two-dimensional FDTD grid.

In Figure 31, the conventional FDTD update equations as a reduced form of Equation (20) are the equations with conventional FDTD parameters represented as follows

$$d_a\mathcal{H}_x + d_b\Delta\mathcal{E}_z \rightarrow \mathcal{H}_x = d_a\mathcal{H}_x - \frac{d_b}{\Delta y}\left[\mathcal{E}_z(+\Delta y) - \mathcal{E}_z\right] \tag{126a}$$

$$d_a\mathcal{H}_y + d_b\Delta\mathcal{E}_z \rightarrow \mathcal{H}_y = d_a\mathcal{H}_y + \frac{d_b}{\Delta x}\left[\mathcal{E}_z(+\Delta x) - \mathcal{E}_z\right] \tag{126b}$$

$$c_a\mathcal{E}_z + c_b\Delta\mathcal{H}_y + c_b\Delta\mathcal{H}_x \rightarrow \mathcal{E}_z = c_a\mathcal{E}_z + \frac{c_b}{\Delta x}\left[\mathcal{H}_y(+\tfrac{\Delta x}{2}) - \mathcal{H}_y(-\tfrac{\Delta x}{2})\right] \tag{126c}$$

$$- \frac{c_b}{\Delta y}\left[\mathcal{H}_x(+\tfrac{\Delta y}{2}) - \mathcal{H}_x(-\tfrac{\Delta y}{2})\right]. \tag{126d}$$

The PML equations in the $-x$ boundary region with the subscripted FDTD parameters from Equation (125) are given by

$$d_{a,s}\mathcal{H}_y + d_{b,s}\Delta\mathcal{E}_z \rightarrow \mathcal{H}_y = d_{a,s}\mathcal{H}_y + \frac{d_{b,s}}{\Delta x}\left[\mathcal{E}_z(+\Delta x) - \mathcal{E}_z\right] \tag{127a}$$

$$c_{a,s}\mathcal{E}_{zx} + c_{b,s}\Delta\mathcal{H}_y \rightarrow \mathcal{E}_{zx} = c_{a,s}\mathcal{E}_{zx} + \frac{c_{b,s}}{\Delta x}\left[\mathcal{H}_y(+\tfrac{\Delta x}{2}) - \mathcal{H}_y(-\tfrac{\Delta x}{2})\right]. \tag{127b}$$

Similarly, the PML equations in the $+y$ boundary region are given by

$$d_{a,s}\mathcal{H}_x + d_{b,s}\Delta\mathcal{E}_z \rightarrow \mathcal{H}_x = d_{a,s}\mathcal{H}_x - \frac{d_{b,s}}{\Delta y}\left[\mathcal{E}_z(+\Delta y) - \mathcal{E}_z\right] \tag{128a}$$

$$c_{a,s}\mathcal{E}_{zy} + c_{b,s}\Delta\mathcal{H}_x \rightarrow \mathcal{E}_{zy} = c_{a,s}\mathcal{E}_{zy} - \frac{c_{b,s}}{\Delta y}\left[\mathcal{H}_x(+\tfrac{\Delta y}{2}) - \mathcal{H}_x(-\tfrac{\Delta y}{2})\right]. \tag{128b}$$

To compare the cosine tapered PML boundary condition versus conventional requirements for a PML boundary condition, I first review the FDTD equation parameters,

$$c_a = \frac{2\epsilon - \sigma\Delta t}{2\epsilon + \sigma\Delta t}, \tag{129a}$$

$$c_b = \frac{2\Delta t}{2\epsilon + \sigma\Delta t}, \tag{129b}$$

$$d_a = \frac{2\mu - \sigma^*\Delta t}{2\mu + \sigma^*\Delta t}, \tag{129c}$$

$$d_b = \frac{2\Delta t}{2\mu + \sigma^*\Delta t}. \tag{129d}$$

Solving for the FDTD material parameters in terms of the FDTD equation parameters, I get

$$\epsilon = \frac{\Delta t}{2c_b}\left(1 + c_a\right), \tag{130a}$$

$$\sigma = \frac{1 - c_a}{c_b}, \tag{130b}$$

$$\mu = \frac{\Delta t}{2d_b}\left(1 + d_a\right), \tag{130c}$$

$$\sigma^* = \frac{1 - d_a}{d_b}. \tag{130d}$$

$$\tag{130e}$$

For a multiplication factor of a between the PML equation parameters, i.e. $c_{a,2} = ac_{a,1}$, I see that the conditions for zero reflection,

$$\frac{\mu_2}{\epsilon_2} = \frac{\mu_1}{\epsilon_1}, \tag{131a}$$

$$\frac{c_b}{d_b}\frac{1 + ad_a}{1 + ac_a} = \frac{c_b}{d_b}\frac{1 + d_a}{1 + c_a}, \tag{131b}$$

$$\frac{1 + c_a}{1 + ac_a} = \frac{1 + d_a}{1 + ad_a}, \tag{131c}$$

and

$$\frac{\sigma^*}{\mu} = \frac{\sigma}{\epsilon}, \tag{132a}$$

$$\frac{1 - d_a}{1 + d_a} = \frac{1 - c_a}{1 + c_a}, \tag{132b}$$

are met for all layers of a PML for a free space region, because $c_a = d_a = 1$ in free space. For a PML layer in a non-free space region, the conditions for zero reflection are approximately met for all layers of the PML if $c_a \approx d_a$. From an evaluation of these equations I find that $c_a = d_a$ for all lossless materials and that $c_a \approx d_a$ unless a material is very lossy in which case very little energy will reach the PML boundary.

Numerical results for a ten cell cosine tapered PML boundary for a two-dimensional problem are shown in Figures 32 – 33. In this example, the PML region is within the FDTD region of the previous example so the fields in Figure 32 are reduced from those in Figure 29. This effect is more noticeable closer to the border. From a comparison of Figure 33 with Figure 30 I see that the ten cell tapered cosine PML boundary condition reflects approximately 25 times less energy (-28 dB) then the first-order, one-way boundary condition implemented as a direct application of the first-order, one-way propagation equation from Section 6.2.

The disadvantage of all PML boundary conditions is the need for between 10 and 20 extra cells around the FDTD grid adding to the computational and memory costs of FDTD. A second disadvantage of all PML boundary conditions is very complicated programming with nine different regions for two-dimensional problems and 27 different regions for three-dimensional problems with interfaces to adjacent regions. The complexity is reduced slightly by expanding the fields in the entire FDTD grid as split-fields. In the case of a two-dimensional problem, this reduces the number of different update equations to twelve equations from as many as 35 and eliminates the need for interface equations between the regions with a one-third memory increase. In this approach the PML update equations are modified by the multiplier from Equation (125). Alternatively, at a cost of a large increase in memory, the PML materials can be defined over the entire combined FDTD-PML grid. In the next section, I use insights from the formulation of the PML boundary condition to reformulate the one-way propagation boundary conditions of Sections 5 and 6.2 into a more correct form for two dimensions.

6.4 Split-Field One-Way Propagation Boundary Condition in Two Dimensions

As I consider the split-field formulation of the PML method versus the one-way propagation equation, Equation (49), it is apparent that for two-dimensional space the electric field is expanded as a sum of waves traveling in each of the four directions, that is, using the PML notation for $\pm x$ and $\pm y$ electric fields I get

$$\overleftarrow{\boldsymbol{\mathcal{E}}}_{zx} = \tfrac{1}{2}\left(\boldsymbol{\mathcal{E}}_{zx} + \eta\hat{x}\times\boldsymbol{\mathcal{H}}\right), \tag{133a}$$

$$\overrightarrow{\boldsymbol{\mathcal{E}}}_{zx} = \tfrac{1}{2}\left(\boldsymbol{\mathcal{E}}_{zx} - \eta\hat{x}\times\boldsymbol{\mathcal{H}}\right), \tag{133b}$$

$$\overleftarrow{\boldsymbol{\mathcal{E}}}_{zy} = \tfrac{1}{2}\left(\boldsymbol{\mathcal{E}}_{zy} + \eta\hat{y}\times\boldsymbol{\mathcal{H}}\right), \tag{133c}$$

$$\overrightarrow{\boldsymbol{\mathcal{E}}}_{zy} = \tfrac{1}{2}\left(\boldsymbol{\mathcal{E}}_{zy} - \eta\hat{y}\times\boldsymbol{\mathcal{H}}\right), \tag{133d}$$

where $\boldsymbol{\mathcal{E}}_{zx} = \overleftarrow{\boldsymbol{\mathcal{E}}}_{zx} + \overrightarrow{\boldsymbol{\mathcal{E}}}_{zx}$ and $\boldsymbol{\mathcal{E}}_{zy} = \overleftarrow{\boldsymbol{\mathcal{E}}}_{zy} + \overrightarrow{\boldsymbol{\mathcal{E}}}_{zy}$. Expanding the equations into the individual field components I get

$$\overleftarrow{\mathcal{E}}_{zx} = \tfrac{1}{2}\left(\mathcal{E}_{zx} + \eta\mathcal{H}_y\right) \tag{134a}$$

$$\overrightarrow{\mathcal{E}}_{zx} = \tfrac{1}{2}\left(\mathcal{E}_{zx} - \eta\mathcal{H}_y\right) \tag{134b}$$

$$\overleftarrow{\mathcal{E}}_{zy} = \tfrac{1}{2}\left(\mathcal{E}_{zy} - \eta\mathcal{H}_x\right) \tag{134c}$$

$$\overrightarrow{\mathcal{E}}_{zy} = \tfrac{1}{2}\left(\mathcal{E}_{zy} + \eta\mathcal{H}_x\right). \tag{134d}$$

a) Two-Dimensional FDTD with Cosine Tapered PML Boundary Condition, Time=25 ns

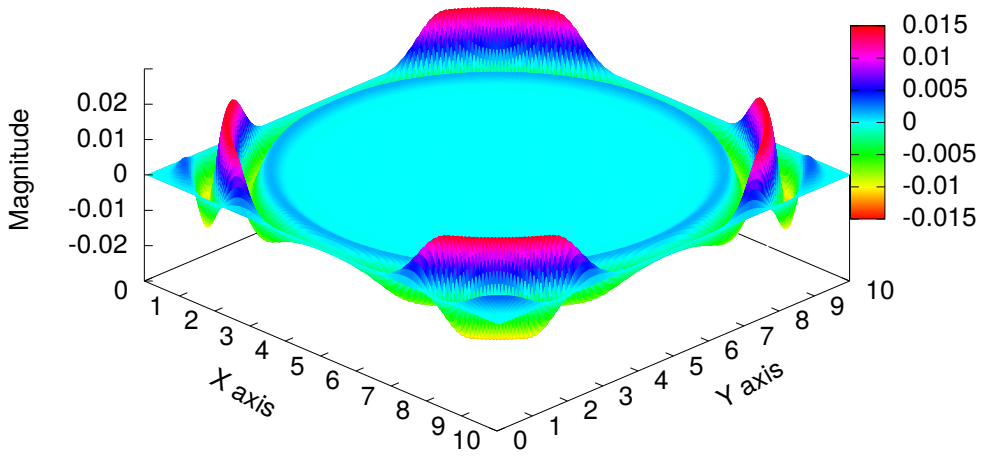

b) Two-Dimensional FDTD with Cosine Tapered PML Boundary Condition, Time=30 ns

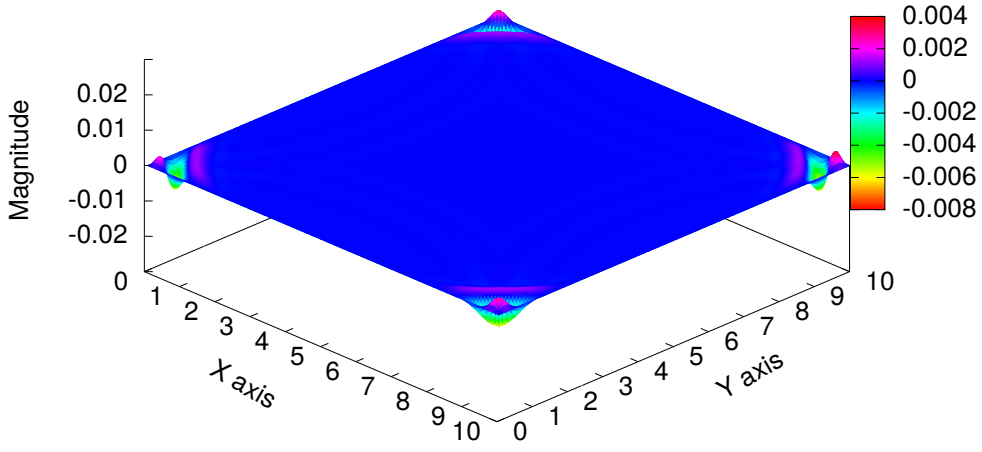

Figure 32—Propagation of a modulated Gaussian pulse (f_c = 300 MHz, f_{BW} = 300 MHz) in a two-dimensional FDTD grid after 25 ns (a) and 30 ns (b) with a ten cell cosine tapered PML boundary condition for $\Delta x = 0.05$ meters and $\Delta t = \Delta x/(c\sqrt{2})$.

a) Two-Dimensional FDTD with Cosine Tapered PML Boundary Condition, Time=35 ns

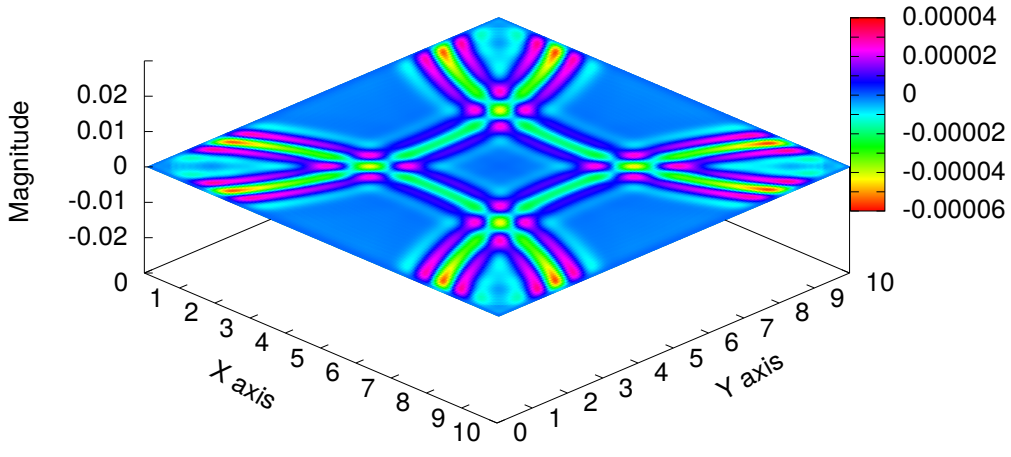

b) Two-Dimensional FDTD with Cosine Tapered PML Boundary Condition, Time=40 ns

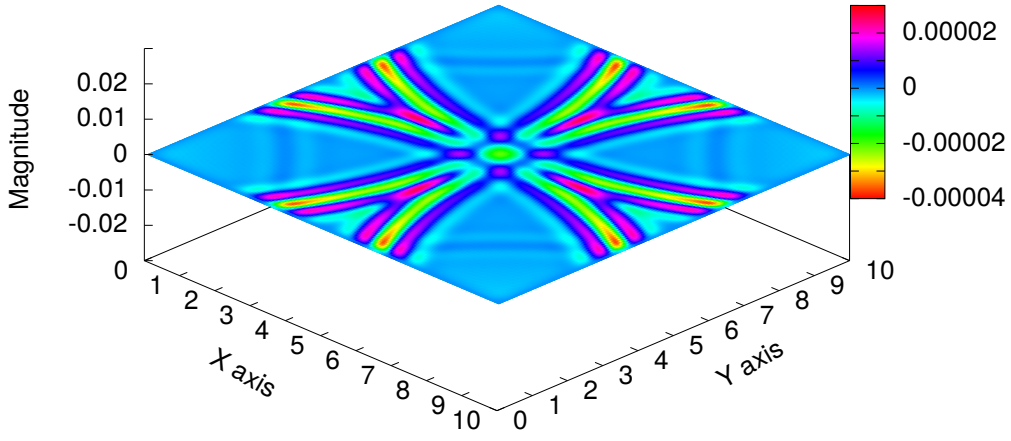

Figure 33—Propagation of a modulated Gaussian pulse (f_c = 300 MHz, f_{BW} = 300 MHz) in a two-dimensional FDTD grid after 35 ns (a) and 40 ns (b) with a ten cell cosine tapered PML boundary condition for $\Delta x = 0.05$ meters and $\Delta t = \Delta x/(c\sqrt{2})$.

Then, from Equation (86), I get the first-order, split-field, one-way propagation boundary condition for the $+x$ boundary to be

$$\mathcal{E}_{zx}(n_x, y, t) = \frac{c\Delta t - \Delta x}{c\Delta t + \Delta x}\mathcal{E}_{zx}(n_x - 1, y, t) - \frac{2\eta\Delta x}{c\Delta t + \Delta x}\mathcal{H}_y(n_x - 1, y, t - \tfrac{\Delta t}{2}). \tag{135}$$

The corresponding equations for the $-x$, $+y$, and $-y$ boundaries are

$$\mathcal{E}_{zx}(1, y, t) = \frac{c\Delta t - \Delta x}{c\Delta t + \Delta x}\mathcal{E}_{zx}(2, y, t) + \frac{2\eta\Delta x}{c\Delta t + \Delta x}\mathcal{H}_y(1, y, t - \tfrac{\Delta t}{2}), \tag{136a}$$

$$\mathcal{E}_{zy}(x, n_y, t) = \frac{c\Delta t - \Delta x}{c\Delta t + \Delta x}\mathcal{E}_{zy}(x, n_y - 1, t) + \frac{2\eta\Delta x}{c\Delta t + \Delta x}\mathcal{H}_x(x, n_y - 1, t - \tfrac{\Delta t}{2}), \tag{136b}$$

$$\mathcal{E}_{zy}(x, 1, t) = \frac{c\Delta t - \Delta x}{c\Delta t + \Delta x}\mathcal{E}_{zy}(x, 2, t) - \frac{2\eta\Delta x}{c\Delta t + \Delta x}\mathcal{H}_x(x, 1, t - \tfrac{\Delta t}{2}). \tag{136c}$$

The numerical results for this first-order, split-field, one-way propagation boundary condition are shown in Figures 34 – 35. From a comparison of Figure 35 with Figure 30, I see approximately a 30% (5 dB) reduction in the reflected energy from the boundary when combining the first-order, one-way boundary condition with the split-field concept in two dimensions. This is with the minimal cost of calculating the split electric field at one cell away from all boundaries. This indicates that a one-dimensional boundary condition can be applied to the split-field formulation and produce a low cost high-quality, two-dimensional boundary condition. However, further testing has shown that the spatial and temporal second-order, one-way propagation boundary condition from Section 5.5 is unstable when implemented in a split-field formulation.

a) Two-Dimensional FDTD with First-Order Split-Field One-Way Boundary Condition, Time=25 ns

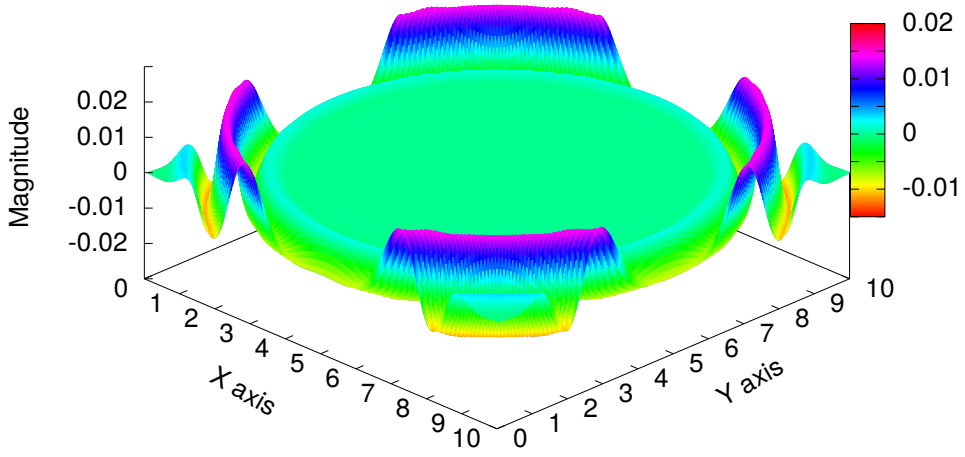

b) Two-Dimensional FDTD with First-Order Split-Field One-Way Boundary Condition, Time=30 ns

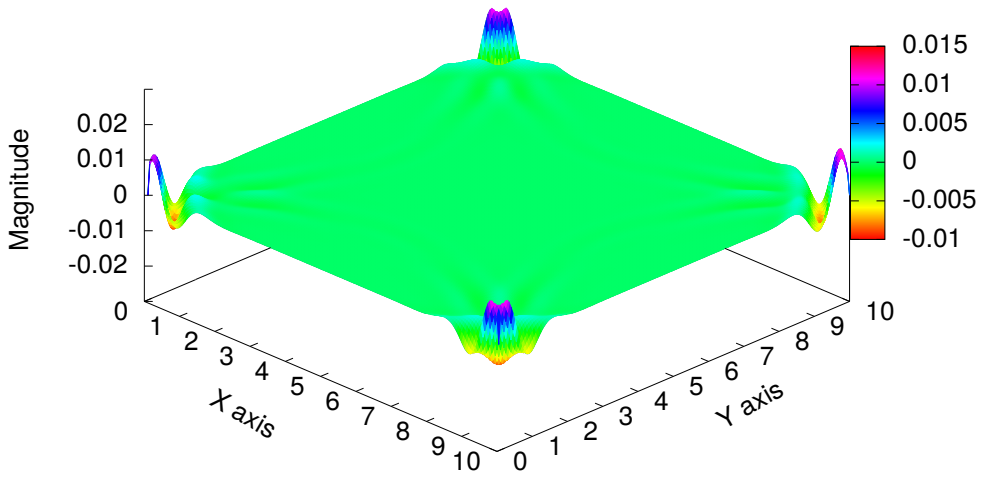

Figure 34—Propagation of a modulated Gaussian pulse (f_c = 300 MHz, f_{BW} = 300 MHz) in a two-dimensional FDTD grid after 25 ns (a) and 30 ns (b) with a first-order, split-field, one-way boundary condition for $\Delta x = 0.05$ meters and $\Delta t = \Delta x/(c\sqrt{2})$.

a) Two-Dimensional FDTD with First-Order Split-Field One-Way Boundary Condition, Time=35 ns

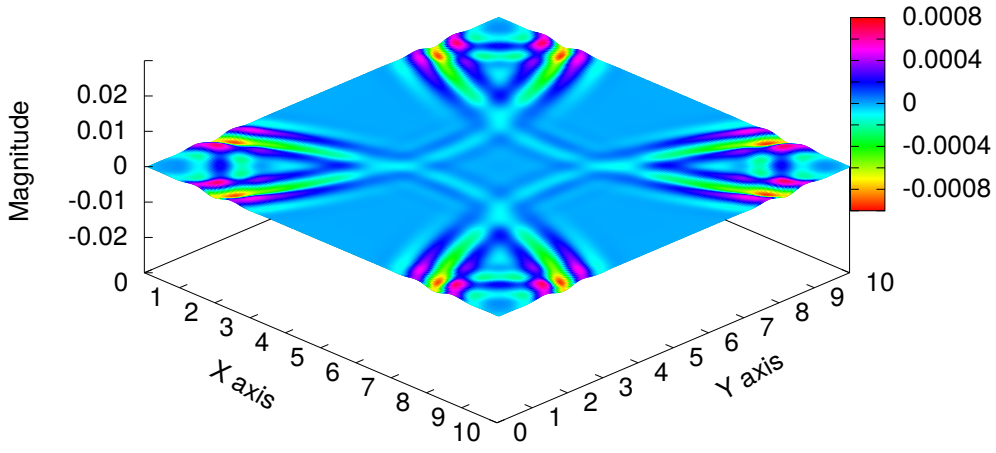

b) Two-Dimensional FDTD with First-Order Split-Field One-Way Boundary Condition, Time=40 ns

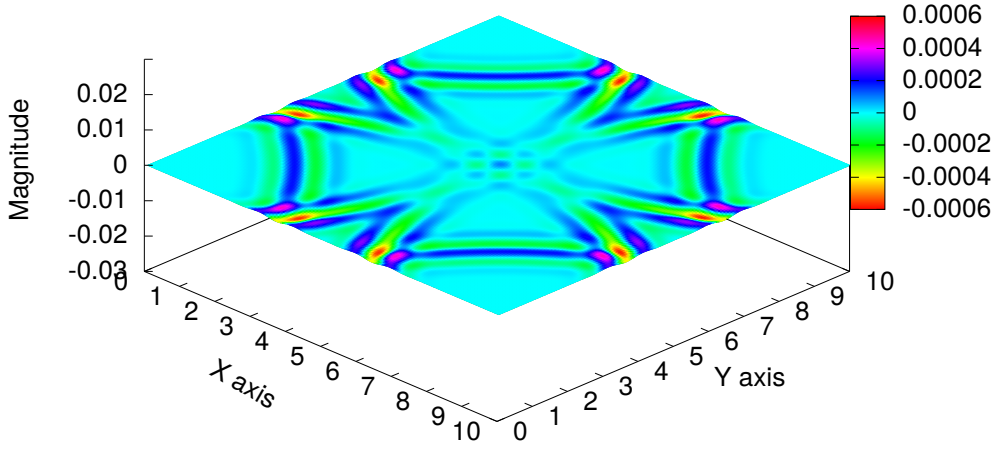

Figure 35—Propagation of a modulated Gaussian pulse (f_c = 300 MHz, f_{BW} = 300 MHz) in a two-dimensional FDTD grid after 35 ns (a) and 40 ns (b) with a first-order, split-field, one-way boundary condition for $\Delta x = 0.05$ meters and $\Delta t = \Delta x/(c\sqrt{2})$.

7. CONCLUSION

This report presented the derivation and evaluation of concepts in the finite-difference time-domain (FDTD) method for electromagnetic modeling. I started with a background on how the electromagnetic properties of materials are treated in FDTD and followed with the foundation of the Yee formulation of FDTD. From this basis, I developed the total-field/scattered-field and scattered-field methods for simulating waves incident on the region modeled in an FDTD grid. For the first method, I showed that a secondary FDTD grid is effective in reducing anomalous scattering at the boundary between the total-field and scattered-field regions. I showed that the incident-field time derivative required for the scattered-field method can be obtained from the spatial derivative of the incident-field and that a sixth-order central difference equation is a cost effective means to generate the derivative of the incident-field as opposed to the analytic derivative.

I presented background on boundary condition concepts starting with one-dimensional FDTD before turning to two-dimensional FDTD, where I showed that the split-field formulation of the Bérenger Perfectly Matched Layer (PML) method can be generalized with other one-dimensional FDTD boundary conditions rather than just lossy material layers. In the development of one-dimensional boundary conditions, I showed that the formula for splitting an electromagnetic field into components traveling in opposite directions can be used to develop a series of one-way boundary conditions, which perform better than those developed from the factorization of the wave equation. In the last section of the report, I developed a split-field, one-way boundary condition for two-dimensional FDTD that is far less expensive than the widely used PML methods, which even for two-dimensional FDTD require over 27 difference PML/FDTD update equations along with interface equations between the nine different PML/FDTD regions.

REFERENCES

1. K. S. Yee, "Numerical Solution of Initial Boundary Value Problems Involving Maxwell's Equations in Isotropic Media," *IEEE Transactions on Antennas and Propagation* **14**(3), 302–307 (Mar. 1966).

2. R. F. Harrington, *Time-Harmonic Electromagnetic Fields* (McGraw-Hill, New York, 1961).

3. C. A. Balanis, *Advanced Engineering Electromagnetics* (Wiley, New York, 1989).

4. A. R. von Hippel, *Dielectric Materials and Applications* (John Wiley and Sons, New York, 1954).

5. J. Li, L. X. Guo, Y. C. Jiao, and R. Wang, "Composite Scattering of a Plasma-Coated Target Above Dispersive Sea Surface by the ADE-FDTD Method," *IEEE Geoscience and Remote Sensing Letters* **10**(1), 4–8 (Jan. 2013).

6. T. Meissner and F. J. Wentz, "The Complex Dielectric Constant of Pure and Sea Water From Microwave Satellite Observations," *IEEE Transactions on Geoscience and Remote Sensing* **42**(9), 1836–1849 (Sept. 2004).

7. R. Somaraju and J. Trumpf, "Frequency, Temperature and Salinity Variation of the Permittivity of Seawater," *IEEE Transactions on Antennas and Propagation* **54**(11), 3441–3448 (Nov. 2006).

8. K. S. Kunz and R. J. Luebbers, *The Finite Difference Time Domain Method for Electromagnetics* (CRC Press, Boca Raton, FL, 1993).

9. A. Taflove and S. Hagness, *Computational Electrodynamics: The Finite-Difference Time-Domain Method, 2 ed.* (Artech House, Boston, MA, 2000).

10. J. B. Schneider and K. Abdijalilov, "Analytic Field Propagation TFSF Boundary for FDTD Problems Involving Planar Interfaces: PECs, TE, and TM," *IEEE Transactions on Antennas and Propagation* **54**(9), 2531–2542 (Sept. 2006).

11. T. Tan and M. Potter, "1-D Multipoint Auxiliary Source Propagator for the Total-Field/Scattered-Field FDTD Formulation," *IEEE Antennas and Wireless Propagation Letters* **6**, 144–148 (2007).

12. I. R. Çapoğlu and G. S. Smith, "A Total-Field/Scattered-Field Plane-Wave Source for the FDTD Analysis of Layered Media," *IEEE Transactions on Antennas and Propagation* **56**(1), 158–169 (Jan. 2008).

13. M. F. Hadi, "A Versatile Split-Field 1-D Propagator for Perfect FDTD Plane Wave Injection," *IEEE Transactions on Antennas and Propagation* **57**(9), 2691–2697 (Sept. 2009).

14. T. Tan and M. Potter, "Optimized Analytic Field Propagator (O-AFP) for Plane Wave Injection in FDTD Simulations," *IEEE Transactions on Antennas and Propagation* **58**(3), 824–831 (Mar. 2010).

15. T. Tan and M. Potter, "FDTD Discrete Planewave (FDTD-DPW) Formulation for a Perfectly Matched Source in TFSF Simulations," *IEEE Transactions on Antennas and Propagation* **58**(8), 2641–2648 (Aug. 2010).

16. H. Kim, I. S. Koh, and J. G. Yook, "Enhanced Total-Field/Scatter-Field Technique for Isotropic-Dispersion FDTD Scheme," *IEEE Transactions on Antennas and Propagation* **58**(10), 3407–3411 (Oct. 2010).

17. R. Bollimuntha, M. F. Hadi, M. J. Piket-May, and A. Z. Elsherbeni, "Dispersion Optimized Plane Wave Sources for Scattering Analysis with Integral Based High Order Finite Difference Time Domain Methods," *IET Microwaves, Antennas & Propagation.* **10**, 976–982 (2016).

18. J. Scarborough, *Numerical Mathematical Analysis* (Johns Hopkins Press, 1958).

19. J. P. Bérenger, "A Perfectly Matched Layer for the Absorption of Electromagnetic Waves," *Journal of Computational Physics* **114**(2), 185–200 (1994).

20. R. Holtzman and R. Kastner, "The Time-Domain Discrete Green's Function Method (GFM) Characterizing the FDTD Grid Boundary," *IEEE Transactions on Antennas and Propagation* **49**(7), 1079–1093 (July 2001).

21. M. Abramowitz and I. A. Stegun, eds., *Handbook of Mathematical Functions*, Appl. Math. Ser. 55 (National Bureau of Standards, Washington, D.C., 1964).

Appendix A

FDTD FORMULAS AS FORTRAN90 CODE

This appendix shows Fortran 90 code for the one-dimensional FDTD equations. The one-dimensional FDTD E-field update equation, Equation (16), is written as

```
ez(2:nx) = ca(icz(2:nx)) * ez(2:nx) &
         + cbx(icz(2:nx)) * ( hy(2:nx) - hy(1:nx-1) )
```

where `nx` is the size of the one-dimensional space, `ca` is Equation (17a), `cbx` is Equation (17b) divided by Δx, and `icz` is the material number at each `ez` field location. I have taken `hy(i)` to be $+\Delta x/2$ relative to `ez(i)`. The H-field update equation, Equation (18), is

```
hy(1:nx-1) = da(idy(1:nx-1)) * hy(1:nx-1) &
           + dbx(idy(1:nx-1)) * ( ez(2:nx) - ez(1:nx-1) )
```

where `da` is Equation (19a), `dbx` is Equation (19b) divided by Δx, and `idy` is the material number at each `hy` field location. The incident-field corrections for Equations (30a) and (30b) are

```
t = ( n + 0.5 ) * dt
x = ( ixleft - 0.5 ) * dx
ez(ixleft) = ez(ixleft) + cos(phi) * cbx(icz(ixleft)) * ezinc(x,t) / eta
x = ( ixright + 0.5 ) * dx
ez(ixright) = ez(ixright) - cos(phi) * cbx(icz(ixright)) * ezinc(x,t) / eta
```

and for Equations (30c) and (30d) are

```
t = n * dt
x = ixleft * dx
hy(ixleft-1) = hy(ixleft-1) - dbx(idy(ixleft-1)) * ezinc(x,t)
x = ixright * dx
hy(ixright) = hy(ixright) + dbx(idy(ixright)) * ezinc(x,t)
```

where `dx` $= \Delta x$, `dt` $= \Delta t$, `n` is the current time step, `ixleft` is the index of the left boundary between the scattered and total-field regions, and similarly for `ixright`. Since I have chosen `hy(i)` on the right of `ez(i)` the equation for Equation (30c) requires `(ix-1)`. The incident-field, `ezinc(x,t)` is calculated from

```
tp = t - 3.0 * tau - cphi * ( x - x_offset ) / cc
ezinc = sin( omega * tp ) * exp( -tp*tp / (tau*tau) )
```

where `x_offset` is either `dx*ixleft` or `dx*ixright` depending on the propagation direction.